A study on the integration of a novel $NaBH_4$ fuelled hybrid system for a small inland vessel

D. Lensing

Technische Universiteit Delft

Delft University of Technology

Challenge the future

A study on the integration of a novel $NaBH_4$ fuelled hybrid system for a small inland vessel

by

D. Lensing

to obtain the degree of Master of Science
at the Delft University of Technology,
to be defended publicly on Monday April 6, 2020 at 10:00 AM.

Report number:	SDPO.20.005.m	
Student number:	4239954	
Project duration:	May 1, 2019 – April 6, 2020	
Thesis committee:	Ir. K. Visser,	TU Delft, Section SDPO
	Dr. Ir. P. de Vos,	TU Delft, Section SDPO
	Prof. Dr. Ir. J.T. Padding,	TU Delft, Section Complex Fluid Processes

An electronic version of this thesis is available at http://repository.tudelft.nl/.

TU Delft

Preface

The energy transition is in full swing and disruptive technologies together with progressive policies force all kind of industries to rethink how they operate and how they can reduce their carbon footprint. The maritime industry has traditionally been slower to adopt innovations but is no exception. Alternative fuels are being researched by all the big players, and more hydrogen and battery electric concepts are being realized. I find this transition fascinating and realize that innovation can change the status quo rapidly. So when I was investigating different subjects for my master thesis and Klaas Visser told me about the H2SHIPS project, I immediately got excited. I already knew that Klaas was working on alternative ways of storing hydrogen and that Floris van Nievelt had just finished his thesis on the application of NaBH4, and the promise of safe and energy-dense hydrogen storage had already grabbed my attention. The H2SHIPS project provided a platform to implement this technology with a pilot vessel that would be built for the Port of Amsterdam. What followed was an on the spot pitch on my studies and why I was suitable for the project. Apparently, this went well because a few weeks later I was starting my research.

In the beginning, the research went slowly, the pilot in Paris for the H2SHIPS project was cancelled at the last minute and with only a few weeks' notices the kick-off meeting got postponed for six months. Whether the Amsterdam pilot would continue became uncertain and as a result, the early phase of my research became very broad. As the project continued it became clear that the project would go ahead and the cooperation between the Port of Amsterdam, H2FUEL, MARIN and the TU Delft improved. I now had more information on the vessel's demand and operation and could apply and test my ideas using the new vessel as a case study. I learned a lot about different hydrogen technologies, implementations and developments through the H2SHIPS project and I enjoyed the international character of the project. In the end, I can say that I am satisfied with the result of my thesis, I would like to think that I realised a comprehensive work on the application of NaBH4 and look forward to the actual implementations on board of the new 'Havenbeheer' vessel.

My research would not have been possible without the help of others and I would first like to thank my supervisor Klaas Visser for his guidance and advise during my thesis research, his positivism and ability to connect people are infectious and inspiring. I would also like to thank Alex Grasman and Karola van der Meij. from MARIN for sharing their results and keeping me up to date on their progress. From the Port of Amsterdam, I would like to thank Patricia Haks and Jan Egbertsen for their work in the H2SHIPS project and their cooperation with the TU Delft. Gerard Lugtigheid and Hans te Siepe from H2FUEL have also been helpful in discussing the working mechanisms of $NaBH_4$, the reaction catalysts and the workings of the reactor prototype.

Last but not least I would like to thank my mother, Ieneke Wiegman, my father, Rene Lensing, and my sister, Jessie Lensing, for their continued love and support during my upbringing and throughout my studies.

D. Lensing
Delft, April 2020

List of Symbols

The next list describes several symbols that will be later used within the body of the document

η Efficiency

ρ Density

A_E/A_O Effective blade area

A_{wp} Area of waterplane

Boa Beam over all

Bwl Beam water line

C_A Incremental resistance coefficient

$C_A A$ Air resistance coefficient

C_B Block coefficient

C_F Friction resistance coefficient

C_m Midship coefficient

C_p Prismatic coefficient

C_T Total resistance coefficient

C_v Specific heat at constant volume

$c_{0.75}$ Chord length at 0.75 percent of blade length

C_{wl} Waterline coefficient

D_p Diameter of propeller

$Disp$ Displacement

DOD Depth of discharge

F Faraday constant

Fn Froude number

g gravimetric constant

I Current

J Advance ratio

k Form factor

k reaction rate

K_Q Torque factor

K_T Thrust factor

LCB Length of centre of buoyancy

Loa Length over all

Lwl Length water line

M Molar density

m_{H_2O} Mass of water

P Power

Q Capacity

R Resistance

Rn Reynolds number

S_{wp} Surface area of waterplane

SOC State of charge

T Draft of a ship

T Temperature

t Thrust deduction factor

$t_{1/2}$ Half life time

t_s Start up time

T_{aft} Draft at the aft

Uf_{H2} Hydrogen utilisation rate

V_a Water speed at propeller

V_s Ship speed

w Effective wake factor

$wt\%$ Weight percentage

x_{NaBH_4} Molar fraction of sodium borohydride

z Nr. of blades

Contents

1 Introduction **1**
1.1 Background . . . 2
1.1.1 Hydrogen as a fuel . . . 2
1.1.2 Hydrogen storage methods . . . 2
1.1.3 Comparison of hydrogen storage methods . . . 4
1.1.4 Working principles of $NaBH_4$ . . . 5
1.1.5 Department of Energy go / no go decision . . . 5
1.1.6 $NaBH_4$ Applications . . . 6
1.1.7 Conclusion . . . 7
1.2 Projects Related to the Research . . . 8
1.3 Problem Definition . . . 8
1.4 Research Question . . . 9
1.5 Structure of the Report . . . 10
1.6 Software . . . 10

2 The $NaBH_4$ System Components and Performance **11**
2.1 System Architecture . . . 11
2.2 Hydrogen generation system . . . 12
2.2.1 Reaction kinetics . . . 12
2.2.2 Possible catalysts . . . 13
2.2.3 Developed Catalyst by University of Gent . . . 14
2.2.4 Reactor Vessel . . . 16
2.2.5 Fuels . . . 17
2.2.6 Spent fuel . . . 18
2.2.7 Ultra Pure Water . . . 20
2.2.8 Tank concepts . . . 21
2.2.9 Subsystem Overview . . . 22
2.3 Propulsion system . . . 24
2.3.1 Fuel cell selection . . . 24
2.3.2 Fuel cell performance . . . 25
2.3.3 Battery parameters . . . 26
2.3.4 Battery selection . . . 27
2.3.5 Electric motor . . . 29
2.3.6 AC-DC Transformers . . . 30
2.3.7 Subsystem Overview . . . 31
2.4 Control system . . . 32
2.4.1 Reactor Control . . . 32
2.4.2 Energy Management Strategies . . . 32
2.4.3 Selection of Strategy . . . 35

3 Ship Characteristics **37**
3.1 Case Study: Port of Amsterdam Vessel . . . 37
3.1.1 Reference Vessel: ”MS Havenbeheer” . . . 37
3.1.2 Port of Amsterdam Design Requirements . . . 38
3.1.3 Parametric Evaluation and Estimation . . . 38
3.1.4 Appendages . . . 41

3.2 Resistance and propulsion . . . 42
3.2.1 Resistance . . . 42
3.2.2 Propulsion factors . . . 45
3.2.3 Open water efficiency . . . 46
3.2.4 Power Requirements . . . 50
3.3 Operational Profiles . . . 51
3.3.1 Techno Fysica B.V. Measurements . . . 51
3.3.2 Cases . . . 52
3.4 Initial Sizing . . . 54

4 Modelling of the System 57
4.1 Model Architecture . . . 57
4.2 Input . . . 58
4.3 EMS Models . . . 59
4.4 Power Transformation . . . 60
4.4.1 Battery . . . 60
4.4.2 Fuel Cell . . . 61
4.5 Batch Reactor Model . . . 62
4.5.1 Injection . . . 62
4.5.2 Reaction Kinetics . . . 62
4.5.3 Flow control . . . 64
4.5.4 Reactor Pressure . . . 65
4.6 Fuel Cell model . . . 66
4.7 Battery Model . . . 67

5 Analysis of Results 69
5.1 Hydrogen Production Process . . . 69
5.1.1 Simulating method . . . 69
5.1.2 Control Strategy . . . 70
5.1.3 Reaction Kinetics . . . 73
5.1.4 Reactor Volume . . . 73
5.1.5 Conclusions . . . 76
5.2 Energy Management Strategy . . . 77
5.2.1 Simulation Method . . . 77
5.2.2 Comparison EMS . . . 78
5.2.3 Configuration . . . 79
5.2.4 Conclusions . . . 80
5.3 Integrated Design . . . 81
5.3.1 Configuration A: Single Reactor . . . 81
5.3.2 Configuration B: Multiple Reactors . . . 83
5.3.3 Conclusion . . . 85
5.4 Comparison Alternatives . . . 86
5.5 Discussion . . . 88

6 Conclusion 91

A Measurements for inland vessels 95

B Measurements Techno Fysica B.V. 101

C Productsheet Nedstack MT-FCPP-40 and FCS 10-XXL 125

D Product sheet Valence XP Modules 131

Bibliography 133

1

Introduction

Even though shipping is one of the mos fuel-efficient modes of transport, the industry was responsible for over 900 million tonnes of CO_2 equivalent emissions in 2015. This is equivalent to the annual emissions of Germany. Besides greenhouse gas (GHG) emissions ships engines also cause particulate matter, NO_x and noise pollution. As a result, the shipping industry is already facing strict rules and regulations, and these are expected to become even more strict in the near future.

These developments have led to an increased interest in zero-emission solutions and one especially promising area is hydrogen-electric propulsion. By combining hydrogen produced from excess renewable energy with oxygen in a fuel cell, water and electricity are produced. The problem, however, is the storage method for hydrogen, traditionally hydrogen is stored in compression tanks under 300 to 700 bar. But due to the low density of hydrogen, this still results in large installations. Additionally dealing with large amounts of hydrogen gas requires extra safety precautions.

An alternative way of storing hydrogen is by binding the gas to another substance like sodium borohydride or $NaBH_4$. This substance is in a solid form and reacts with water to produce hydrogen and sodium metaborate ($NaBO_2$). The $NaBH_4$ crystals can be stored as a powder and are safe to handle under atmospheric conditions. Also, the substance has a high energy density, even comparable to that of conventional diesel fuel.

This study focuses on $NaBH_4$ as a hydrogen carrier and addresses three problems related to the application of a $NaBH_4$ system.

- First, a suitable configuration for the maritime application of $NaBH_4$ is researched. The $NaBH_4$ reacts with water to produce hydrogen, in the automotive and aviation industry the water needs to be carried on-board. Since a ship can use water from the outside environment a higher energy density is possible compared to what is proposed in the literature.
- Secondly, the hydrolysis reaction takes place in a batch reactor utilizing a catalyst. A model describing the reaction kinetics and the required control settings for such a reactor needs to be developed to understand what is required for viable operations.
- And thirdly, an efficient fuel cell system requires batteries to reduce the size and cost of the fuel cell installation. The integration of a $NaBH_4$ installation in a hybrid system is investigated and a suitable energy management strategy (EMS) for dividing the loads is identified.

The Port of Amsterdam (PoA) is developing a small inland vessel to be powered by hydrogen as a pilot for the North West Europe inter-regional (NWE Interreg) H2SHIPS project. This new build vessel is used as a case study to validate and apply the results of this research. A comparison is made with existing zero-emission technologies and areas for further development are discussed.

1.1. Background

Environmental regulations and increasing pressure from the public domain is leading to more innovation and opportunities for zero-emissions solutions throughout the transportation sector. In the automotive industry, for example, an increasing trend towards batteries can be seen. Unfortunately, the cost and volumetric energy density of Lithium-ion batteries pose an impossible situation for the maritime sector.

Alternatively, the sector is now researching alternative energy carriers such as LNG, methanol, ammonia and hydrogen that all have significantly higher energy densities than batteries. LNG and methanol are seen as an intermediate solution since they are still combustible fuels and thus will still produce greenhouse gasses. Ammonia and hydrogen, on the other hand, can be used in fuel cells, producing zero-emission electrical energy. Of these two, hydrogen is easiest to convert to energy and can be used in a well developed Proton Exchange Membrane (PEM) fuel cell to deliver electrical energy.

1.1.1. Hydrogen as a fuel

To use hydrogen as a power source a fuel cell is needed. Since the 2000's many fuel cell applications have been developed for the maritime industry such as the Nemo H2, a hydrogen-powered canal boat in Amsterdam developed in 2012. The Energy observer, a French vessel that stores on-site produced solar and wind energy into hydrogen to circumnavigate the world. And of course, the Type 212 submarine that uses hydrogen-powered fuel cells as an Air Independent Propulsion systems designed to prolong its submerged mission time.

(a) Nemo H2 (b) Type 212 (c) Energy observer

Figure 1.1: Hydrogen powered vessels

The use of hydrogen in shipping is a fast growing industry due to the increase in volumetric energy density that hydrogen has to offer when compared to batteries. However when compared to diesel oil conventional hydrogen storage is not dense enough to be competitive, the next section will therefore evaluate the different possibilities for on-board hydrogen storage.

1.1.2. Hydrogen storage methods

Safely storing hydrogen is one of the biggest challenges in creating a viable hydrogen-powered system. One way to avoid this problem is to use different fuels and reform it on-board using steam reforming. With this system, conventional fuels such as diesel and LNG can be used. A significant amount of maritime fuel cell studies have been conducted on the use of conventional fuels since the existing infrastructure can be used and the conventional fuels are cheaper and more energy-dense then hydrogen [1]. The problem with steam reforming systems is that they still emit CO_2 emissions. The system is also very complicated, driving up the volume and cost. One example of a ship that uses a more traditional fuel in combination with a fuel cell is the Viking lady, this offshore supply vessel uses LNG in a Molten Carbonate Fuel Cell (MCFC) to generate 320 kW of electrical power.

Then there is storing of actual hydrogen, this is mostly done by compressing the hydrogen to 350 or 700 bar. At 700 bar this results in a gravimetric density of 5.2 wt% and a volumetric density of 0.7 kWh/L for the storage system [2]. Without the storage tanks, the volumetric density of hydrogen at 700 bar is around 1.4 kWh/L. Compressing the hydrogen also consumes energy, for 700 bar this is around 3.7 kWh/kg H_2 or an 11% energy loss [3]. Despite the large volumes required, hydrogen storage by compression is still the most common solution in both the automotive and the maritime industry. This is because refuelling can be done quickly, the costs are relatively low and the process is simple. Another way of storing hydrogen is by liquefying, this is called cryogenic storage and is done

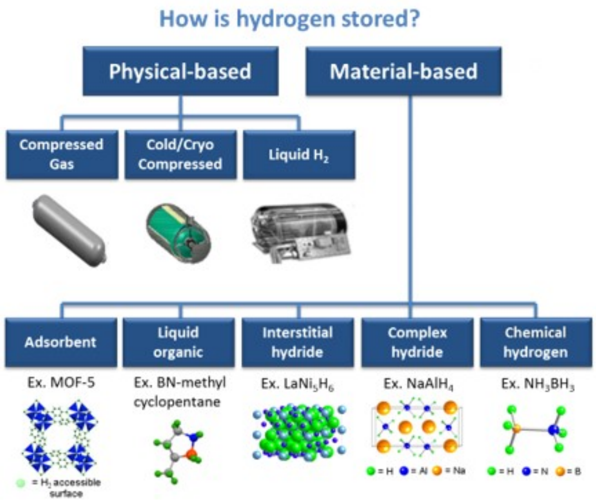

Figure 1.2: Different storage methods for hydrogen [4]

at a temperature of 20°K. When cooled down the hydrogen has an energy density of 2.2 kWh/L [2], which is a 37% improvement compared to the compressed hydrogen. Because of this potential, a lot of research was done in the '90s and a test vehicle was build called the GM hydroGen3. This automotive vehicle had a 90 kg tank that could carry 4.6 kg of LH_2, resulting in a gravimetric density of 5.1 wt%. To achieve this extremely cold state however a lot of energy is required, it takes around 35% of the fuels energy content to achieve cryogenic conditions [2]. The high energy penalty together with the high cost and complexity of the system is the reason that liquid hydrogen storage is not a very popular solution.

Besides compression and cryogenic storage, there is also the possibility of chemical hydrides and adsorption materials. chemical hydrides are often favoured because they are much more stable. When chemical hydrides contain metals such as boron or lithium, they are referred to as metal hydrides. In figure 1.3 the performance of different metal hydrides is shown. On the y-axis is the hydrogen content expressed in weight percentage (wt%) and on the x-axis the reaction temperature needed for hydrogen release. A high hydrogen content and a low reaction temperature are desired, so from this graph, the two best options for hydrogen storage are sodium borohydride, $NaBH_4$, and ammonia borohydride, NH_3BH_3. Of these two the $NaBH_4$ reaction is more studied because it is safer then the reaction of NH_3BH_3 [2].

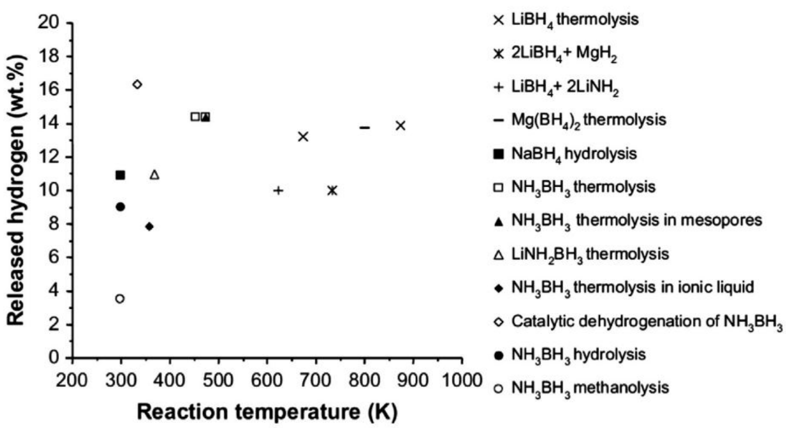

Figure 1.3: Boron based metal hydrides [5]

1.1.3. Comparison of hydrogen storage methods

In figure 1.4a a comparison is made for the volumetric and gravimetric energy densities of different fuels. The fuels include Li-ion batteries, Compressed Hydrogen (CH_2), Liquid Hydrogen (LH_2), Sodium Borohydride, ($NaBH_4$) and Marine Diesel Oil (MDO). The blue bar illustrates the energy densities based on the LHV of different fuels and their densities as well as the wt% of different storage methods as discussed in this chapter. The red line illustrates the effective energy densities and thus includes the losses made for storage as well as in the conversion to electric power. For Li-ion batteries a charge/ discharge efficiency of 80% is assumed [6], for the conversion of hydrogen to electricity in a PEM fuel cell efficiency of 50% is assumed and for a diesel generator, an efficiency of 40% is assumed.

These efficiency's together with the storage losses are also illustrated by the blue graph in figure 1.4c and are known as the Tank to Propeller (TTP) efficiency. Since ultimately hydrogen is only used as a medium to store electrical energy, the red graph in figure 1.4c illustrates the efficiency of the fuel in its capacity to store electricity, known as Well to Propeller (WTP) efficiency. For the production of hydrogen, electrolysis is assumed with rather high efficiency of 80% based on the more efficient hydrolysis plants. The production of $NaBH_4$ is assumed to be around 20% based on the prognosis of H2Fuel. Compared with compressed hydrogen there is a 26% difference in efficiency when storing electricity in $NaBH_4$. It should be noted however that the production of $NaBH_4$ to store hydrogen is still a very novel technology and that increases in efficiency are likely in the near future. And when the regeneration process approaches a 70% energy efficiency it becomes economically competitive with compressed hydrogen storage.

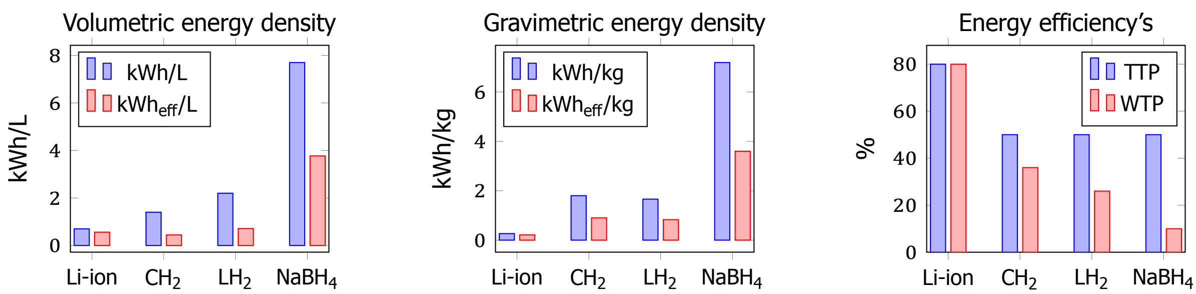

(a) Volumetric energy density

(b) Gravimetric energy density

(c) Efficiency

Figure 1.4: Properties of different energy storage options.

In conclusion, there are four major ways of obtaining and storing hydrogen onboard of vessels these are: Steam reforming, Compression, Cryogenic storage and material based. Steam reforming can be used as an intermediate solution, but due to its inefficiency and the fact that it still emits greenhouse gasses, it is not a very viable option. Compression is simpler and more efficient storage method, however, the limited energy densities could become a problem for larger vessels. Cryogenic storage has a sizeable energy penalty and is still very limited in its energy densities as a storage method. Chemical hydrides and especially sodium borohydride seem very promising as an energy storage method due to its high energy densities both volumetric and gravimetric. The regeneration process, however, is still very inefficient leading to higher costs, however, only limited research is done into the improvement of the hydrolysis process and larger improvements can be expected. Furthermore, the implications of a hydrogen fuel that can be handled safely under atmospheric conditions could have an important impact on the maritime sector.

1.1.4. Working principles of $NaBH_4$
Sodium borohydride is a chemical bond that can be used to store hydrogen, it reacts with water to release hydrogen in a process called hydrolysis, see equation 1.1 [7]. This process can be accelerated by adding heat, acid or a catalyst. When using Ultra Pure Water (UPW) the hydrolysis reaction can reach efficiency's of 98%, realising a very high hydrogen yield.

$$NaBH_4 + 2H_2O = 4H_2 + NaBO_2 + 217kJ \tag{1.1}$$

The hydrolyses reaction is extra efficient in creating hydrogen because it not only releases the bonded hydrogen from $NaBH_4$ molecules, but it also releases the hydrogen-bonded in the H_2O molecules, effectively doubling the hydrogen yield. The gravimetric hydrogen density of $NaBH_4$ is 10.8 wt% [7], however, since not only the $NaBH_4$ hydrogen but also the H_2O hydrogen is released the gravimetric density of the storage method is double that of $NaBH_4$ at 21.6 wt%. With a density of 1.074 kg/L and a Lower Heating Value (LHV) of 33.3 kWh/kg for hydrogen, this results in a volumetric energy density of around 7.7 kWh/L.

$$NaBH_4 + (2+x)H_2O = 4H_2 + NaBO_2 \cdot xH_2O \tag{1.2}$$

There are two methods of storing the fuel, it can either be stored as dry bulk in the form of powder or small crystals or an aqueous solution. Theoretically, one mole of $NaBH_4$ requires two moles of water. However, the actual reaction requires much more water as is described in equation 2.1, where x is the excess water. The excess water is required to solve the reaction product, or spent fuel, $NaBO_2$. If the spent fuel is not completely dissolved, some precipitation will be left in the reactor, this can then lead to degradation of the catalyst performance and the reaction in general.

Using sufficient water has been one of the major concern for the development of $NaBH_4$ systems and usually a solution of between 20-30 wt% of $NaBH_4$ is commonly used [8]. Because all this extra water is required the energy density of the system has always been rather poor, however, the research has always been focused on on-board concepts for the automotive industry. A maritime concept was the water can be sourced from the outside environment has never been truly analysed, even though it has the potential of reaching a very high energy density.

1.1.5. Department of Energy go / no go decision
This section will discuss some of the research done into the use of sodium borohydride as an hydrogen carrier as well as some of the prototype projects that have been developed in different industries. First the automotive industries and the role of the U.S. Department of Energy (DOE) will be discussed. Then some notable projects and prototypes developed as UAV's and UGV's, and their performance will be discussed. Finally the advances made in the regeneration process will aslo be shortly discussed.

The U.S. Department of Energy (DOE) has been one of the main drivers of research and innovation into hydrogen applications and storage. The focus has been on developing an hydrogen powered vehicles that can provide an alternative to the fossil fuel dependant cars. In order to push innovation the DOE has issued targets that serve as a road map to the implementation of hydrogen in the automotive industry. The targets for storage are shown in table 1.1, the ultimate goal for the gravimetric and volumetric energy densities for example are 6.5 wt% and 1.7 kWh/L.

STORAGE PARAMETER	UNITS	2020	2025	ULTIMATE
System Gravimetric Capacity				
Usable, specific-energy from H2 (net useful energy/max system mass)	kWh/kg(kg H2/kg system)	1.5(0.045)	1.8(0.055)	2.2(0.065)
System Volumetric Capacity				
Usable energy density from H2 (net useful energy/max system volume)	kWh/L(kg H2/L system)	1.0(0.030)	1.3(0.040)	1.7(0.050)
Storage System Cost				
Storage system cost	$/kWh net($/kg H2)	10(333)	9(300)	8(266)
Fuel cost	$/gge at pump	4	4	4

Table 1.1: DOE targets for hydrogen storage [4]

In 2003 the company Millennium Cell Inc. developed two prototype vehicles, one with the Fuel Cell

(FC) system as main power source and one with the FC system as range extender. Both vehicles used Sodium Borohydride as an energy carrier [9]. The Fuel cell Vehicle (FCV) was called Natirum and was a converted Chrysler Town model, it had a range of 300 miles with a 60 kW FC power plant. This system used sodium borohydride dissolved in water at a 30 wt% rate, the whole storage system had a hydrogen density of around 4.0 wt% and was projected to be around 8.4 wt% in 2010 by recycling the water produced in the fuel cell. Unfortunately the company seized its operations in may 2008, presumably following the No Go recommendation from the DOE in 2007.

In 2007 the DOE appointed a committee to evaluate the viability of future implications for different hydrogen storage applications. The goal of the committee was to give a simple Go/ No Go advice for the sodium borohydride technology. After evaluation the committee decided to give a No Go recommendation based on the following concerns [10]:

1. The insufficiently proven volume exchange tank concept required to reduce the overall system volume.
2. The requirement for a large amount of water on board of vehicles, especially the 30 wt% of $NaBH_4$ used by Millennium Cell since this is very close to the solubility limit and could be below, depending on the temperature.
3. The precipitation in the system due to the spent fuel of $NaBO_2$ that could potentially clog up the system was not sufficiently addressed.
4. The $NaBH_4$ costs are currently high due to the inefficient regeneration process and more research is necessary to convince the committee.

The first two points emphasise the belief of the committee that for an automotive vehicle the gravimetric and volumetric energy densities could not meet the 2010 target of 5.5 wt% and 1.5 kg/L respectively. It should be noted however that the current 2025 goal is still well below the original 2010 goal and the ultimate goal is only slightly above these values. In the report, the committee recognised the potential of hydrogen released by the hydrolysis of $NaBH_4$ but eventually decided to focus on different technologies instead. It should also be noted that the committee acknowledges that breakthrough advances in the production process of $NaBH_4$ are not easy, especially since the current production model is 50 years old [10]. Ultimately the committee decided to give a No Go advice for the automotive sector based solely on the failing of reaching the 2007 goals and the lack of prospect of meeting the 2010 goals. They recommended however that research into the cost-effective production of $NaBH_4$ should continue in ordered to stimulate other borane related hydrogen storage options.

1.1.6. $NaBH_4$ Applications

Besides the automotive industry, the aviation industry has also been developing $NaBH_4$ fuelled hybrid systems. The U.S. military has been working together with the company Protonex to develop Unmanned Aerial and Ground Vehicles (UAVs and UGVs). From 2006 to 2007 Protonex refitted and tested one of their existing UAVs called the Puma with a $NaBH_4$ fuelled FC system and reported a 4 fold increase in flight duration. The total power system including fuel, fuel cells and electronics had an energy density of 515 Wh/kg [11]. The fuel was stored in a cartridge that could easily be replaced after it was used. Protonex then applied the same cartridge system to a UGV called the Talon. The FC system fitted in the original envelope of the battery and increased the range of the vehicle with a factor 3, according to Protonex this has two main reasons. First, the stored fuel had twice the energy density compared to the li-ion battery pack. The second reason is that the FC system was hybridised with a li-ion battery to handle peak demands. This increased the efficiency of the system since the original battery pack showed low efficiencies at peak load conditions [11].
Not just the U.S. military showed interest in developing $NaBH_4$ fuelled UAVs. From 2010 to 2018 the South Korean ministry of science funded research that focused on implementing and improving a cartridge-based, $NaBH_4$ fueled Fuel Cell system [12–14]. In 2011 a UAV was developed using a catalytic hydrolyses process and a 15 wt% $NaBH_4$ solution with Co as the catalyst by Kim et al[12]. The researchers completed test flights but concluded that a larger fuel capacity and lighter fuel cells were necessary to further improve the range and energy density. In 2014 Kim et al.[13] further improved their design by integrating a fully functioning volume exchange tank to reduce the volume and thus

(a) UGV Talon developed by Protonex in 2007

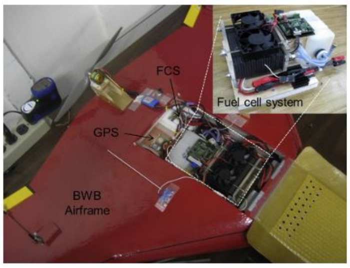

(b) UAV developed in 2014 by Kim et al.

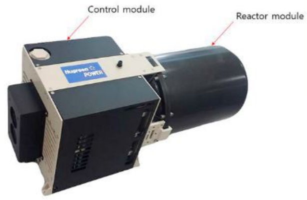

(c) UAV cartridge developed in 2019 by Kwon et al.

Figure 1.5: Different prototypes developed from 2007-2019

increase the fuel capacity. Furthermore, they improved the hydrolysis reaction by using a Co-b catalyst supported on a porous material. Finally in 2019 Kwon et al.[14] focused on improving the end-user experience by fabricating a replaceable cartridge. The hydrogen temperature was maintained at 23°C and the system reported an energy density and hydrogen storage of 463 Wh/kg and 3.5 wt% respectively.

For the successful implication of $NaBH_4$ as a commercial fuel, the regeneration aspect should be evaluated as well. A more efficient regeneration process will lead to a lower fuel cost and thus adaptation will become more likely. The original method developed in 2003 by Kojima et al.. regenerated $NaBO_2$ by annealing dehydrated $NaBO_2$ and MgH_2 at high temperature and high hydrogen pressure [15]. However, this was an expensive process due to the inefficiency and the high cost of Mg. In 2009 Hsueh et al. developed a method of high energy ball milling, increasing the energy efficiency but still relying on the expensive MgH_2 [16]. Another problem is that the previously mentioned methods rely on dehydrated $NaBO_2$ as starting product however the actual by-product of the $NaBH_4$ hydrolysis is $NaBO_2 * xH2_O$ meaning that it is an aqueous solution of $NaBH_4$. In 2017 Ouyang et al. developed a simple and efficient method for regenerating $NabH_4$ by ball milling starting from either $NaBO_2 * 2H2_O$ or $NaBO_2 * 4H2_O$ with Mg [7]. Because the cheaper material of Mg is used instead of MgH_2 the researchers claim a cost reduction of 34-fold.

1.1.7. Conclusion

In conclusion, $NaBH_4$ emerged at the beginning of the century as a serious contender for hydrogen storage leading to the automotive industry developing a few prototypes. However, due to the need for water on board, the unproven volume exchange concept and the inefficient regeneration process the United States Department Of Energy gave a no go recommendation for this technology. Even though the $NaBH_4$ systems couldn't realise the DOE goals, they did show increased energy density compared traditional hydrogen systems and for this reason, the aviation industry continued to develop different prototypes. These systems validated the concept of the volume exchange tank and showed a significant increase in the energy density of around 2-4 times that of a battery system. It should be noted that when considering maritime systems much higher numbers can be expected due to the abundance of water from the outside environment. Finally, some significant research has been done on the regeneration side to decrease the fuel cost and even though some serious steps are realised, more research is needed. It should also be noted that not a lot of research in this area has been done and that when the demand for cheap $NaBH_4$ will grow, the attention of researchers for this subject will grow as well.

1.2. Projects Related to the Research

This research is done within the framework of the North-West Europe inter-regional (NWE Interreg) project and as such other parties and projects are also involved in the development of the technology. H2FUEL is a start-up dedicated to the development of $NaBH_4$ technologies. H2SHIPS is an NWE Interreg project aimed at demonstrating the technical and economical feasibility of hydrogen bunkering and propulsion systems.

H2FUEL

H2FUEL b.v. is a partner in this research and is cooperating closely with the University and other project partners. H2FUEL holds a patent on the use of ultrapure water (UPW) for the hydrogen production process, or hydrolysis, of NaBH4 and is actively developing new technologies to implement NaBH4 fuelled hydrogen technologies. H2FUEL holds the patent and researches new technologies such as durable catalysts and better regeneration processes, H2CIF is a spin-off company from H2FUEL and develops the reactor and technologies needed for implementing the hydrogen production process.

H2CIF has developed a prototype reactor using acid as a catalyst, the reactor is being tested in an experimental environment at the Botlek Plant One location. Currently, the company is developing a more powerful version of the reactor as well as implementing it in a containerised solution that includes storage and all necessary safety features such as ventilation. The prototype for this system is supposed to be operational around the summer of 2020 so that a demonstration can be given at the Amsterdam SAIL event.

Finally, the H2FUEL & H2CIF companies are developing a reactor that functions on a cobalt-based catalyst, thus eliminating the requirement for acid, increasing safety as well as storage density. The container used during the Amsterdam Sail event will then be repurposed for the Cobalt catalyst and the results of this development are to be expected around the end of 2020 / start of 2021.

H2SHIPS

H2SHIPS is a North-West Europe inter-regional project (NWE Interreg) and aims to: "demonstrate the technical and economical feasibility of hydrogen bunkering and propulsion for shipping and will identify the conditions for successful market entry for the technology." The H2SHIPS project involves two pilot projects, an H2 refuelling system in Belgium and a hydrogen-powered port vessel for the Port of Amsterdam to be powered by $NaBH_4$. The Amsterdam vessel will be used as a case study in this research to validate the configuration and sizing of components.

1.3. Problem Definition

In this section, the gap in knowledge between the literature and the objective of realising a $NaBH_4$ maritime system will be identified. Identifying the knowledge gaps will help to define the problem and this, in turn, will shape the research question and sub-questions.

$NaBH_4$ in Maritime applications

After the no go decision the interest for $NaBH_4$ fueled systems declined within the automotive industry. The aviation industry, however, has continued to research the possibilities an energy-dense $NaBH_4$ system can provide for UAVs. Yet, applications of a $NaBH_4$ system in the maritime industry have not been realised and have hardly been researched. As such, questions regarding the application of such a system in a maritime environment remain unanswered. Especially the use of water sourced from the outside environment could result in high energy-dense solutions if proven feasible.

Reaction Kinetics and Reactor Model

The reactor being developed is a batch reactor with a cobalt-based catalyst. The catalyst is developed by the University of Gent and some research is done into the reaction speed and reaction order [17]. However, the research is mainly focused on limiting the degradation of the catalyst over multiple cycles and thorough research on the reaction kinetics of the selected catalyst is missing. Furthermore, the integration of a batch reactor into a hydrogen-electric system has not been done as such the behaviour of such a reactor and the impact it has on the system has not been studied.

Integration of $NaBH_4$ in a Hybrid System
Other questions regarding the integration of a $NaBH_4$ system for maritime applications concern the power-sharing and energy management between the hydrogen energy storage and the batteries. EMS systems have been studied for pure hydrogen systems but the integration of a batch reactor into the system could result in different requirements. The size of the battery and the degree of hybridisation between the battery and hydrogen storage system for certain maritime applications also needs to be determined, and the boundary conditions that affect the right sizing need to be identified.

1.4. Research Question

This section will elaborate on the structure of the report. The scope of this report will be defined and the research questions to be answered in this researched are introduced. Then the structure of the report is discussed, briefly introducing the chapters and relating them to the various sub-questions. Finally, the software used in this research is shortly discussed.

Research Questions
A research question is formulated relating the general questions regarding a maritime $NaBH_4$ fueled system to the pilot vessel being developed by the Port of Amsterdam (PoA). The research question is then further divided into five sub-questions.

What is a suitable design for a $NaBH_4$ hybrid propulsion system for a small inland vessel and how can the design and different control strategies be improved using dynamic modelling?

To find an answer the research question is further divided into the following sub-questions:

1. *What are the possibilities and limitations of the subsystem components, and how can a $NaBH_4$ system be integrated into a maritime application?*
    - *NaBH4 storage and hydrogen production.*
    - *Electric components including batteries.*
    - *Control strategies.*
2. *What is the correct sizing of components for the Port of Amsterdam new build vessel?*
3. *How can the batch reactor be modelled and what other models can be used to validate the initial design?*
4. *What is an effective energy management system for the power distribution of the Port of Amsterdam vessel and how can the hydrogen production system be integrated?*
5. *How does the final design perform when compared to traditional (zero emission) alternatives?*

Scope
The hybrid propulsion system as introduced in the research question contains the power train from energy storage to the propeller. The hydrodynamics of the vessel are also considered to estimate the load characteristics of the new build vessel. The power distribution between fuel cell and batteries will be discussed in terms of energy management. The secondary control settings such as voltage control and torque characteristics of the electric motor, however, will be out of scope for the modelling.

The reactor vessel where the hydrogen is produced from the $NaBH_4$ is being developed by the H2FUEL company and as such the dimensions of the reactor type of reactor is out of scope. How to control the output and input of the reactor however will be discussed. H2FUEL is also responsible for the development of a suitable catalyst for the reaction, however, the workings of the catalysts will be discussed since these are crucial for the reaction kinetics.

1.5. Structure of the Report

This report is structured so that it will answer the various sub-questions before concluding the main research question. First, the possible solutions will be explored and evaluate in chapter 2, answering sub-questions 1.a to c, resulting in a recommendation on how to implement the various subsystems of $NaBH_4$ propulsion system.

Chapter 3 will answer sub-question 2 and will result in an estimation for the Port of Amsterdam's vessels resistance. This resistance can then be used to create an operational profile as well as provide a basis for the model input. The operational profile will lead to an estimation for the energy and power requirements of the vessel and thus answer sub-question 3.

Then in chapter 4, the Simulink model will be introduced based on the decisions made in the previous chapters. The model is first divided into different subsystems before being integrated into one model. The details on the Simulink mechanics as well as the physics and theories behind the models will be discussed in this chapter.

In chapter 5 the models will first be evaluated separately to find optimal settings and to evaluate different EMS systems. By doing so, sub-question 4 will be answered. After recommending the most likely configurations the behaviour of the combined models is tested to compare different configurations of a $NaBH_4$ system. The optimal solution will be evaluated on power and energy density and compared to conventional solutions, answering sub-question 5.

Finally, chapter 6 will be used to recap on the made conclusions to answer the main research question. Furthermore, this chapter will include recommendations for further research.

1.6. Software

For this research, the Matlab and Simulink environment is used for analysing the dynamic behaviour. Within the Simulink environment, Simscape is used, this add-on allows for the modelling of electric networks.

2

The $NaBH_4$ System Components and Performance

This chapter will introduce the maritime $NaBH_4$ propulsion concept in which the water necessary for the hydrogen production process will be sourced from the outside environment. Conventional applications use an aqueous solution with only 30 wt% of $NaBH_4$, However, by using dry $NaBH_4$ fuel and sourcing water from the outside environment it is expected that the energy density of this system will increase even further. In this chapter the concept will be reviewed from a system design point of view, options for different components will be discussed and analysed, and at the end of each chapter, an overview of the subsystem is given.

2.1. System Architecture

First a system layout of the maritime $NaBH_4$ concept is given in figure 2.1. The dry $NaBH_4$ crystals are mixed with the UPW from the filters and enter the converter. Here the hydrolysis reaction takes place and the resulting hydrogen is delivered at the fuel cell and the spent fuel is pumped to a storage tank. The rest of this chapter divides $NaBH_4$ system into three subsystems. The hydrogen production system focuses on the chemistry and the reaction kinetics of the $NaBH_4$ hydrolysis reaction. The propulsion subsystem examines the energy storage in batteries and the efficiency losses in the drive train. And finally, the control subsystem focuses on the injection and pressure control of the hydrogen generator, as well as the energy management strategy that determines the power-sharing between the fuel cell and battery systems.

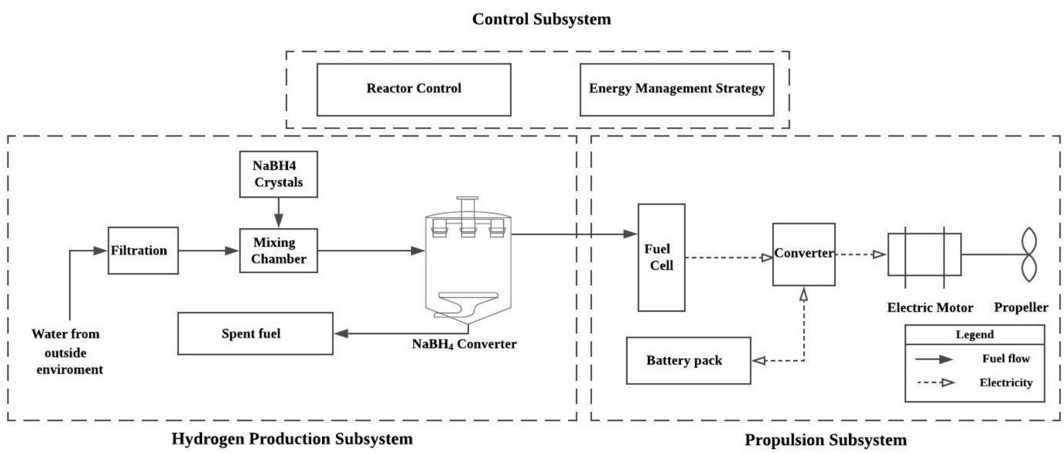

Figure 2.1: System lay out of the maritime $NaBH_4$ propulsion concept.

2.2. Hydrogen generation system

This section will evaluate all the components of the hydrogen production system. First, the $NaBH_4$ conversion reactor will be discussed. The different methods for controlling the conversion rate of the reaction will be evaluated as well as the prototype for the reaction chamber built by H2FUEL. Secondly, the problems concerning fuel storage will be addressed, including the concept of the volume exchange tank as well as the different fuel compositions that can be used. Thirdly the different tank concepts will be evaluated in terms of density as well as their advent ages and disadvantages. Finally, an hydrogen production process will be proposed for the H2SHIPS project taken into account all the factors discussed in this chapter.

2.2.1. Reaction kinetics

As discussed in chapter 1, the hydrolysis reaction of $NaBH_4$ is exothermic as described in equation 2.1. In this section, the reaction kinetics will be described as well as ways of controlling the reaction and hydrogen release by acid, heat or catalysts. Finally, the reaction chamber designs and size will be discussed.

$$NaBH_4 + 2H_2O = 4H_2 + NaBO_2 + 217kJ \tag{2.1}$$

The hydrolysis reaction of $NaBH_4$ as given in equation 1.1 is affected by the pH levels of the solution, as can be seen in table 2.1. High levels of acidity will result in a fast reaction, whereas base solutions can stabilise the hydrolysis process. At normal conditions, the half-life time of a sodium borohydride solution is 3.7 seconds and given that it takes around 7 cycles of half-life time to reach a conversion efficiency of 99.2%, then under normal conditions with sufficient water, most of the hydrogen will be released after 25.9 seconds or roughly half a minute. In batch operations with limited water however, this is not the case. This is because the pH of the solution increases as the hydrogen is produced due to the dissolved by-product of $NaBo_2$, and this slows down the reaction drastically [18].

When the $NaBH_4$ is stored as a solution in water it thus needs to be stabilised using a base such as NaOH (sodium hydroxide). The reason that NaOH is used, is that the base is sodium-based so it does not add any new elements to the process and thus it will not contaminate the spent fuel or hydrogen in any major way. The amount of NaOH necessary depends on the $NaBH_4$ solved in the solution. H2fuel uses for example an experimentally determined solution of 5 wt% NaOH for a 30 wt% $NaBH_4$ solution, 7.5 wt% NaOH for a 50 wt% solution and 10 wt% for a 66 wt% solution in order stabilize the solution. If the fuel will be used in a certain form in an industrial scale these percentages could be further optimised.

Besides preventing the reaction from happening, the pH value can also be used to activate and accelerate the reaction. As can been seen in table 2.1 the half time life of the $NaBH_4$ reaction increases dramatically when the pH value drops. Different kinds of acids can be used such as HCL, H_2SO_4, HNO_3, H_3PO_4, or HCOOH [19]. The exact amount of acid necessary again depends on the amount of $NaBH_4$ and NaOH in the water solution and the desired hydrogen production rate.

pH	Half-life of NaBH4	99.2% Conversion	
4	0.0037	0.0259	sec
5	0.037	0.259	sec
6	0.37	2.59	sec
7	3.7	25.9	sec
8	36.8	257.6	sec
9	6.1	42.7	min
10	61.4	42.98	min
11	10.2	71.4	h
12	4.3	30.1	d
13	42.6	298.2	d
14	426.2	2983.4	d

Table 2.1: Half-life of $NaBH_4$ at various pH values [20]

Alternatively, a catalyst can be used to accelerate the reaction. The catalyst will provide an alternate reaction pathway for the reaction thus requiring less activation energy. A catalyst will not be consumed by the reaction, however, some research has suggested that the effect of the catalyst degrades over multiple cycles. The alternative reaction path occurs at the surface of the catalyst so an increased surface area will increase the effectiveness of the catalyst, this can be achieved by using a powdered form of the catalyst. Due to the importance of the surface area of the catalyst, it is also crucial that no precipitation of the spent fuel in the crystalline form of $NaBO_2$ x $2H_2O$ is formed. So extra water is required in the reaction tank to ensure the complete solvation of the spent fuel.

Another method of accelerating the hydrolysis reaction is by increasing the heat of the reaction, this method is very hard to describe by simple formulas due to the complexity of the reactions involved so experimental tests will need to be executed to quantify the exact hydrogen production when the heat is used as the prime accelerator. However, it is fair to say that reaction speeds will be slow and operation temperatures will become very high. A comparison between the different acceleration methods can be found in table 2.2.

Accelerator	**Half life**	**Advantages**	**Disadvantages**
Acid	<1 min	High reaction speed, High performance on dynamic behaviour, HCL highly available, Fast reactor start up	Safety hazard Additional weight and volume for storage Extra refuelling component
Catalyst (Cobalt)	~10 min	Catalyst is not 'consumed', Low cost, No additional spent fuel	Catalyst degradation over cycles, Higher reactor volume and weight
Temperature	~1 hour	Low OPEX, Low maintenance, Less additional water needed	Slow start up, Large and heavy reactor

Table 2.2: Overview of different acceleration methods [21]

2.2.2. Possible catalysts

Of all the accelerator options, adding acid seems like the most promising candidate for fast and well controlled reactions. However the safety implications of using an aggressive acid, as well the significant amounts of acid that would be necessary would become a great problem [21]. Thus catalysts could be the better option if the performance is sufficient. In this subsection different catalysts will be evaluated in order to identify the most promising candidate.

Catalyst are usually divided into noble and non-noble catalysts. Even tough noble metal based catalysts are in general one or two order in magnitude more effective, they are also much more expensive. It has been estimated that for a 75 kW vehicle, using a noble catalyst would be an order of magnitude more expensive compared to using a non-noble alternative [22]. The large difference in price and also the limited availability of rare metals has lead to increased research into non-noble catalyst, often cobalt based. In the table 2.3 three viable non-noble catalysts options are evaluated. These three options have been selected due to their high effectiveness and are further evaluated based on cycle efficiency and practicality.

Catalysts	**Co-B nano particles** [23]	**Co-W-B/Ni Foam** [24]	**Fe-Co-B/Ni Foam** [25]
Cycle efficiency	Not tested	90% after 6 cycles	54% after 6 cycles
Form	Black precipitate/ Powder	Electrolessly plated on Ni foam	Electrolessly plated on Ni foam
Max reaction rate (mL_{H2} min^{-1} $g_{cat}{}^{-1}$)	26000	15000	22000
$NaBH_4$ solution used	15 wt% / 3.2 gram	20 wt% / 2 gram	15 wt% / 20 ml
g_{cat} used	0.1287	0.0447	0.0250
Max reaction rate (L_{H2} min^{-1})	3.3457	0.6700	0.5500
A_0 ($NaBH_4$)	0.0847	0.0528	0.0847
Rate coefficient (s^{-1} (experiment))	0.0073	0.0024	0.0012
Rate coefficient (s^{-1} $g_{cat}{}^{-1}$)	0.0569	0.0527	0.0481
Half-life time $t_{1/2}$ (s $g_{cat}{}^{-1}$)	12.19	13.16	14.4

Table 2.3: Three selected non-noble cobalt based catalysts for $NaBH_4$ hydrolysis [23] [24] [25]

The effectiveness of a catalyst is often evaluated by their max reaction rate in litres of H_2 produced in one minute per gram catalyst used. For some catalysts with reaction rates of only 500-16000 (mL_{H2} min^{-1} $g_{cat}{}^{-1}$) the reaction is zero-order and thus the reaction rate is independent from the reactant concentration. More effective catalysts, however, show the behaviour of a first-order reaction, where the reaction rate is dependant on the concentration of the reactant [23]. This behaviour is defined by the rate law given in equation 2.2.

$$Rate = -\frac{d[A]}{dt} = k[A] \tag{2.2}$$

The "rate" is the reaction rate of reactant [A], in this case $NaBH_4$ and is in units of molar s^{-1}. The unit k is the rate coefficient and is given in s^{-1}, for higher order reaction k may vary, however for first order reactions k can be considered constant. By rewriting and solving the integral the second form of the rate law can be found as defined in equation 2.3.

$$[A_t] = [A_0]e^{-kt} \tag{2.3}$$

Since the rate coefficient is constant, the maximum rate will coincide with the maximum amount of reactant [A] so we can calculate k. First, we convert the max rate of H_2 to molar rate, then to max rate of $NaBH_4$ by molar ratio and then calculate the number of reactants used in the experiments, finally, we can determine what the k value is for the different catalysts using table 2.3 and equation 2.3. If we know k we can also determine the half-life time as given by equation 2.5.

$$\frac{[A_{1/2}]}{[A_0]} = \frac{1}{2} = e^{-kt_{1/2}} \tag{2.4}$$

$$t_{1/2} = \frac{ln(2)}{k} \tag{2.5}$$

It is important to note that the effectiveness of the catalytic reaction is of course determined by the amount of catalyst available. And even tough k is constant, it is dependant on how much catalyst is used. There is, therefore, some room in the reactor design to speed up the reaction if more catalyst is used, finally the design limitation for the catalyst support material will determine the exact reaction rate constant.

Furthermore, parts of the catalyst can react with the substance in a process called leaching and this will decrease the cycle effectiveness of the catalyst. This is most likely the case for the iron-cobalt-boron (Fe-Co-B) catalyst, where it is suspected that the $NaBH_4$ reacts with the catalyst to form $Fe(OH)_3$ [22]. Other factors that can decrease cycle efficiency is lost of the catalyst due to mechanic grinding when the reactants are stirred or pumped and the catalyst is damaged as a result.

From the three catalysts selected in table 2.3 the Cobalt-Born nanoparticles show the highest rate coefficient per gram of catalyst. This is most likely due to the high surface area that is realised by using nanoparticles. The problem, however, is that the catalyst is not supported and is used in a powder form, making placing it in a reactor difficult. Furthermore, the cycle efficiency of the catalyst is not properly tested. However due to its high reaction rate and lack of side reaction that can cause leaching H2FUEL decided to further develop the Cobalt Boron nanoparticles catalyst with the help of the University of Gent.

2.2.3. Developed Catalyst by University of Gent

In 2015 H2FUEL asked the University of Gent to further develop a Co-B nanoparticle catalyst using commercially available resins to support the powder. The research was conducted by S. Basting under supervision of professor G. Haesart [17]. A method was developed to produce the catalyst using reduction and the performance was tested under varying circumstances, most notably the temperature. Finally, the IRC7481J catalysed was selected as the best catalyst, optimised for efficiency, reaction rate and cycle efficiency.

Resin	TP207	TP207	TP207	IRC 7481 J	IRC 7481 J
Temperature (C)	30°	50°	75°	50°	50°
Order of reaction	Zero	Zero	First	Zero	Zero
Max activity (mL_{H2} min^{-1} n_{cat}^{-1})	14	85	721	451	662
Max activity (mL_{H2} min^{-1} g_{cat}^{-1})	383	2370	20189	12628	18536
NaBH4 solution used	5 wt%/ 10 ml	5 wt%/ 10 ml	5 wt%/ 10 ml	5 wt%/ 10 ml	10 wt%/ 10 ml
resin used (g)	0.11	0.11	0.11	0.10	0.10
$n_{catalyst}$ / g_{resin} (mol kg^{-1})	1.53	1.53	1.53	1.29	1.29
$g_{catalys}$ / g_{resin} (g kg^{-1})	42.78	42.78	42.78	36.12	36.12
g_{cat} used	4.71E-03	4.71E-03	4.71E-03	3.61E-03	3.61E-03
L_{H2} min^{-1}	0.0018	0.0112	0.0950	0.0456	0.0670
Rate coefficient k (1 s^{-1})	3.39E-07	2.07E-64	2.30E-03	8.46E-06	1.24E-05
Rate k (1 s^{-1} g_{cat}^{-1})	7.21E-05	4.39E-04	4.89E-0	2.34E-03	3.44E-03
$t^{1/2}$ (s g_{cat}^{-1})	97.94	16.07	1.42	3.02	4.11
$t^{1/2}$ experiment (min)	346.91	56.94	5.03	13.92	18.96

Table 2.4: Resin supported Co-B catalysts as developed by Rijks Universiteit Gent [17]

The Co-B nanoparticles catalyst is supported in an ion exchange resin. This allows the catalyst to be in an insoluble solid form compared to the liquid reactant whilst remaining ion exchange properties that allow for the reaction to occur. The University of Gent decided to use commercially available resins of the Amberlite brand produced by Rohm and Haas, most notably the TP207 and the IRC748 resins.

The TP207 resin was used to examine the effects that the reaction temperature has on the reaction rate and these results can be seen in figure 2.2. From this figure, it becomes clear what a huge impact the temperature has on the reaction rate of the substance. Increasing the temperature from 50°to 75°Celsius even seems to change the reaction kinematics from a zero-order to a first-order reaction and as a result, the reaction rate increased 12 times as can be seen in table 2.4.

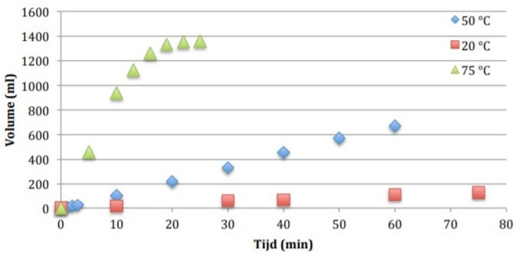

Figure 2.2: The effect of the reaction temperature on the catalytic performance of Co-B on the TP207 resin [17]

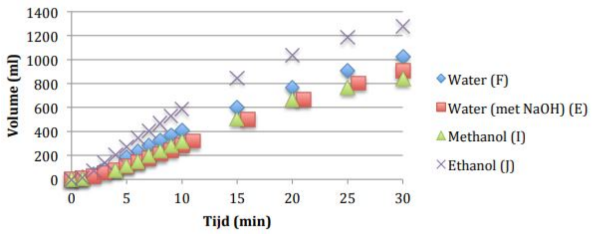

(a) Hydrolysis reaction with a 5 wt% $NaBH_4$ solution

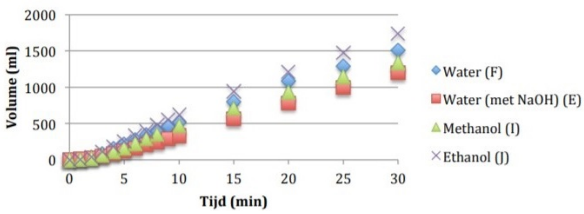

(b) Hydrolysis reaction with a 10 wt% $NaBH_4$ solution

Figure 2.3: The effect of using different solvents in the reduction process, leading to the creation of catalyst IRC7481 F, E, I and J and their hydrogen production performance [17]

After evaluating different resins and different formation conditions, it was concluded that the so called IRC7481 J was the best performing resin supported Co-B catalyst. In figure 2.3 the hydrolysis of a 5 wt% $NaBH_4$ solution is shown, it was found to have no leaching effects and a reaction efficiency of 99.2% with a decent half life time of 13 minutes at 50°Celsius.

From figure 2.3 it appears that the reaction of IRC7481 J is again zero order. Although it could also be a very slow first order reaction it is assumed that the reaction is zero order and behaves similar to the TP207 resin that was tested. A first order reaction rate law is defined by equation 2.7.

$$Rate = \frac{-d[A]}{dt} = k \tag{2.6}$$

Integrating the law gives an expression for k based on measurements as can be seen in equation 2.7 and gives an expression for the half life time as defined by equation 2.8.

$$[A] = [A]_0 - kt \tag{2.7}$$

$$t_{1/2} = \frac{[A]_0}{2k} \tag{2.8}$$

It is reasonable to assume that the reaction rate will increase and that the reaction kinetics will become first order at higher temperatures of around 75°Celsius, as was the case with the TP resin. Sadly this was not tested and thus no accurate conclusion can be made on the performance of this catalyst at higher temperatures. However, based on the results of the testing with the TP207 resin it is not unlikely to think that the reaction rate increases with a 10 fold when increasing temperature to 75 °Celsius.

Finally, it should be mentioned that the exact reaction rate of the reactor is not constant and can be varied by adjusting certain reaction conditions such as:

- Changing the temperature of the reaction.
- Changing the movement of the reactants by e.g. stirring or pumping.
- Changing the amount of catalyst.
- Changing the concentration of $NaBH_4$ in the solution.
- Changing the concentration of stabiliser NaOH in the solution.

For the modelling, an average half-life time of 10 minutes will be assumed as a reference value. However given the high tune-ability of this parameter due to the factors mentioned above, a sensitivity analysis will be done varying the reaction rate to evaluate its effect on the system and the reactor sizing.

2.2.4. Reactor Vessel

Throughout the literature, different reactor designs have been proposed for the application of a $NaBH_4$ power system. Most of the researched systems, however, were focused on the automotive and industry and thus focused on a continues flow reactor to ensure a continues process and avoid the use of heavy batteries. To achieve complete hydrogen conversion, however, excess amounts of catalyst needed to be used. In the feasibility research that has preceded this research, many different forms of reactors were evaluated and in consideration with H2fuel systems form of the multi-purpose batch reactor was selected [21].

A multi-purpose batch reactor has the advantage that small experiments can still be executed and analysed with relative ease, while still being able to scale up the reactor to an industrial level. On the other hand, a system including a batch reactor requires more control systems to function properly, as well as the need for extra batteries to achieve the required load in time and to bridge the gap between demand and supply caused by the slow reaction kinetics of the catalytic reaction.

H2FUEL has developed, build, and tested two prototypes for the batch reactor. The first version was a 5 kW reactor, meaning that it had a capacity of 0.15 kg H_2 per hour. This version is used to demonstrate and validate the hydrogen production rate using acid and ultrapure water. Conversion rates of 98% were observed and using acid the conversion rate was almost instantaneous.

The V2 version of the prototype is being developed and will have a capacity of 3.75 kg H_2 per hour or 125 kW and will function using a catalyst. The reactors demonstrate the viability of the technology in a relevant environment meaning that they have a technology readiness level (TRL) of 6. When integrated with a fuel cell the technology will show its viability as part of an integrated system reaching TRL 7. The reactor volume and specifics will increase further when developed, however, for now, these specifics of the V2 reactor will be used as a basis for the design of the propulsion system.

Reactor	Internal volume	External volume	Capacity (kg H_2/h)	Power (kW H_2)	Density (kW/L)	TRL	Pressure	Temperature
V1	38 L	49 L	0.15	5	0.10	5-6	50 bar	60-110 C
V2	38 L	49 L	3.75	125	2.55	6	110 bar	60-110 C

Table 2.5: Specifications of the reactor prototype versions one and two developed by H2FUEL.

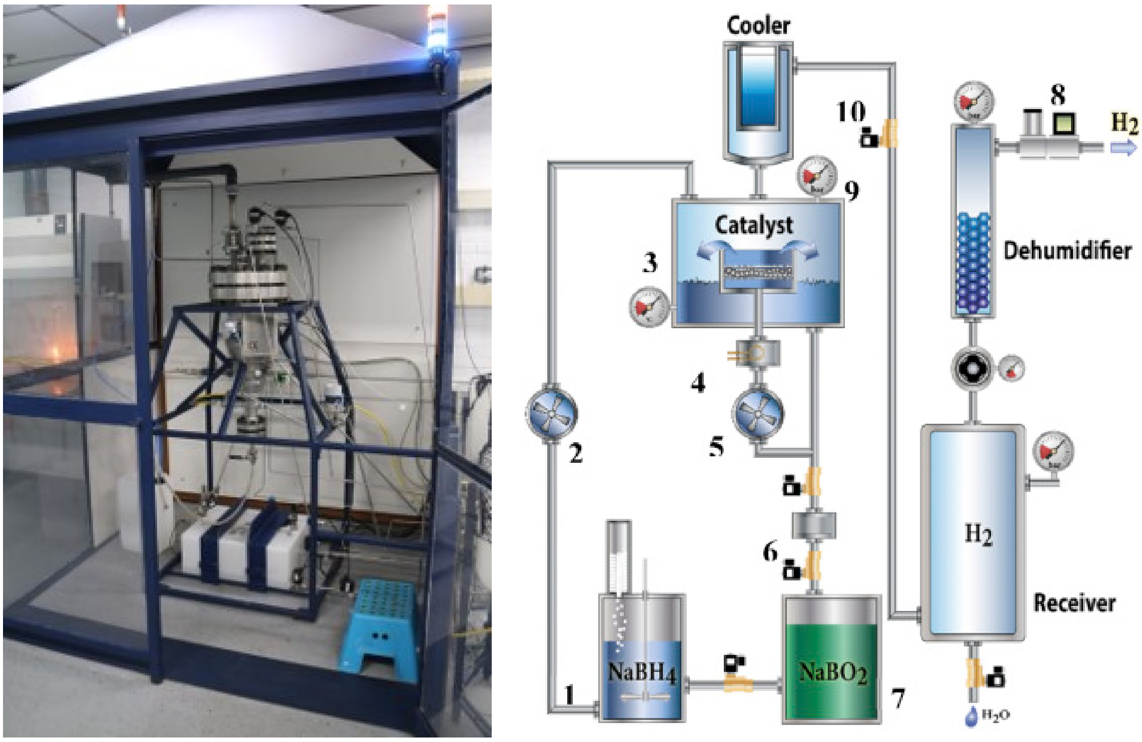

(a) V1 prototype

(b) Scheme for multipurpose batch reactor

Figure 2.4: The V1 prototype of a $NaBH_4$ batch reactor build en tested by H2FUEL (a), Multi purpose batch reactor using dry fuel [26] (b)

2.2.5. Fuels

The $NaBH_4$ can be delivered and stored in different solutions. Four storage methods for the $NaBH_4$ fuel are defined as: Fuel 30, Fuel 50, Fuel 66 and Dry fuel. The number indicates the weight percentages of $NaBH_4$ in the solution and dry fuel is a substance of small powder or crystals that can be mixed with water to achieve the desired solution for the reaction. In this section the different fuels will be shortly evaluated, in table 2.6 the gravimetric and volumetric densities are calculated based on 1 kg of H_2 and assuming a lower heating value (LHV) of 33 kWh, efficiency losses are neglected. Furthermore, NaOH is not added to the solution yet since the precise percentages may differ and will increase the weight and volume per kg H_2.

Fuel 30 is based on a mole ratio of 1 $NaBH_4$ to 5 H_2O so that enough water is present after the hydrolysis reaction for the $NaBO_2$ side product to dissolve and thus prevent precipitation in the reactor that could clog the system or contaminate the catalyst. The gravimetric density can easily be determined since the solution is based on weight percentage. The volumetric density, however, is a lot more difficult to accurately determine since salts in solutions cannot be determined analytically and require an experiment. On such experiment tested the hydrogen production of a 30 wt% solution with HCL acid and 1 wt% NaOH, and determined that the density of the solution be 1.01 g/ml [27].

Fuel 50 is the fuel proposed when using an acid accelerator. In this case, the acid will be used as the catalyst of the reaction, however, the acid needs to be diluted in water as well. The acid solution is added to the fuel 50 solution in the reactor and the total water available will be enough to prevent precipitation. Calculating the volumetric density of this fuel is again difficult without experiments especially so since not all the $NaBH_4$ will be solved in the solution given that the solubility limit of a $NaBH_4$ solution at 20°C is 35% [21]. However, an estimation is made based on equation 2.9 using the solubility limit, the density of fuel 30 and the density of $NaBH_4$. ρ_1 and ρ_2 are the different densities and w_1 an w_2 are the weight percentages of the dry $NaBH_4$ and saturated NaB_4 solution respectively.

$$\rho = \rho_1 w_1 + \rho_2 w_2 \tag{2.9}$$

$$\rho = 1.07(0.50 - 0.35) + 1.01(1 - (0.50 - 0.35)) = 1.02[g/ml] \tag{2.10}$$

Fuel 66
Fuel 66 is called the slurry fuel and is based on the theoretical amount of water that can be recirculated from the fuel cell and has a 66 wt%. The slurry fuel needs constant circulation in the tank to prevent clogging and formation of $NaBH_4$ x H_2O crystals. The density can is calculated using equation 2.11 and is

$$\rho = 1.07(0.66 - 0.35) + 1.01(1 - (0.66 - 0.35)) = 1.03[g/ml] \tag{2.11}$$

Dry fuel has the highest energy density and can be mixed with water from the outside environment after it is filtered, a feature that is unique to the maritime sector. Another advantage dry fuel has over the mixed fuels is that no NaOH stabiliser is needed and that the fuel can be stored safely without any decay. Because even though NaOH stabilises $NaBH_4$ solutions by increasing the pH value, it does not stop the hydrolysis completely. Over years there will still be some hydrogen boil off, dry $NaBH_4$ fuel does not have this problem. Disadvantages of dry fuel, however, are the increased complexity in fuel handling since the crystals cannot be pumped through the system. A solution could be to store the dry fuel above the water mixing chamber, where they are dropped by gravity or a pneumatic device when needed, similar to the device discussed in figure 2.4. Another problem can occur when the dry fuel is in small powder form, due to the high surface area the substance tends to become sticky in humid environments. This problem could be mitigated by using coarser crystals and thus reducing the surface area.

Fuel	kg/kg_H2	L/kg_H2	kWh/kg	kWh/L	Advantages	Disadvantages
Fuel 30	15.63	15.47	2.13	2.17	Easy fuel handling, No extra water	Needs NaOH to stabilize
Fuel 50	7.18	9.19	3.55	4.84	Easy fuel handling, More dense	Needs NaOH to stabilize, Requires acid solution or water mixing chamber, Requires circulation in the tank
Fuel 66	5.97	6.90	4.69	5.87	Easy fuel handing, More dense	Needs NaOH to stabilize, Needs water mixing chamber, Requires circulation in the tank
Dry fuel	4.69	4.38	7.10	7.60	Very dense, No stabilizer needed, No decay over time	Fuel handling is difficult, Needs water mixing chamber, Humidity could make the substance sticky

Table 2.6: Different type of $NaBH_4$ fuels and their densities, NaOH for stabilising is not included

2.2.6. Spent fuel
As mentioned before, the precipitation of the by-product $NaBO_2$ in water is one of the more difficult problems in achieving an energy-dense system. So much so that the U.S. Department of Energy listed it as one of the main reasons behind the no go decision in 2007 [10]. In this chapter, the precipitation reactions will be evaluated and different options for filtering out the excess water will be evaluated.

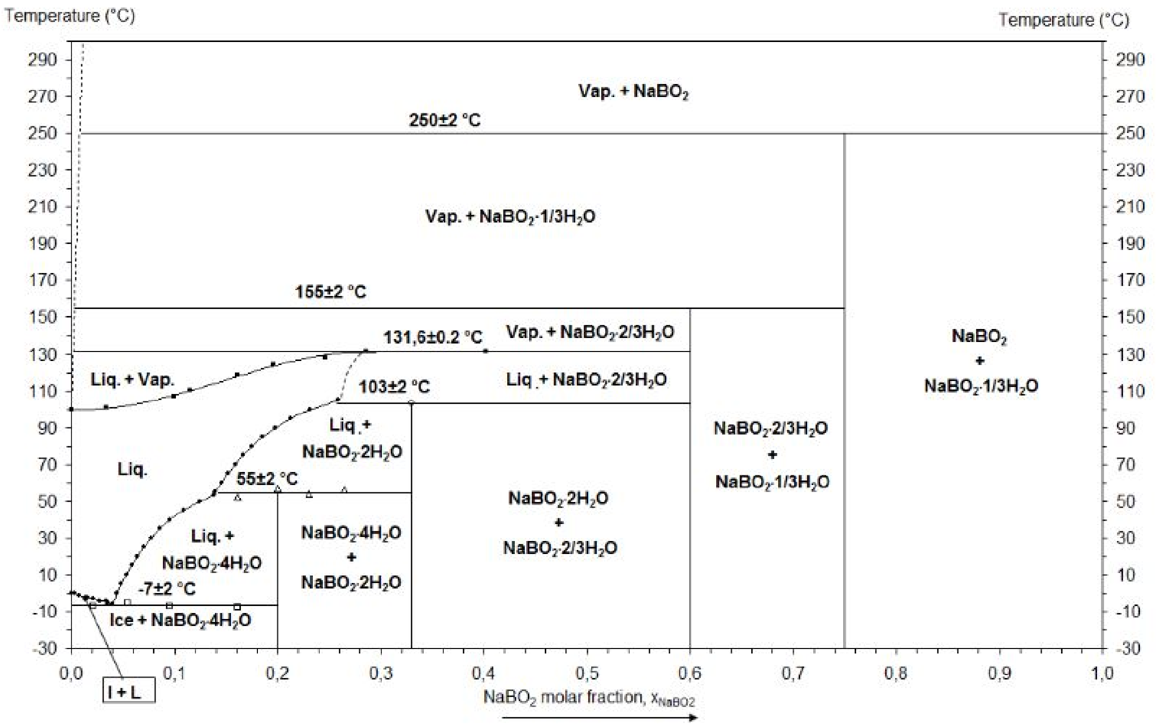

Figure 2.5: Binary phase diagram of the system $NaBO_2$-H_2O [28]

In figure 2.5 the phase diagram of the $NaBO_2$ is shown, besides the complete solution, shown in the graph by liq., $NaBO_2$ also forms five different types of crystals namely: $NaBO_2$x $4H_2O$, $NaBO_2$x $2H_2O$, $NaBO_2$x $2/3H_2O$, $NaBO_2$x $1/3H_2O$ and anhydrous $NaBO_2$. The formation of these crystals can become a problem and can lead to clogging of the system making the substance unpumpable. These crystals are formed depending on the molar concentration of $NaBO_2$ shown in equation 2.12 and 2.13

$$NaBH_4 + (2+y)H_2O = 4H_2 + NaBO_2 \cdot yH_2O \tag{2.12}$$

with x is:

$$x = \frac{1}{1-y} \tag{2.13}$$

In general, the formation of crystals will increase with increasing molar concentration, as a result of filtering, and with decreasing temperature during storage. One method of dealing with the clogging problem is thus by re-heating the storage tank before pumping, increasing the solubility of the mixture and reversing the formation of crystals that cause the clogging problem. For a solution with a molar fraction of 0.2 $NaBO_2$ the tank would need to be reheated to 90 degrees to fully prevent clogging and thus maintain the pump-ability of the fluid. After x=0.25 it becomes impossible for the solution to return to a fully dissolved liquid without adding extra water. The conditions for maintaining a pump-able flow are summarised in table 2.7.

Another factor in the formation of hydrated crystals is the temperature of the solution. Some crystals will only form under high enough temperature, $NaBO_2$x $2/3H_2O$, for example, will only form between $103\pm2°$and 155 ± 2°C as can been seen in figure 2.5. A substance with a molar rate of 0.66 $NaBO_2$ only contains the $NaBO_2$x $2/3H_2O$ crystals. To realise this substance, the solution would first need to be heated until 103 ± 2 °C and then filtered until the molar concentration reaches 0.66. A similar process can be applied when heating and filtering the solution at a temperature higher then 155 ± 2°C. At this stage $NaBO_2$x $1/3H_2O$ crystals will be formed and a molar concentration of 0.75 becomes possible. In both cases, the result is a sludge of crystals that can be stored very densely but can not be transported easily.

Furthermore the heating up of the solution has an energy cost that is calculated in table 2.7, using equation 2.14 and assuming a reactor temperature of 90°C and a C_v of 0.0098 kWh/kg/T. Considering that hydrogen has an LHV of 33.3 kWh/kg and assuming a fuel cell efficiency of 50% the relative energy cost is 8.8% and 39.4% for x=0.66 and x=0.75 respectively.

$$P_{heat} = c_v m_{H_2O} \Delta T \tag{2.14}$$

x_{NaBO2}	kg/kg_H2	L/kg_H2	Energy cost (kWh/kg_H2)	Method of filtration using fuel 30	Conditions for pumping
x=0.05	55.55	49.02	0.00	Adding water	Ambient until 10 degrees
x=0.10	30.60	24.61	0.00	Adding water	Heating until 35 degrees
x=0.15	22.28	16.69	0.00	Adding water	Heating until 67 degrees
x=0.20	18.12	12.83	0.00	Adding water	Heating until 90 degrees
x=0.25	15.63	10.57	0.00	None	Heating until 105 degrees
x=0.33	13.14	8.37	0.00	Liquid filtration	Unpumpable
x=0.60	9.81	5.23	1.47 (8.8%)	Heating (105) + liquid filtration	Unpumpable
x=0.75	8.89	4.29	6.55 (39.4%)	Heating (157) + gas filtration	Unpumpable

Table 2.7: Densities for different concentrations of spent fuel.

Finally the densities of different spent fuel concentrations are calculated and summarised as well in table 2.7. As with the $NaBH_4$ solutions it remains difficult to estimate the densities of the solution due to the formation of crystals over time. However there has been some research into the densities of $NaBO_2$ solutions for a mole ratio of x=0 to 0.13 and a linear relation was found that fitted the equation 2.15 [29].

$$\rho = \rho_{water} + 0.0607 \cdot M \tag{2.15}$$

Where ρ is the density in g/ml and M is the molar density in mol/kg. The equation was interpolated until x=0.25 after which the solution becomes completely crystalline and another method had to be applied. For x=0.33 to x=0.75 the density is based on the relative density of anhydrous $NaBO_2$ and H_2O. In reality the density for this range differs due to the formation of crystal with varying sizes and additional research is necessary if such a spent fuel solution is applied.

2.2.7. Ultra Pure Water

The hydrolysis reaction also requires water and how much depends on the fuel that is used. For fuel 30 no extra water is needed and this results in a molar fraction of $NaBO_2$ in the spent fuel of 0.25. for other fuels the water either needs to be stored somewhere on-board or it can be sourced from the outside environment. If the water is sourced then it first needs to be filtered. The main energy consumer for this process is the reverse osmosis (RO) process. It is difficult to say with certainty what the energy consumption of an RO process since it depends on the plant design. To pass the semi-permeable membrane the water needs to reach a pressure of around 60 bars, this costs a lot of energy however most of the energy is recovered by using turbines, in general, the energy consumption is around 4 to 10 kWh per cube meter [30]. A conservative estimate of 10 kWh per cube meter is used in this study and the results for some relevant combinations are shown in table 2.8.

	x_{NaBO2}	L UPW/kg_{H2}	Energy cost RO kWh/kg_{H2}	Energy cost RO (%)
Fuel 30	x=0.15	8.21	0.082	0.49%
	x=0.20	4.04	0.040	0.24%
	x=0.25	1.54	0.015	0.09%
Dry Fuel	x=0.15	19.17	0.192	1.15%
	x=0.20	15.00	0.150	0.90%
	x=0.25	12.50	0.125	0.75%
	x=0.60	6.67	0.067	0.40%

Table 2.8: Ultra pure water requirements depending on the fuel type.

2.2.8. Tank concepts

Different possibilities and configuration for the storage tanks are introduced. First, the concept of the volume exchange tank will be discussed, then conventional options using separate tanks will be discussed. Finally, the concept of replaceable cartridge tanks will be discussed. In table 2.9 a few configurations of these different tanks are proposed and compared.

The safest option would be to use separate tanks, the design would need tanks for spent fuel and the fuel (e.g. fuel 30) or the ultrapure water if dry fuel is used. By replacing the water tanks with a reverse osmosis system the density could be increased further and only tanks for the dry fuel and spent fuel would be necessary.

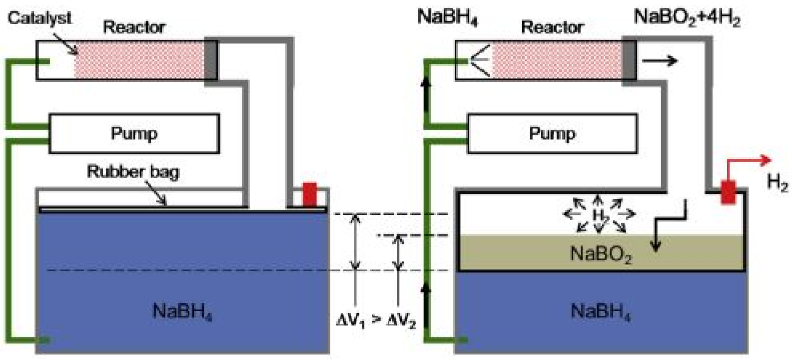

Figure 2.6: Volume exchange tank as developed by Kim et al.[13]

Another option is the volume exchange tank concept as shown in figure 2.6. The volume exchange tank stores the fuel and the spent fuel in the same tank separated by a membrane. The spent fuel and the used fuel concentration need to be of comparable volumetric energy densities. So for example fuel 30 and spent fuel of x=0.25 could be used however a solution of x=0.15 could also be used since the volumetric densities of fuel 30 and spent fuel x=0.15 are similar. In this case spent fuel with x=0.15 would be preferred since the risk of crystal formation is smaller, and crystals could damage the membrane. The volume exchange tank has been tested on small scale however large scale application has not yet proven itself.

A combination of conventional tanks and the volume exchange concept can be realised by utilising a buffer tank. At the beginning of the operation the tanks would be filled with fuel 30 or UPW. During operation first the buffer tank would be filled until one of the fuel tanks is empty and can be refilled with the spent fuel either from the buffer tank or from the reactor directly. In this cased it is assumed that 10 tanks plus one buffer tank is installed, thus increasing the required volume with 10%. In table 2.9 this option is called interchangeable tanks.

Finally it could be possible to create a very dense system using a crystalline spent fuel with x=0.60. However such a system can not be pumped dry, instead the entire tank would need to be replaced resulting in a cartridge system. In this case the tank would need to be easily accessible, creating some enormous design limitation as well as possible high costs. None the less it remains an interesting concept that could create new possibilities in the future.

Tank concepts	kg/kg_2	L/kg_2	wt%	vol%	Advantages	Disadvantages
Interchangeable tanks Fuel 30 - x=0.25	20.63	20.42	4.8%	4.9%	No filtering	Density is actual lower due to NaOH, Fuel degradation over time, UPW installation
Interchangeable tanks Dry fuel - UPW - x=0.20	31.26	29.59	3.2%	3.4%	No filtering, No fuel degradation	Low density,
Volume exchange tanks Fuel 30 - x=0.25	18.75	18.57	5.3%	5.4%	High energy density No filtering	Vulnerable membrane poses safety risk, Density is actual lower due to NaOH, Fuel degradation over time, UPW installation
Volume exchange tanks Fuel 30 - x=0.15	22.28	18.57	4.5%	5.4%	High energy density Less risk on crystal formation	Vulnerable membrane poses safety risk, Density is actual lower due to NaOH, Fuel degradation over time, Need to produce extra water
Cartridge system Dry fuel - UPW - x=0.60	14.50	9.61	6.9%	10.4%	Very high energy density	Spent fuel needs to be heated and filtered, UPW installation, Cartridge needs good accessibility
Separate tanks Dry fuel - on-board water - x=0.20	36.88	31.30	2.7%	3.2%	Low safety risk, No energy cost	Low energy densities,
Separate tanks Dry fuel- UPW - x=0.20	22.81	17.21	4.4%	5.8%	Low safety risk	Low energy densities UPW installation

Table 2.9: Energy densities of different storage concepts

2.2.9. Subsystem Overview

Since the H2SHIPS project is the first time a propulsion system like this will be applied, a few consideration should be taken into account when designing the system. First, the safety, hydrogen itself is a very flammable substance and therefore there is a justified concern from the public and classification societies for the safety of a hydrogen vessel. Therefore less complex safe solutions are given priority over more energy-dense and more efficient solutions.

Secondly, the dry fuel solutions are given priority over the mixed solutions because even when stabilised the mixed solution will deteriorate over time. Since the vessel that is being designed will on occasion have long periods of inactivity, it is undesirable to use mixed fuels. Another advantage is that the intake and filtering of water can be tested and the concept can be proven during operations, paving the way for more energy-dense solutions in the future.

In figure 2.7 the schematics of the proposed hydrogen system is shown. The solution after mixing is chosen to be 25 wt% to achieve a molar fraction of x=0.20 $NaBO_2$ after the reaction and thus ensuring pump ability of the spent fuel. Also minimising the risk of crystal formation while still maintaining an energy-dense storage system for the spent fuel.

According to table 2.7 the tanks would need to be heated up until 90 degrees to achieve complete solubility for pumping out the spent fuel. However, based on experiments based from H2FUEL it seems that a solution with suspended particles could also be acceptable and pump-ability is achieved at lower temperatures as well. For now, it is assumed that a spent fuel solution of x=0.20 is indeed a viable solution, either with heating or without. However, it should be noted that the spent fuel conditions are one of the most critical design aspects and will need to be investigated further before implementation.

The intake of new fuel and discharge of spent fuel is controlled by a pressure transmitter and level indicator respectively. When a certain threshold is reached the valves will be activated thus maintaining a constant hydrogen buffer and preventing the flooding of the catalyst by spent fuel. The data are shown in figure 2.7 are used in the rest of this research to size the different systems and to asses the volumes that are needed and available for other subsystems such as the battery packs.

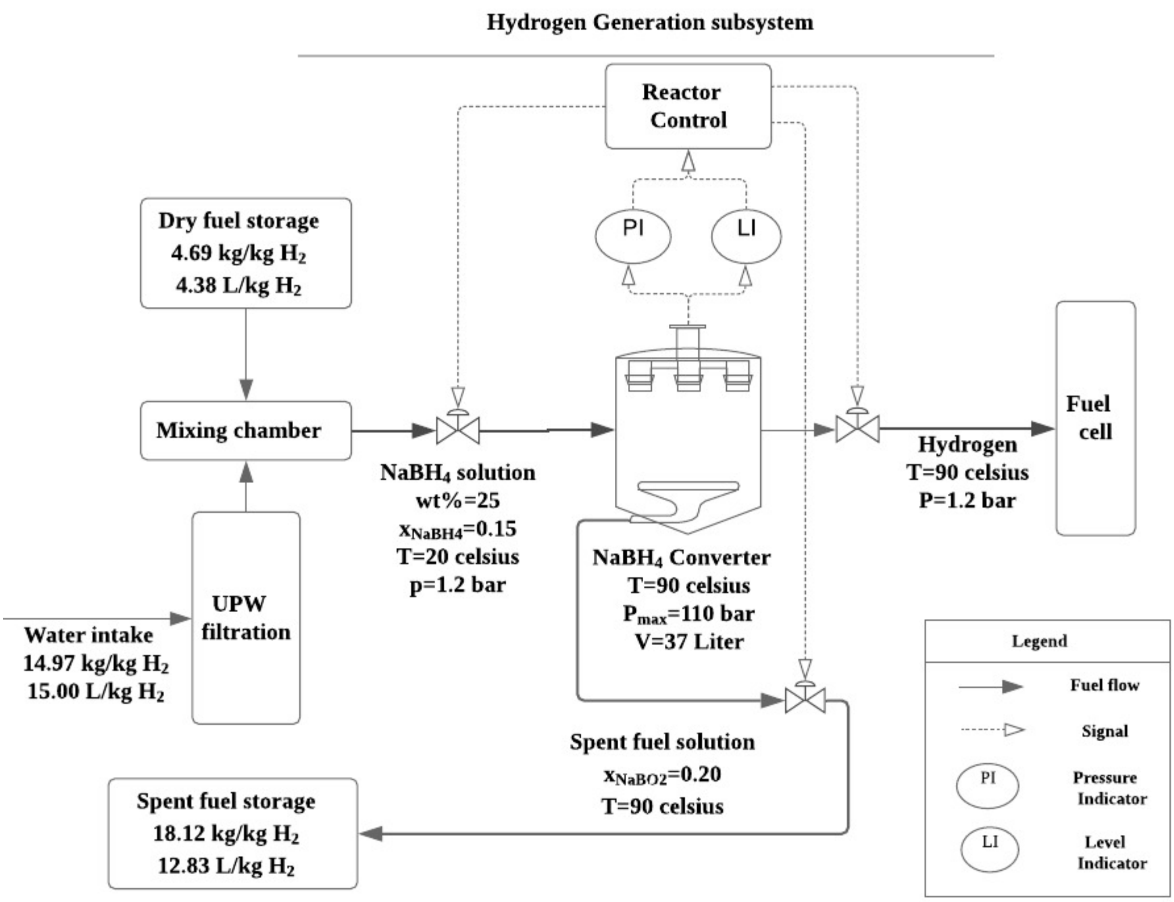

Figure 2.7: A schematic overview of the hydrogen production subsystem including Pressure Transmitter (PT) and Level Indicator (LI) for control and including densities per kg H2 being produced

2.3. Propulsion system

In this section, the propulsion subsystem will be evaluated. The Fuel cell options will be examined and a suitable fuel cell will be selected and the typical fuel cell performance will be evaluated. Different Li-ion batteries are examined as well as different electric motors. Finally, an overview of the chosen configuration is given to determine the electrical efficiency of the propulsion train.

2.3.1. Fuel cell selection

Many projects are now being developed using fuel cell technology ranging from bulk carriers to cruise ships, to high-speed ferries. These projects are very well documented in a study from 2017 called "Study on the use of fuel cells in shipping" [31] commissioned by the European Maritime Safety Agency (EMSA). This study also evaluated different types of fuel cells used in the maritime industry and found three types of fuel cells to be the most promising. These are the Proton Exchange Membrane Fuel cell (PEMFC), the High-Temperature PEM Fuel cell (HT-PEMFC) and the Solid Oxide Fuel Cell (SOFC).

The PEMFC has an anode and cathode, separated by a membrane that conducts protons. Hydrogen is fed to the anode side, here the H_2 reacts with a catalyst, usually platinum-based, creating H^+, protons and e^-, electrons. The protons travel through the membrane to the cathode side and the electrons travel through an external electrical circuit, thus creating a current. The cathode side is being fed with oxygen, here the H^+ protons, the e^- electrons and the O_2 molecules react to form H_2, see figure 2.8a. The PEMFC technology is relatively mature resulting in a relatively low cost, the efficiency is moderate around 50-60 % [31] and the FC has a high tolerance for cycling operations. Disadvantages of the PEMFC are the low operating temperature, around 100°C, resulting in waste heat that is unsuitable for energy recovery, the high hydrogen purity necessary for proper operations and the need for a complex water management system [31].

The HT-PEMFC is similar to the conventional Low-Temperature PEM Fuel Cell (LT-PEMFC) however the operating temperature is higher at around 200°C. This results in more useful waste heat, slightly increasing the efficiency if used effectively. This also results in a higher fuel tolerance and a less complex water management system since water is only present in the gaseous phase. The technology is less mature than the conventional LT-PEMFC and thus costs will be higher. The main reason for using an HT-PEMFC is better fuel tolerance. When reforming an alternative fuel onboard such as LNG or ammonia, this can greatly reduce the complexity, cost and volume of the overall system.

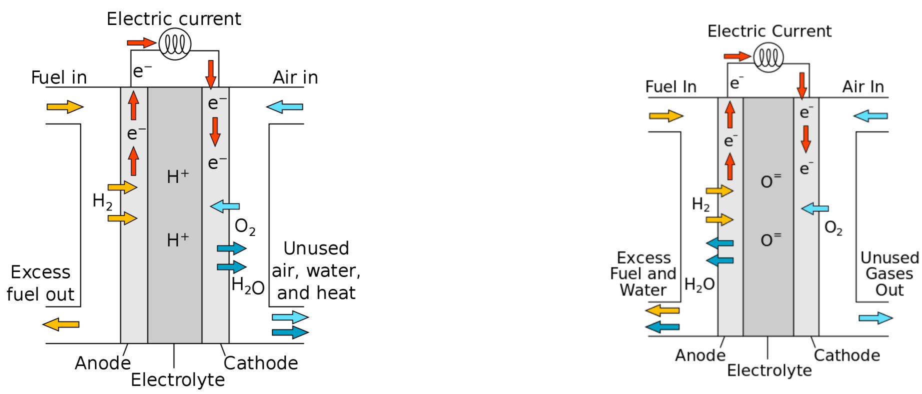

(a) Proton Exchange Membrane Fuel Cell [32]

(b) Solid Oxide Fuel Cell [33]

Figure 2.8: The reaction of different fuel cells

The SOFC fuel cell works slightly different then the proton exchange fuel cell. Here it is not the positive H^+ protons that travel trough the membrane, but rather the negatively charged O^- ions that are created at the cathode side. At the anode side the O^- react with the H_2 creating H_2O molecules and $2e^-$ electrons. The SOFC is highly efficient, reaching 85% efficiency when waste heat is included and this number is expected to rise with further development [31]. It is also possible to reform hydrocarbon fuels such as LNG in the cell itself, this will however release CO_2 and NO_x into the atmosphere. The SOFC is not matured yet as an technology and is therefore still very costly. The high temperature required for a SOFC to function of around 800-1000°C leads to very slow start up times and can pose a safety risk as well.

From the fuel cells that were selected, the HT-PEMFC and the SOFC are more resilient against fuel impurities. Therefore these fuel cells look very promising on the short term future where perhaps pure hydrogen on board ships will not yet be realised and fuel cells instead depend on on-board reforming. If however pure hydrogen is available, the PEMFC is considered to be the superior choice outranking the alternatives on important parameters such as cost, size, maturity and safety [31].

	Relative cost	**Size**	**Maturity**	**Sensitivity to fuel impuririties**	**Safety aspects**	**Efficiency**
LT-PEMFC	Low	Small	High, extensive experience from several applications including ships	Medium	Hydrogen	50-60%
HT-PEMFC	Moderate	Small	Low, experience some aplications including ships	Low	Hydrogen and high temperatures (200 C)	50-60%
SOFC	High	Medium	Moderate, experience from several applications including ships	Low	Hydrogen and high temperatures (600 C)	60% (electrical) 85% (Heat recovery)

Table 2.10: Summary of fuel cell technologies [31]

2.3.2. Fuel cell performance

When integrating the fuel cell in the system it is important to understand the power performance of a fuel cell system. In figure 2.9 a power performance curve of typical 30 kW fuel cell is shown. Fuel cell systems tend to perform better at part load conditions with an optimal efficiency around 1/3 and 2/3 of the rated power. This information will be important for the implementation of an energy management system since the load can be optimised to achieve maximum efficiency.

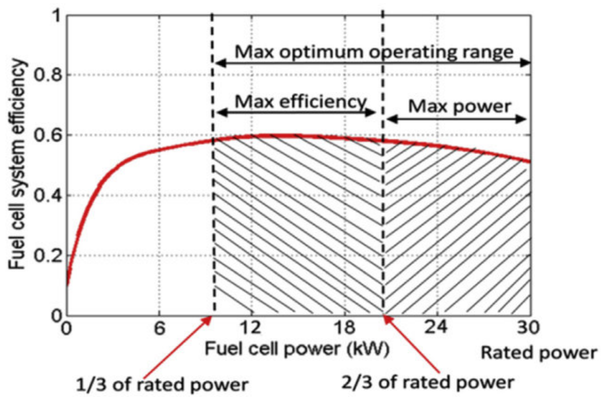

Figure 2.9: A typical power performance curve for a fuel cell system [34]

It should be noted that the difference in efficiency depends heavily on the fuel cell system design and may differ depending on the manufacturer. However the indications for maximum efficiency and maximum power as given in figure 2.9 can be used in order to create an energy management strategy in section 2.4.2.

2.3.3. Battery parameters

This section will shortly introduce some important battery parameters that will be used in the selection and modelling of the battery systems. The State of Charge (SOC) and Depth of Discharge (DOD) will be introduced as well as the cycle durability and the charge/ discharge C rates.

The state of charge is the percentage of the battery that is charged, so SOC of 100% means that the battery is fully charged and SOC of 0 % means that the battery is empty. SOC is used for indicating the battery status and is, therefore, an important parameter for energy management. For example, a complete discharge of the battery results in only 500 expected lifetime cycles and discharge of only 30% results in 2050 expected lifetime cycles. It also not desirable to recharge your battery completely to 0% DOD, the desirable range for batteries between recharge cycles is considered between 80% and 30% DOD, or a SOC of between 70% and 20%.

Depth of Discharge is the inverse of SOC with DOD 0% being fully charged and DOD 100% being fully discharged. DOD can also be expressed in units of Ah. DOD is mostly used to discuss the effects of charging on the number of lifecycles of the battery system. In figure 2.10 the effect of DOD on the expected lifecycles is illustrated.

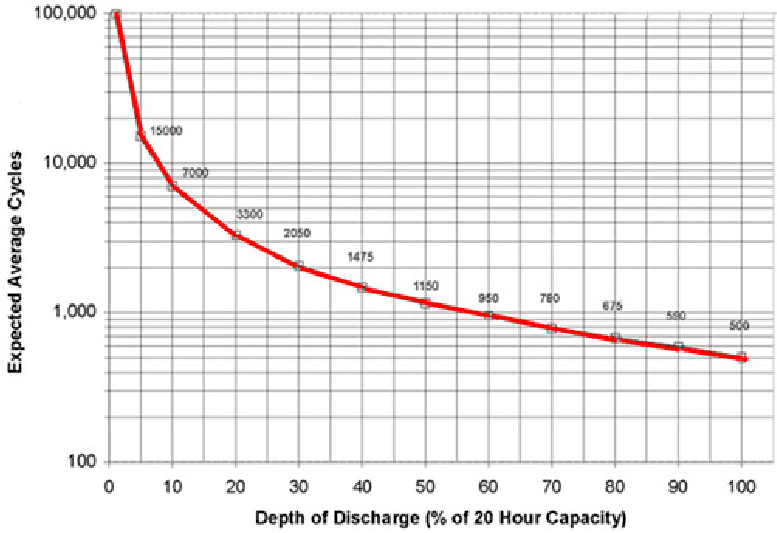

Figure 2.10: Effect of DOD on expected life cycles for a typical rechargeable battery [35]

Another important parameter for battery design is the C-rate of the battery. The C rate is defined as the time it takes for the battery to charge or discharge and has the SI unit of h^{-1}. When a battery has a nominal capacity of 40 Ah and a C rate of 1, then the maximum allowed current is 40 A and the battery will be discharged in one hour. The relation between the max current and C rate is given in equation 2.16, where Q is the nominal capacity in Ah.

$$C = \frac{I_{max}}{Q_{nominal}} \tag{2.16}$$

Batteries with a high discharge C rate will also have a higher power density since more ampere can be drawn from the battery. Unfortunately, however, an analytical relation between C rates and specific power is not possible since depending on the battery the voltage profile also changes depending on the discharge current, as can be seen in figure 2.11. In fact, both the nominal voltage, the nominal capacity and the battery efficiency decrease when more power is required from the battery system and this should be taken into account when designing the control system.

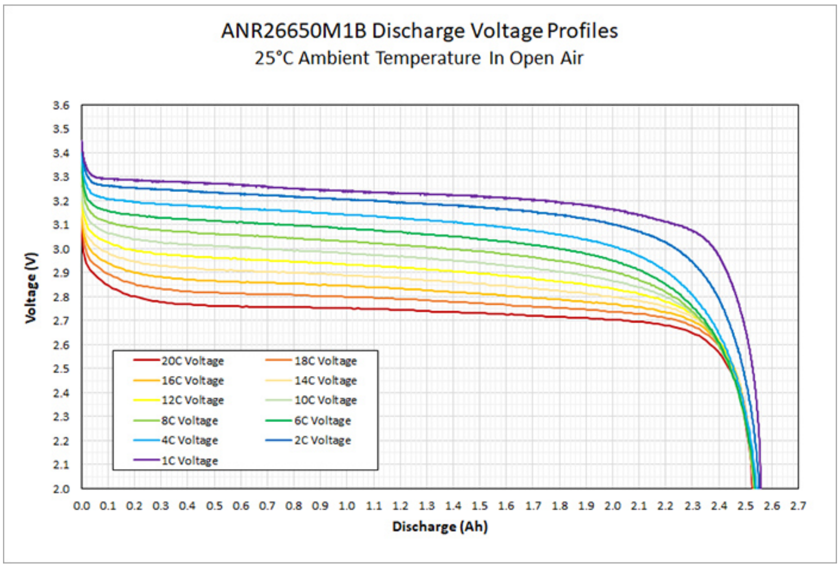

Figure 2.11: Discharge voltage profiles with different C-rates for a typical Li-ion battery [36]

2.3.4. Battery selection

Lithium-ion batteries have become the standard for battery systems in the recent decade however still many different types of Lithium-ion batteries exist. This chapter will introduce the different options for Li-ion batteries and will evaluate and compare their performance.

Lithium Cobalt Oxide (LCO)

The lithium cobalt oxide battery has a high specific energy and therefore it used to be a popular choice for mobile phones and laptops. The disadvantages are low cycle life, low specific power and low thermal stability making it relatively unsafe. The charge and discharge C rate are both around 1 resulting in average charging and poor power performance. Finally, Cobalt is an expensive material. The LCO was an early version of the Li-ion battery and has now become mostly irrelevant.

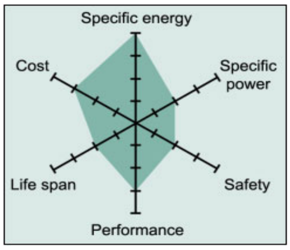

Figure 2.12: Spider graph of the LCO battery [37]

Lithium Manganese Oxide (LMO)

The LMO battery has lower specific energy but very good specific power performance with a discharge C rating of up to 10 C and a maximum charge C rating of 3 C. During longer operations at high load thermal runaway begins to become a problem however. The batteries are often used for power tools and medical devices. A combination of LMO and NMC are often used in the Power-train of electric vehicles such as the Nissan Leaf, the Chevy Volt and the BMW i3. Nowadays however the technology has become less relevant due to advancements in NMC batteries

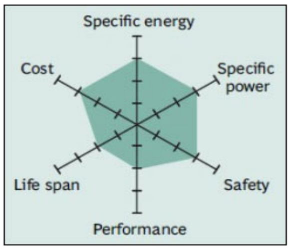

Figure 2.13: Spider graph of the LMO battery [37]

Lithium Nickel Manganese (NMC)

The NMC is one of the most common and fastest-growing Li-ion batteries on the market because of its good overall performance. The NMC battery systems can be optimised for either high specific energy of high specific power. The battery is used in E-bikes, medical devices and electric vehicles. It is regarded as a hybrid cell since it has a good specific energy, Long lifetime, a discharge rate of 2 C and high energy density makes this one of the leading battery systems.

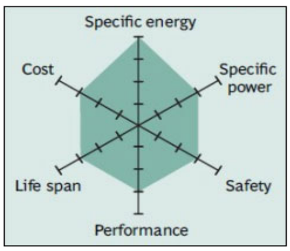

Figure 2.14: Spider graph of the NMC battery [37]

Lithium Iron Phosphate (LFP)
The LFP battery excels in safety, cycle life and specific power. Discharge C rates of up to 25 C is possible. The drawbacks of LFP batteries are the relatively high cost and the increased self-discharge. The battery system is mostly used for applications that have very high peak loads. The electric Amsterdam canal boats are equipped with the Lithium Iron Magnesium Phosphate (LFMP) a more advanced version of the LFP type batteries. Due to their long lifetimes and high safety, these batteries are a good option for the maritime sector.

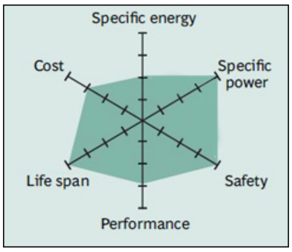

Figure 2.15: Spider graph of the LFP battery [37]

Lithium Nickel Cobalt Aluminium (NCA)
The NCA battery has very high energy density and has, therefore, a similar function to the NCA. The drawbacks, however, are the cost and safety of these battery packs. These batteries are mostly being developed by Panasonic and Tesla because they have the highest specific energy of all the li-ion batteries.

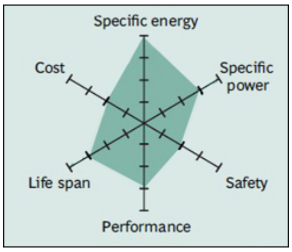

Figure 2.16: Spider graph of the NCA battery [37]

Lithium Titanate (LTO)
The LTO battery is one of the safest li-ion batteries and is capable of delivering high amounts of power with a discharge C rate of up too 10 C. Furthermore it has a very high cycle life with up to 7000 cycles being possible. Unfortunately the specific energy is very low at only 50-80 kWh/kg. These battery systems are used in the electric power train of the Mitsubishi i-MiEW and the Honda Fit EV as well as for solar powered street lights. The high costs of the battery systems limits the use to special applications.

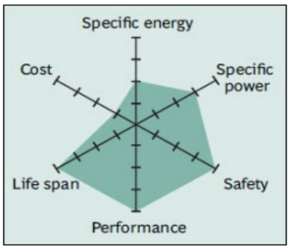

Figure 2.17: Spider graph of the LTO battery [37]

In table 2.11 the different characteristics of the discussed Li-ion batteries are summarised. It appears that a trade off exist in the battery design between high specific energy and high specific power. In the automotive industry it seems that the energy dense batteries are preferred. In the maritime industry however, the cycle lifetime, safety and specific power are of more importance then in the automotive industry. Therefore it seems that batteries of the Lithium iron phosphate (LFP) or lithium titanate (LTO) could be preferred over more cost effective and energy dense batteries such as the nickel cobalt (NCA) and the nickel manganese cobalt (NMC). In order to make a final decision, the energy and power demand of the ship needs to be known as well as any space limitations. However it seems likely that the LFP battery will be the preferred choice due to good safety, lifetime and high power capabilities.

	Specific energy (capacity)	Charge C rate	Discharge C rate	Cycle life (avg.)	Cost	Safety	Comments
LCO	150-200 Wh/kg	0.7-1 C	1 C	500-1000	Unknown	Thermal runaway at 150 C	Early Li-ion battery no longer relevant.
LMO	100-150 Wh/kg	3 C	10 C	300-700	Unknown	Thermal runaway at 250 C	Good power battery but has become less relevant, good safety.
NMC	150-220 Wh/kg	0.7-1 C	2 C	1000-2000	$ 420 per kWh	Thermal runaway at 210 C	High C rates lead to thermal run away, leading system, good hybrid cell.
LFP	90-120 Wh/kg	1 C	25 C	>2000	$ 580 per kWh	Thermal runaway at 270 C	One of the safest Li-ion batteries.
NCA	200-260 Wh/kg	0.7 C	1 C	500	$350 per kWh	Thermal runaway at 150 C	Predicted to reach 300 Wh/kg, used by Tesla and market share is growing.
LTO	50-80 Wh/kg	5 C	10 C	3000-7000	$1005 per kWh	Safest battery	Long life and ability to ultra-fast charge but very low specific energy.

Table 2.11: Summary of different Li-ion battery systems [37]

2.3.5. Electric motor

The transformation from electrical power to mechanical power is done using an electric motor. The behaviour of the chosen motor is important for the ship designer since the envelope can affect the operation of the propeller. A DC motor, for example, has a different speed-torque signature then a traditional diesel engine, as illustrated in figure 2.18. However, other electric motors such as the induction motor can use sophisticated frequency control to deliver max torque at the required rpm. To understand the requirements of the drive train better, three main types of electric motors are discussed in this section.

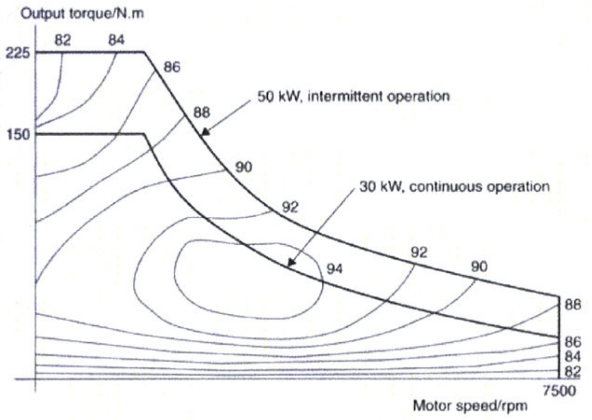

Figure 2.18: Typical efficiency map of a 50 kW permanent magnet brushless DC motor (BLDC) [38]

Brushed DC Motor (DC)

The brushed or commutator DC motor is one of the oldest and well known electric motors. It functions by creating a magnetic field in the stator, using either a separate DC circuit or a permanent magnet, and an electrical current in the rotor. Because current needs to be delivered to the rotating rotor, some kind of brushes are required. These parts increase the maintenance requirements of the machine significantly since they will wear over time. Brushed DC motors are cheap and easy to build and are therefore widely used for everyday appliances. However, when the required power increases, the size of the DC motor could become a problem due to the poor power density of the motor. DC motors have been applied to on various ships, Submarines, ice breakers and military ships have all used the conventional DC motor because of its easy control-ability and low noise characteristics [39].

Induction Motor (IM)

The most commonly used electric motor is the induction ”squirrel cage” motor. The motor is driven by AC current in the stator and has conductive bars on the rotor in a sort of squirrel cage form. The AC current creates a magnetic field and as the conductive bars move trough the field they create a current that then accelerates the motion further, creating a torque. Control is done by applying different frequencies and voltage to the motor so even though the squirrel cage is very simple, it does require a sophisticated control system increases the cost and the size of the system. Advantages of the induction motor are low costs, high reliability due to the lack of commutators and good control-ability, however, the controls do require a variable frequency controller that increases the size and cost of the system. Induction motors are widely used in electric vehicles such as the Tesla Model 3.

Permanent Magnet Motor (PM)

Due to the developments of high powered magnets such as neodymium-iron-boron permanent magnets, it has become possible to create very energy-dense electric motors. The permanent magnets are installed in the rotor with copper windings around the stator to induce current, making it essentially an inside out brushless DC motor. The PM motor can be operated on both AC (BLAC) and DC (BLDC) power however a different control unit will be required. The control of the PM motors is based on at least three-phase currents, either in AC as sinus shapes or in DC as trapezoid shapes, making the control relatively complex. The main advantage of the PM motors is the increased power density and efficiency due to the presence of the magnets, for this reason, PM motors have become widely used in electric vehicles such as the Nissan Leaf, the Chevrolet Bolt and also in heavy electric vehicles such as trains and forklifts [40]. Finally, there is a safety risk associated with large magnets. In case of a malfunction with the control unit the motor will keep turning, and because of the permanent magnets will create a current that can cause acute damage to the wiring and the control unit [39].

The three electric motors that are discussed are summarised in table 2.12. The brushed DC motor is the most applied engine in the maritime industry due to its easy controllability and low cost however it does have the major drawback of relying on maintenance-heavy commutators. The induction motor is the most widely used engine for appliances due to its extremely low cost and simple working principle although the control can become complex when a wide range of speeds and torque is required. The permanent magnet motor is an increasingly popular motor offering high energy densities and efficiencies but it is a costly motor due to the required magnets, furthermore, the magnets create a safety risk and further complications in the design.

	Power Density	**Efficiency**	**Reliability**	**Controllability**	**Cost**	**Advantages**	**Disadvantages**
DC	Low	78%	Low	Very High	Low	Well known technology, Easy to control	High maintenance, Low efficiency
IM	Medium	87%	High	High	Very Low	Cheap to build, Easy to control	Requires complex frequency transformation
PM	High	90%	Medium	Medium	Medium	Very energy dense, High efficiency	Expensive, Safety risks due to magnets

Table 2.12: Comparison of different Electric motors [38]

For smaller ships the power density of the electric motor is less critical then the cost thus the IM and DC are preferred over the PM motors. Unless very high efficiency is required, then the PM engine is the preferred option. Both IM and DC motors are well developed, cheap and have good controllability, however, both options also have disadvantages. Eventually, the choice for electric motor depends on the desired grid (AC or DC) and the inverters and their performance that are required and on design specific considerations.

2.3.6. AC-DC Transformers

A typical performance of electricity transformers is shown in figure 2.19. As can bee seen using below 20% of the rated power should be avoided. This means that charging and discharging at low powers will be avoided when designing the power and energy management systems. Typical efficiency of 0.95 is assumed for the transformers in the system.

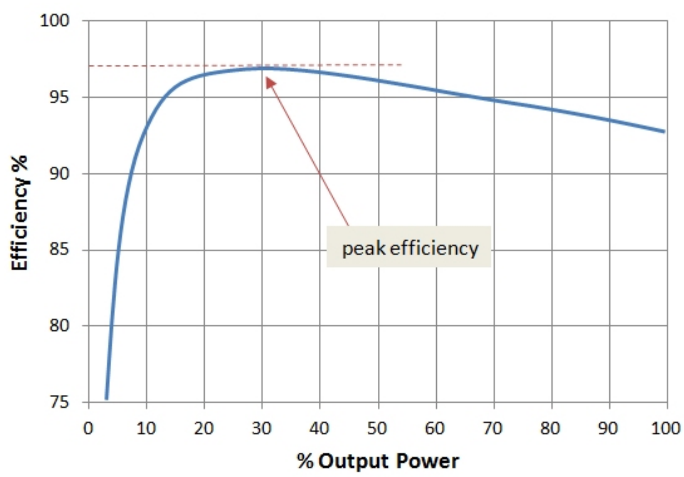

Figure 2.19: Typical efficiency curve for both AC/DC and DC/DC converters [41]

2.3.7. Subsystem Overview

As with the hydrogen production subsystem, a few H2SHIPS related concerns will be taken into account with designing the propulsion subsystem. Since one of the aims of the Port of Amsterdam is to create a circular vessel (excluding the batteries) it is not desired to use permanent rare earth magnet motors for propulsion. The supply chain of recycling PM motors is non-existent and the rare earth magnets used are in short supply. Another important consideration is the reduction of complexity both in control as in the components. The hydrogen supply chain is already a very novel technology and by minimising the complexity in the propulsion system the risk of dangerous malfunctions is decreased. Given these considerations, a commutator (or brushless) DC motor has been selected for the propulsion, the technology is safe and well known in the maritime sector and is easy to control. The AC induction motor is a more efficient option however the complex controls and conversion to an AC grid are considered to be undesirable in the design of this vessel.

Another major concern with the design of a hydrogen vessel is the safety considerations, especially regarding the battery system. Lithium-ion batteries have a large risk on overt heating and this should be taken into account when designing the battery space and cooling system. To reduce the risk however, the decision is made for a less energy-dense but safer battery option of the LFP batteries. These batteries are produced by for example Lithiumwerks and were also used on the electric canal boats in Amsterdam. The high thermal runaway temperature of 270°C and high discharge rate of 25 C will provide the safe and high power performance necessary for the electric motors. The bad performance in energy density will be compensated by the high energy density of the $NaBH_4$ on board.

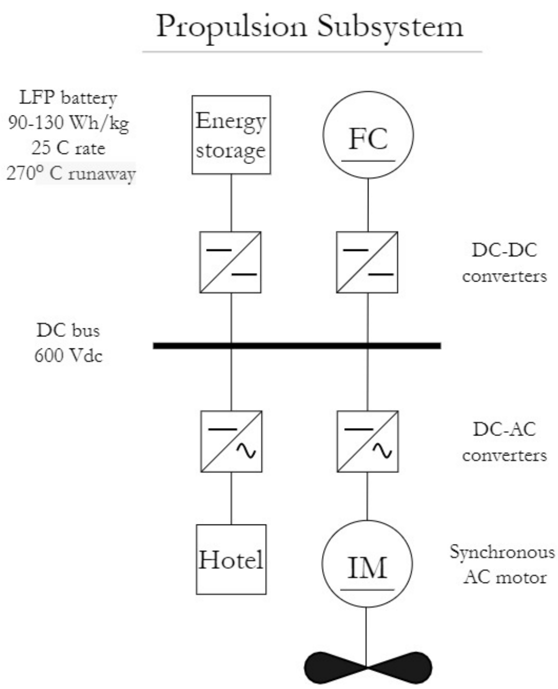

Figure 2.20: A schematic overview of the propulsion subsystem

2.4. Control system

The control system can be divided into several levels as defined by R.D. Geertsma et al. [42] and illustrated in figure 2.21. This particular system design defines three levels of control where the primary control is the actual system settings and communication between components, the secondary control is defined as power management and governs among others the start / stop commands. The Energy Management Strategy system (EMS) is defined as the tertiary level of control and, together with the start-stop control, will be the main focus of this section.

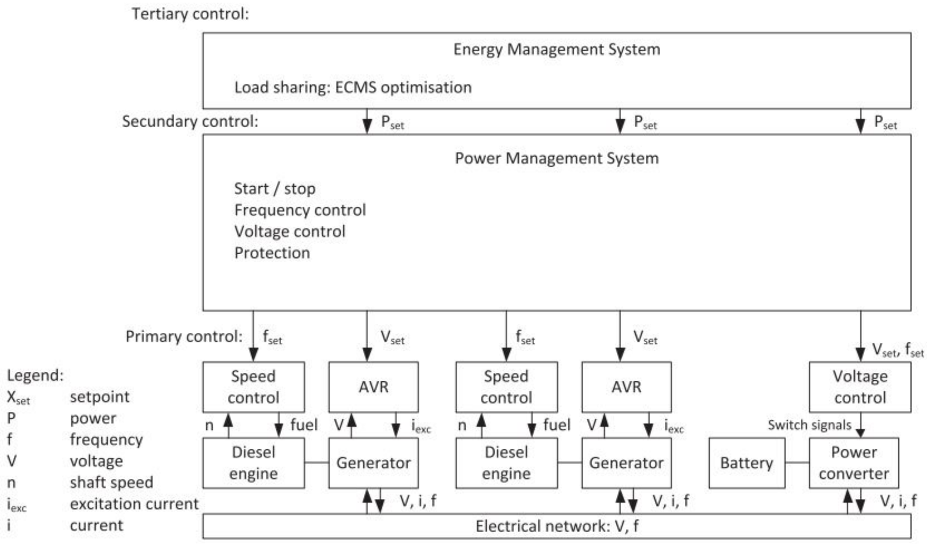

Figure 2.21: A complete control strategy using ECMS as proposed by R.D. Geertsma et al. for a diesel-electric hybrid vessel [42]

2.4.1. Reactor Control

The reactor will provide the hydrogen to the fuel cell and will thus function as a sort of start / stop control for the hydrogen system. The injection timing of $NaBH_4$, the pressure in the tank and the management of spent fuel when the reactor is full will be the most critical components of this control mechanism. There is little information within the literature for these control mechanisms of a catalyst drove $NaBH_4$ hydrogen reactor, so the actual management of these systems will have to be invented and evaluated in chapter 4 and 5 respectively. A starting point is provided however by F. Nievelt in the research thesis before this thesis in [21], where several injection methods where tested and evaluated for an acid catalyst $NaBH_4$ reactor.

2.4.2. Energy Management Strategies

Different energy managements strategies for fuel cell - battery hybrid systems have been proposed in [43], [42] and [44]. In this section, the methods will be briefly discussed so that a suitable method can be selected.

Classic PI control

PI or PID control is widely used for simple control problems due to its simplicity and ease of tuning. In a hybrid system fuel cell - battery system a PI controller is used to sustain a certain battery SOC according to figure 2.22. The PI controller determines the required Battery power to sustain a certain reference SOC, this power is then deducted from the load power, resulting in the fuel cell power. This method is advantageous for prolonging the lifetime of the battery if the reference value is kept at a relative high SOC, preferring to use the fuel cell over the battery as the primary energy source.

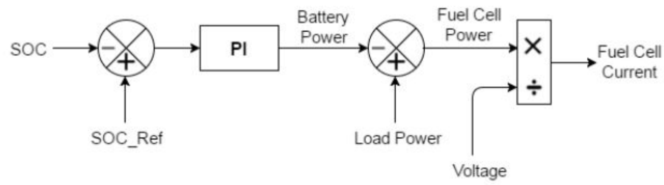

Figure 2.22: Classical PI control strategy scheme [44]

Charge Deplete - Charge Sustain

Charge Deplete - Charge Sustain, or CDCS, is an energy management method that prioritises the use of the battery over the fuel cell. The required power supply is delivered by the battery until a certain SOC threshold is reached. Then the charge sustain mode takes over, using the fuel cell to keep the SOC level until the end of the journey. By prioritising the batteries the consumption of hydrogen is minimised, often leading to a lower operational cost, making it a popular and widely used strategy for hybrid systems.

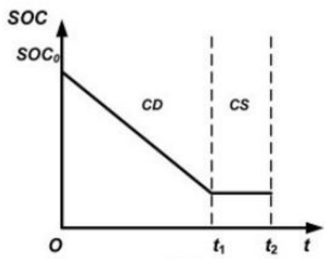

Figure 2.23: Charge Deplete Charge Sustain (CDCS) strategy scheme [43]

Heuristic rule based

State-based, rule-based or sometimes called heuristic control strategy is based on a set of rules that split the load over the battery and fuel cell based on the state of the system to optimise system efficiency. The state-based method often uses SOC and the load as a reference value and determines the output for the fuel cell and battery. An example is given in figure 2.24, where the state is determined on the battery SOC and the load power, the output is the fuel cell reference power and is either minimum, optimal, following the load and or charging, and maximum.

Battery SOC	State	Load Power	Fuel cell reference power
SOC > 80%	1	$P_{\text{load}} \leq P_{\text{FCmin}}$	P_{FCmin}
	2	$P_{\text{load}} \leq P_{\text{FCmin}} + P_{\text{optdis}}$	P_{FCmin}
	3	$P_{\text{load}} \leq P_{\text{FCmax}} + P_{\text{optdis}}$	$P_{\text{FC}} = P_{\text{load}}$ - P_{optdis}
	4	$P_{\text{FCmax}} + P_{\text{optdis}} < P_{\text{load}}$	P_{FCmax}
50% ≤ SOC ≤ 80%	5	$P_{\text{load}} \leq P_{\text{FCmin}}$	P_{FCmin}
	6	$P_{\text{load}} \leq P_{\text{FCopt}}$ - P_{BATopt}	P_{load}
	7	$P_{\text{load}} \leq P_{\text{FCopt}} + P_{\text{BATopt}}$	P_{FCopt}
	8	$P_{\text{load}} \leq P_{\text{FCmax}}$	P_{load}
	9	$P_{\text{load}} > P_{\text{FCmax}}$	P_{FCmax}
SOC < 50%	10	$P_{\text{load}} \leq P_{\text{FCmax}}$ - P_{optchar}	$P_{\text{load}} + P_{\text{optchar}}$
	11	$P_{\text{load}} > P_{\text{FCmax}}$ - P_{optchar}	P_{FCmax}

Figure 2.24: Example of state based strategy scheme [43]

Equivalent Fuel Consumption Minimisation Strategy
Equivalent consumption minimisation strategy, or ECMS, is a real-time optimisation control method that uses an objective function to minimise the equivalent fuel costs. The equivalent fuel cost is based on the idea that using a battery now, will eventually cost hydrogen when the battery needs to be recharged. Thus using battery power has a hydrogen consumption cost, that can be compared with the fuel cell hydrogen consumption cost. The optimal fuel cell power is then determined using an optimisation problem as defined in 2.17 [44]. Moreover, the ECMS strategy uses a penalty coefficient of α, which increases as the SOC drops, thus pushing the system towards a stable SOC level.

$$
\begin{aligned}
\text{Minimise} \quad & C_{FC} \cdot P_{FC} + \alpha \cdot C_{battery} \cdot P_{battery} \\
\text{Constraints} \quad & P_{load} = P_{FC} + P_{battery} \\
& \alpha = 1 - 2\mu \frac{SOC - 0.5(SOC_{max} + SOC_{min})}{SOC_{max} + SOC_{min}} \\
& P_{FC,min} \leq P_{FC} \leq P_{FC,max} \\
& P_{battery,min} \leq P_{battery} \leq P_{battery,max} \\
& 0 \leq a \leq 100 \\
\text{With} \quad & x = [P_{FC}, a, P_{battery}] \forall \quad \mathbb{R}
\end{aligned}
\tag{2.17}
$$

Multi Scheme
The multi scheme strategy was developed for the fuel cell driven passenger ship the FCS Alsterwasser in Germany and tries to combine the best of given strategies to optimise efficiency [43]. The multi scheme contains different strategies and switches between these strategies, choosing a suitable strategy at each instant. In figure 2.25 an example of a multi scheme strategy is shown, differentiating between three distinct power modes and SOC regions. Depending on the state of the system the optimal strategy is chosen to minimise fuel consumption.

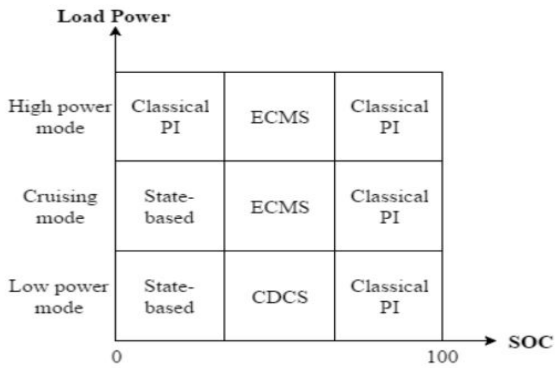

Figure 2.25: FCS Alsterwasser multi scheme strategy [43]

2.4.3. Selection of Strategy

In this section the different strategies will be evaluated based on the expected characteristics of the vessel and three methods will be determined to be analysed in the SIMULINK model. The vessel will have a significant amount of energy storage in the battery system, with the fuel cell functioning as a range extender. When onshore the battery system can be recharged, thus functioning as a so-called plug-in hybrid.

Charge Deplete - Charge Sustain

The vessel will function as a so-called plug-in hybrid with the capability of recharging when onshore, so in essence, any implemented strategy should always be an adaption of the Charge Deplete - Charge Sustain strategy. The method of sustaining the charge, however, is not defined and other strategies will be used to determine a suitable charge sustaining method.

Classic PI control

One method that can be used for charge sustaining is a classical PI control. When implementing, however, an anti wind up mechanism should be considered as well so that the correction factor does not ramp up during the charge deplete section of the cycle. One of the methods to be evaluated will be a PI controller with a reference value of 40% SOC. The implementation of the strategy and the PI settings will be determined in chapter 4.

Heuristic rule based

Rule-based strategies are very flexible in its application and can, therefore, be applied as a form of charge sustain. Based on some basic rules a very effective charge sustain strategy can be realised. Two methods of rule-based strategy will be implemented, as illustrated in table 2.13 and equation 2.18. The second set of rules is inspired by the penalty coefficient as proposed in the ECMS system of [44].

The first strategy is a binary decision, with the fuel cell working at max efficiency between 50-70% SOC and at max power below 50% SOC. The second strategy is more continues with the delivered power ramping up from minimum to maximum between 50-70% SOC.

$$P_{FC}(SOC) = P_{FC,min} + \frac{SOC_{high} - SOC}{SOC_{high} - SOC_{low}} * (P_{FC,max} - P_{FC,min}) \tag{2.18}$$

	Heuristic 1		Heuristic 2	
	Pbatt	**Pfc**	**Pbatt**	**Pfc**
SOC >= 70	Pload	0	Pload	0
50 <SOC <70	Pload - Pfc_min	Pfc_min	Pload - Pfc(SOC)	Pfc(SOC)
SOC <= 50	Pload - Pfc_max	Pfc_max	Pload - Pfc(SOC)	Pfc(SOC)

Table 2.13: Heuristic rules for EMS 1 and EMS 2

Equivalent Fuel Consumption Minimisation Strategy

The ECMS strategy is developed for mild hybrid vehicles that cannot recharge such as plug-in hybrids do. As such the strategy is based on the assumption that the difference between initial and final SOC is very small, with the battery functioning only as an energy buffer, eventually all energy comes from the fuel. This is different from a plug-in system that also recharges and actively consumes part of the batteries energy by design. However, when in Charge sustain mode an ECMS strategy could be applied to efficiently maintain the desired SOC value.

The ECMS is a popular solution in the automotive industry because the results come close to the optimum solution, and thus result in minimum fuel consumption. This becomes especially important when dealing with internal combustion engines where the efficiency depends heavily on the required torque and rpm. However, the binary nature of the cost function results in many start/stop cycles for the engine. This might not be a big problem for gasoline engines that can easily be run on stand-bye, but start/stop cycles and excessive load changing are the main reason for degradation in fuel cells, with 33% being caused by the start/stop cycle [45]. So even though ECMS results come close to optimal fuel consumption it is deemed more important to prioritise fuel cell lifetime over fuel consumption.

Multi Scheme
Multi scheme EMS was found to be very effective for the hydrogen-fueled FC Alsterwasser. However, this vessel was not recharged onshore and thus required the difference between the initial and the final SOC to be very small. This is illustrated by the use of classical PI and state-based at low SOC, designed in such a way that the SOC recovers faster to its desired value.

Furthermore, to implement a multi scheme EMS more information is required on the load profile of the vessel. Since this strategy is not been proven to be effective for a plug-in hybrid system, and because more input is required, it is deemed unsuitable. However, a Multi scheme inspired EMS that also interacts with the captain is recommended for further studies. Such a system could have different modes that influence the control of the system. Resulting for example in full battery-electric operation for silent city tours, or for a range extender mode allowing for more range, depending on the requirements and input from the captain.

Conclusion
The application for the Energy Management Strategy system within this project aims to create a hybrid system with a fuel cell as a range extender. This differs from some application, especially in automotive, where the objective is to maintain a steady SOC value and use hydrogen or other fuels as a single energy source. The strategies that are most suited for this task, such as ECMS and multi scheme, are less suitable for the application as range extender where the batteries can be recharged daily. The best strategy for a plug-in hybrid is a form of Charge sustain - Charge Deplete strategy and three methods of sustaining the charge will be further analysed, two rule-based strategies and one PI controlled strategy:

- EMS1, is a heuristic strategy, the fuel cell runs at max efficiency, starting at SOC<70% taking over the load and charging when possible at SOC<50% the fuel cell runs at max power. Once activated the fuel cell will run for a minimum amount of time to prevent zero crossings at a given SOC value.
- EMS2, is a heuristic strategy, fuel cell runs at max efficiency, starting at SOC<70% taking over the load and charging when possible, then the fuel cell ramps up based on the SOC as seen in equation 2.18 until it reaches max power at SOC<50%. Once activated the fuel cell will run for a minimum amount of time to prevent zero crossings at a given SOC value.
- EMS3, is PI controlled strategy, the system will prioritise the use of the battery until the battery reaches a SOC of 40%, after which a PI controller will try to maintain a 40% SOC of the system.

3

Ship Characteristics

3.1. Case Study: Port of Amsterdam Vessel

To estimate the power requirements necessary for the PoA vessel a reference vessel is chosen to determine some critical parameters such as beam width, draft and displacement. The PoA vessel will be operated in and around the canals of Amsterdam and will be used during tours for important guests of the port. As such, the characteristics in size and operational profile are similar to that of the well-known canal boats of Amsterdam. These vessels will, therefore, serve as a reference for the initial design of the PoA vessel. Finally, some consideration for safety will be given by evaluating the safety concept of the ”FCS Alsterwasser”, one of the first hydrogen hybrid vessels built-in 2007 as part of the ZEMSHIPS project.

3.1.1. Reference Vessel: ”MS Havenbeheer”

The current port vessel of the Port of Amsterdam is called the ”MS Havenbeheer”, this vessel is used to accommodate important guests as well as facilitating work visits around the port area. The new build vessel will be a slightly enlarged version of the current vessel, therefore analysing the current vessels characteristics will give good insights into the characteristics of the new build. The characteristics can be found in table 3.1 and are obtained from the official inland vessel measurements provided in appendix A. The length and beam at the waterline, however, are estimated and the propeller diameter was requested from the Port of Amsterdam.

	Disp.	Loa	Lwl	Boa	Bwl	T	Taft	Cb	D_p	Power
Light ship	30.778 m^3	16.75 m	16.3 m	3.8 m	3.5 m	0.76 m	0.49 m	0.85	0.76 m	138 kW
Dead weight	35.547 m^3	16.75 m	16.3 m	3.8 m	3.5 m	0.86 m	0.59 m	0.73	0.76 m	138 kW

Table 3.1: The characteristics of the current PoA vessel

Figure 3.1: Reference vessel the ”MS Havenbeheer” [46]

The reference vessel will be used to evaluate the results of the parametric design and power requirements from section 3.1.3 and 3.2 respectively. Based on the requirements from PoA, the reference vessel and the Parametric design a good estimation can be made of the power requirements and efficiencies of the vessel.

3.1.2. Port of Amsterdam Design Requirements

This section will evaluate the Port of Amsterdam requirements for the new vessel resulting in main dimensions and three design speeds. This information is then used to evaluate and determine the parameters necessary for calculating the resistance.

Main Dimensions

The main dimensions of the PoA vessel are limited by the Amsterdam canals and regulations on passenger ships. The length of the vessel is limited by regulations at 19.99 metres. The beam is limited to 4.15 metres due to the width of the canals and bridges in the Amsterdam canals. The height is also limited by bridges at 1.90 meters and the draught of the vessel should be limited to 1.50 metres. Furthermore, the headroom should be 2.00 metres if possible. The draft, propeller diameter and block coefficient are considered to be the same for the new build, resulting in the characteristics as shown in table 3.2. The required power for the new build vessel is still unknown and will be the result of the calculations in this chapter.

	Disp.	Loa	Lwl	Boa	Bwl	T	Taft	Cb	D_p	Power
Current PoA vessel	35.547 m^3	16.75 m	16.3 m	3.80 m	3.5 m	0.86 m	0.59 m	0.73	0.76 m	138 kW
New PoA vessel	48.901 m^3	20.00 m	19.5 m	4.15 m	4.0 m	0.86 m	0.59 m	0.73	0.76 m	- kW

Table 3.2: The characteristics of the new PoA vessel

Design speed and Froude number

The design speeds of the PoA vessel depends on where it is sailing. In the canals of Amsterdam, the vessel is limited to 6 km/h and in the harbour area the cruising speed is around 12 km/h, the max speed is 15 km/h. The Froude number is used for the relative speed of the vessel and plays a major role in the wave resistance of the vessel. The Froude number is defined in equation 3.1 and depends on the speed of the vessel in m/s, the gravimetric constant and the length of the waterline (LWL). The PoA vessel is limited in length at 20 meters overall so the length over the waterline is assumed at 19 meters. The resulting Froude numbers and design speeds are shown in 3.3, for the design parameters the harbour cruising speed will be used as reference speed.

$$Fn = \frac{V_{design}}{\sqrt{g * LWL}} \tag{3.1}$$

	V canal	**V cruise**	**V max**
km/u	6	12	15
m/s	1.7	3.3	4.2
knts	3.2	6.5	8.1
Fn	0.12	0.24	0.31

Table 3.3: Design speeds of PoA vessel

3.1.3. Parametric Evaluation and Estimation

The parametric design focuses on the statistical analysis and first-order principles of build ships and as such are based on empirical relations that are highly dependant of the data set used, as a result, many different approaches and formulas exist. Micheal G. parsons have done a great job in summarising different methods in the chapter parametric design of the book ”Ship design a construction vol. 1-2” and he remarks that although most methods are outdated, Schneekluth and Bertram, and Watson and Gilfillan are excellently updated and general approaches [47]. This section will evaluate and estimate the parameters required for calculating the resistance of the vessel.

Block Coefficient C_b

The block coefficient measures the fullness of the submerged hull and affects the resistance and wetted surface area of the vessel. Early in the design process, the C_b can be estimated based on the Froude number of the vessel at design speed. The Watson and Gilfillan (W & G) line as seen in 3.2 coincides with the Jensen line and is recommended as best practice in Germany, with a $\pm$ of 0.025. According

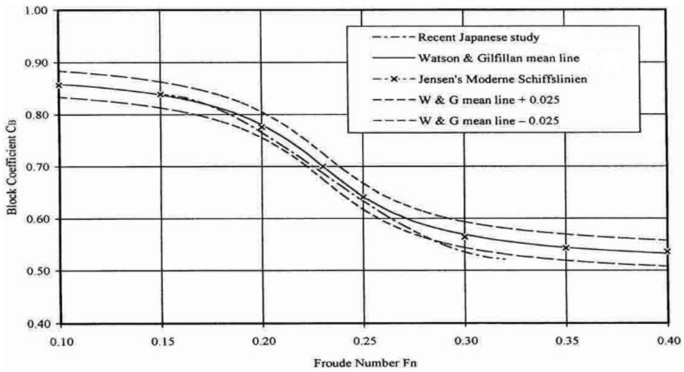

Figure 3.2: Recommended C_b based on Froude number according to Parsons [47]

to Parson, a more recent Japanese study showed some lower results for ships with a higher Froude number however still within the W & G range.

The methods described in figure 3.2 are mostly used for merchant ships with heavy displacement hulls. Telfer analysed series 60 hull data that match more closely with the light displacement hull of a canal cruiser. Parson examined the resistance per tonne of Telfer's analysis and concluded that the optimal block efficient for minimal resistance is defined by equation 3.2 with speed in knots and length in feet. Resulting in a C_b of 0.61.

$$C_b = 1.18 - 0.69\frac{V_{kts}}{\sqrt{L_{ft}}} \tag{3.2}$$

The current PoA vessel has a block coefficient of 0.73 which is in the W & G range for lower Froude numbers but at higher speeds, the block coefficient seems too high. Also when comparing to the Telfer's optimal block coefficient of 0.61 at full speed the PoA vessels C_b seems high. The new vessel is assumed to have the same block coefficient as the current vessel, however, the vessel might become more efficient if the vessel can be designed with a lower C_b.

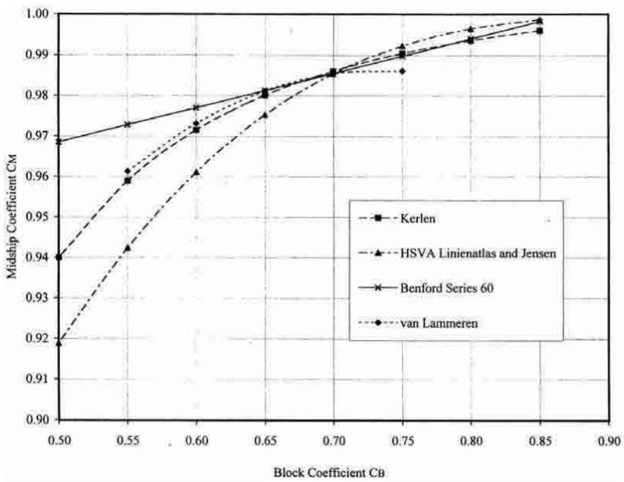

Figure 3.3: Different methods for midship area calculations, the HSVA method is recommended as best practice in Germany [47]

Midship and Prismatic Coefficient

The midship coefficient determines how full the midship, or maximum section, is and the prismatic coefficient determines the fullness of the ship. They are both related to the block coefficient with equation 3.3. In figure 3.3 from Parsons four methods of C_m calculation is shown. The HSVA method is recommended as best practice in Germany according to Jensen and is calculated using equation . This results in a C_m of 0.96 and a C_p of 0.64.

$$C_b = C_p C_m \tag{3.3}$$

$$C_m = \frac{1}{1 + (1 - C_b)^{3.5}} \tag{3.4}$$

Length - Beam Ratio
The L/B ratio of the vessel is predetermined by the Port of Amsterdam requirements. The PoA requires the vessel to be just under 20 meters due to regulations regarding the crew, the Loa will be lower and is assumed at 19.5 meters. Furthermore, the PoA requires a width of 4.25 meters however around the waterline, however, this will also be lower around the waterline and is assumed at 4.00 meters, resulting in an L/B of 4.75. Watson en Gilifan recommend an L/B of 4 for ships below 30 meters up to 6.5 for merchant ships of 130 meters, so 4.75 is within the range of nominal values.

Beam - Draft Ratio
The canals of Amsterdam form a limitation for the draft of the vessel. Including propeller, the draft is limited to 1.45 meters so a high B/T ratio is required to meet this limitation. According to Parson typical values for B/T range from 2.25 to 3.75 although higher values of up to 5 are found. The new PoA vessel will have a B/T of 4.65, A bit higher then is normally found. However, this is to be expected for a draft limited vessel such as a canal cruiser.

Waterplane Coefficient
The waterplane coefficient can be determined early in the design when C_p is known and with some basic understanding of the hull form a good estimation of the waterplane coefficient can be made. Different type of sterns are of importance and the V shape hulls versus the U shaped hulls are important. V-shaped hulls give better sea keeping abilities and U shaped hulls give better calm water abilities. Since the PoA vessel will mostly operate on inland waters a U shaped hull is very logical, the waterplane coefficient can then be estimated using equation 3.5 resulting in a C_{wp} of 0.73 with a waterplane area of 5.55 m^2.

$$C_{wp} = 0.95C_p + 0.17(1 - C_p)^{\frac{1}{3}} \tag{3.5}$$

$$C_{wp} = \frac{A_{wp}}{L_{wl}B_{wl}} \tag{3.6}$$

Wetted Surface Area
The wetted surface area S_w is a crucial parameter in determining the frictional resistance of a vessel. Holtrop and Mennen tested extensively in 1978 and created equation 3.7 based on the form coefficients [48]. Using the parameters determined so far the wetted surface is estimated at 65.42 m^2.

$$S_w = L_{wl}(2TB_{wl})\sqrt{C_m}(0.453 + 0.4425C_b - 0.2862C_m - 0.003467\frac{Bwl}{T} + 0.369C_{wp}) \tag{3.7}$$

$$S_w = 1.025(\frac{\nabla}{T} + 1.7L_{pp}T) \tag{3.8}$$

An alternative method by Mumford uses equation 3.8 resulting in a wetted surface of 65.47 m^2, which is nearly identical to the method proposed by Holtrop and Mennen. The wetted surface area used for calculations will be 65.4m^2 and can be found in table 3.4.

Longitudinal Centre of Buoyancy
The longitudinal centre of buoyancy is necessary for some resistance calculation and to check the design process. However, this parameter can and will change through the design process, for this reason, Benford defined an acceptable bandwidth for the LCB position shown in 3.4. Harvald recommends the best possible LCB as a function of the Froude number with equation 3.9, for the PoA vessel this leads to an LCB of -1.0% Lwl from midship, or 9.7m from the front perpendicular.

$$LCB = 9.7 - 45.0Fn \pm 0.8 \tag{3.9}$$

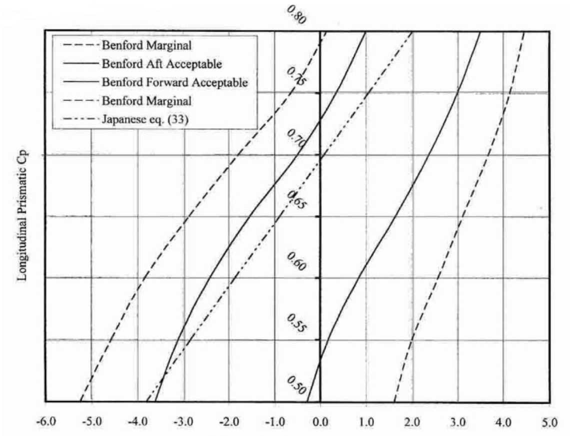

Figure 3.4: Benfords recommended design lane for the longitudinal centre of buoyancy LCB [47]

The parameters determined and estimated in this section for the PoA vessel based on some design limitations are summarised in table 3.4. These parameters will prove useful for resistance calculations and hull efficiency leading to an estimation for the required installed power for the PoA vessel. Two things are most notable about these parameters, first, the length displacement ratio is unusually and the B/T ratio is very high. This means that the ship design is quite different from traditional designs, yet this is to be expected considering that the vessel is a very lightweight cruiser, with a low height and small draft, specifically designed to include tours in the Amsterdam canals.

	L/B	B/T	C_b	C_m	C_p	C_{wl}	A_{wp}	S_w	LCB
Current PoA vessel	4.66	4.07	0.73	0.99	0.74	0.81	46 m2	65.5 m2	-1.0%
New PoA vessel	4.88	4.65	0.73	0.99	0.74	0.81	63 m2	86.0 m2	-1.0%

Table 3.4: Parametric design for the PoA vessel

3.1.4. Appendages

Several appendages are necessary for the PoA vessel and these will be determined in this section such as the Propeller diameter, the rudder options and the skeg area.

Propeller diameter
Starting with the propeller. Although a ducted propeller could be chosen to increase efficiency, for now, a conventional propeller is assumed. In general, a propeller becomes more efficient when increasing the diameter however due to the operating area of the Amsterdam canals, the PoA vessel is restricted in propeller diameter by its maximum draft. Therefore it is assumed that the new vessel will have the same propeller diameter as the current vessel of 0.76 meters.

Rudder
Conventionally a ship requires a rudder for steering. However, by using electric motors the conventional drive shaft can be replaced by podded motors such as azimuth thruster. These thrusters can rotate around their axis giving the ability to steer. This will reduce resistance since it reduces the wetted surface of the vessel and will increase the steerability of the vessel. It is therefore likely to assume that instead of a rudder, an azimuth thruster will be utilised on the PoA vessel.

Skeg
Due to the flat bottom design of a canal cruise and lacking a keel or fin, it is likely to assume that a small skeg will be used to both protect the propeller from debris found in the canals as well as provide some directional stability. An example can be seen in the H2 Nemo vessel design in figure 3.5. Assuming the height of 1 meter from the D_p, and a length of 3 meters, a wetted surface area of 3 m^2 is assumed. The surface area of the supportive struts is neglected due to their small size.

Figure 3.5: The propeller and skeg of the H2 Nemo vessel [49]

3.2. Resistance and propulsion

To estimate the power and energy requirements for the propulsion of the PoA vessel, first, the resistance and efficiencies need to be determined for different speeds. The resistance will be estimated using the parameters determined in section 3.1 using empirical resistance models based on systematic hull testing. Then an estimation for the hull efficiency will be made using an appropriate method. The open water efficiency is determined by selecting a propeller from the Wageningen B series [50]. Finally, other losses such as the conversion and electric engine losses are considered and an estimation for the resistance based on vessel speed is made.

3.2.1. Resistance

The ITTC 1957 method of the international towing tank committee (ITTC) recommends using equation 3.10 for the calculation of resistance where: R_T is the total resistance, ρ is the density of water, S_w is the wetted surface area and V is the design speed. Furthermore: C_T is the total resistance coefficient, C_F is the frictional resistance coefficient based on the ITTC method, C_A is the incremental resistance coefficient, or model-ship correlation factor, and is related to the difference in roughness between the model and the actual ship, C_{AA} is the air resistance coefficient and C_R is the residual coefficient usually based on model testing. However, usually, there is no model available to test and equation 3.11 is used. With R_F being the frictional resistance based on the method proposed by ITTC, using C_F and C_A and the surface area, and R_F being the residual resistance estimated using a statistical model based on systematic testing of hull forms.

$$C_T = C_F + C_A + C_{AA} + C_R = \frac{R_T}{0.5\rho S_w V_s^2} \tag{3.10}$$

$$R_T = R_F(1+k) + R_{APP} + R_W + R_A \tag{3.11}$$

Systematic hull models

Many different models have been developed based on various testing series, these methods and their limitations are summarised in table 3.5. Delft systematic Yacht Series has been developed and is based on yacht hulls, this is reflected in the low C_m and C_p ranges. Harvald developed a fast calculation requiring little input, however, the range is very limited and not applicable to the PoA vessel due to its high B/T value. Hollenbach comes close however the length displacement ratio is too high. The barge model is sufficient in terms of B/T, however, the C_b is not compliant. Of all the examined methods the Holtrop and Mennen method seems to be the most appropriate. The method was developed using 191 models tested up to a maximum Froude number of Fn=0.45, and thus applicable to the PoA vessel. The Holtrop and Mennen estimation are valid for seawater so the resistance might be estimated slightly higher than is the case.

Method	L/displ	L/B	B/T	Cp	Cm	Cb	Extra remarks
DSYS	4.3-8.5	2.7-5.9	Na	0.52-0.60	0.65-0.79	Na	Focuses on sailing yachts with low Cp values
Harvald	4.0-8.0	Na	Na	0.50-0.80	Na	Na	Requires little input but works for a limited range
Hollenbach	4.5-6.0	4.7-7.1	2-6.1	Na	Na	0.51-0.83	Can be used for double screw ships
British Columbia	Na	2.0-4.5	1.5-3.5	Na	Na	0.53-0.61	Only applicable for small vessel with Fn <0.5
Holtrop & Mennen	Na	3.5-9.5	Na	0.40-0.93	0.5-1.0	Na	For displacemt vessels
Oortmerssen	Na	3.0-6.5	1.9-4.0	0.50-0.73	0.72-0.97	Na	Only applicable for small vessel with Fn <0.5
Barge	Na	2.3-8.0	<10	0.7-1	Na	Na	Applicable to barges with Fn<0.6
PoA vessel	2.9	4.75	7.4	0.64	0.96	0.61	Holtrop and Mennen is compatible

Table 3.5: Ranges for different resistance models from the PIAS manual [51]

Frictional resistance coefficient

The frictional resistance is defined with equation 3.12 where C_F is the friction factor as defined by the 1957 ITTC formulation and the C_A is the model ship correlation factor, calculated according to Holtrop and Mennen at C_A=0.0026. (1+k) is a form factor that can be determined using equation 3.13, equation 3.15 with a C_{stern} value of +10 for U shaped Hogner sterns and equation 3.14 for 0.02 < T/L < 0.05 (T/L is 0.028). Finally L_R is the length of run which can be determined by equation 3.16.

$$R_F = 0.5\rho S_w V_s^2 (C_F(1+k) + C_A) \tag{3.12}$$

$$(1+k) = c_{13}(0.93 + c_{12}(B/L_R)^{0.92497}(0.95 - C_p^{-0.52145})(1 - C_p + 0.0225LCB)^{0.69060}) \tag{3.13}$$

$$c_{12} = \begin{cases} (T/L)^{0.2228446}, & \text{when } (T/L) > 0.05 \\ 48.20((T/L) - 0.02)^{2.078} + 0.479948, & \text{when } 0.02 < (T/L) < 0.05 \\ 0.479948, & \text{when } (T/L) < 0.02 \end{cases} \tag{3.14}$$

$$c_{13} = 1 + 0.003C_{stern} \tag{3.15}$$

$$\frac{L_r}{L} = 1 - C_p + \frac{0.06C_pLCB}{4C_p - 1} \tag{3.16}$$

The friction factor C_F can be determined according to the ITTC method using equation 3.17, with the Reynolds number as defined in equation 3.18 and with υ as the kinematic viscosity of water with an value of $1.19 \cdot 10^{-6}$ m^2/s at 15°C.

$$C_F = \frac{0.075}{(log(R_n) - 2)^2} \tag{3.17}$$

$$Rn = \frac{V_s L_{wl}}{\upsilon} \tag{3.18}$$

Frictional resistance appendages

The appendages also cause a frictional resistance component based on the surface area, a form factor as defined in 3.6 and the friction factor C_F following equation 3.19. Since the skeg used is very narrow the minimum form factor of 1.5 is assumed.

$$R_{APP} = 0.5\rho V_s^2 S_{APP}(1 + k_2)C_F \tag{3.19}$$

Wave Resistance Coefficient

The residual resistance is calculated per displacement tonnes Δ and can be calculated using equation 3.20, with the variables defined in equations 3.22, 3.24, 3.25, and the half angle of entrance i_E that can be determined using equation 3.26.

$$R_w/\Delta = Ce^{m_1 Fn^{-0.9} + m_2 cos(\lambda Fn^{-2})} \tag{3.20}$$

$$C = 2223105(B/L)^{3.78613}(T/B)^{1.07961}(90 - i_E)^{1.37565} \tag{3.21}$$

$$m_1 = 0.0140407(L/T) - 1.75254(\Delta^{1/3}/L) - 4.79323(B/L) - c_{16} \tag{3.22}$$

Approximate $1+k_2$ values	
Rudder behind skeg	1.5-2.0
Rudder behind stern	1.3-1.5
Twin-screw balance rudder	2.8
Shaft brackets	3.0
Skeg	1.5-2.0
Strut bossings	3.0
Hull bossings	2.0
Shafts	2.0-4.0
Stabiliser fins	2.8
Dome	2.7
Bilge keels	1.4

Table 3.6: $1+k_2$ values from Holtrop and Mennen [48]

$$c_{12} = \begin{cases} 8.07981C_p + 13.8673C_p^2 - 6.984389C_p^3, & \text{when } C_p < 0.80 \\ 1.73014 - 0.7067C_p, & \text{when } C_p > 0.80 \end{cases} \tag{3.23}$$

$$m_2 = -1.69385C_p^2 e^{-0.1/Fn^2} \tag{3.24}$$

$$\lambda = \begin{cases} 1.446C_p - 0.03(L/B), & \text{when } (L/B) < 12 \\ 1.446C_p - 0.36, & \text{when } (L/B) > 12 \end{cases} \tag{3.25}$$

$$i_E = 125.67(B/L) - 162.25C_p^2 + 234.32C_p^3 + 0.155087LCB^3 \tag{3.26}$$

Total Resistance

Adding the frictional and the residual resistance as determined by the Holtrop and Mennen method, leads to the resistance curve as seen in figure 3.6. The "humps" and "hollows" in the wave resistance part can be explained by the interaction between the waves and the hull length. At the design speed of 12 km/h, there is a small drop trough one of these "hollows" indicating better performance.

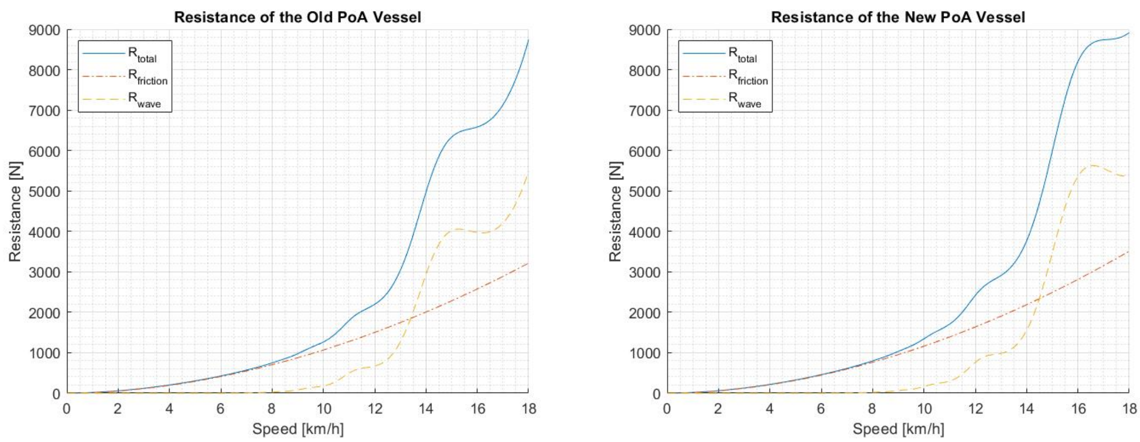

Figure 3.6: Ship resistance based on the Holtrop and Mennen method

3.2.2. Propulsion factors

The propulsion factors can also be determined using the Holtrop and Mennen method and can be used to estimate the hull efficiency of the vessel.

Effective Wake Fraction

The effective wake fraction is the effect of the viscous layer below the bottom of the vessel due to friction. The water speed at the propeller, V_A, is slowed down due to this friction according to equation 3.27 with the effective wake factor w. the wake factor can be determined using equation 3.28.

$$V_A = (1 - w)V_s \tag{3.27}$$

$$w = c_9 C_V \frac{L}{T_{aft}}(0.0661875 + 1.21756 c_{11} \frac{C_V}{1 - C_{P1}} + 0.24558 \sqrt{\frac{B}{L(1 - C_{P1})}} - \frac{0.09726}{0.95 - C_P} + \frac{0.11434}{0.95 - C_B} + 0.75 C_{stern} C_V + 0.002 C_{stern} \tag{3.28}$$

The constant that are not already known can be determined using equations 3.30, 3.31, 3.32, 3.33 and table 3.7.

$$c_8 = \begin{cases} \frac{B S_w}{L D_p T_{aft}}, & \text{when } (B/T_{aft}) < 5 \\ \frac{S_w(7(B/T_{aft}) - 25)}{L D_p((B/T_{aft}) - 3)}, & \text{when } (B/T_{aft}) > 5 \end{cases} \tag{3.29}$$

$$c_9 = \begin{cases} c_8, & \text{when } c_8 < 28 \\ 32 - \frac{16}{c_8 - 24}, & \text{when } c_8 > 28 \end{cases} \tag{3.30}$$

$$c_{11} = \begin{cases} T_{aft}/D_p, & \text{when } T_{aft}/D_p < 2 \\ 0.083333(T_{aft}/D_p)^3 + 1.333, & \text{when } T_{aft}/D_p > 2 \end{cases} \tag{3.31}$$

$$C_v = (1 + k)C_F + C_A \tag{3.32}$$

$$C_{P1} = 1.45 * C_P - 0.315 - 0.0225 LCB \tag{3.33}$$

Thrust deduction factor

When the propeller delivers thrust, the flow speed of the water below the hull is accelerated and thus the pressure of the flow just before the propeller drops. This means that more power is necessary then measured in the tank tests, this effect is accounted for using the thrust deduction factor following equation 3.34. According to Holtrop and Mennen the thrust deduction factor t can be estimated using equation 3.35 with the known constants and equation 3.36 for L/B < 5.2.

$$R = T_p(1 - t) \tag{3.34}$$

$$t = 0.001979 \frac{L}{B - B C_{P1}} + 1.0585 c_{10} - \frac{0.00524 - 0.1418 D^2}{BT} + 0.0015 C_{stern} \tag{3.35}$$

$$c_{10} = \begin{cases} B/L, & \text{when } L/B > 5.2 \\ 0.25 - \frac{0.003328402}{(B/L) - 0.134615385} & \text{when } L/B < 5.2 \end{cases} \tag{3.36}$$

Hull efficiency
Using the effective wake factor and the thrust deduction factor the hull efficiency can be determined according to equation 3.37, the results and the factors necessary to determine the constants can be found in table 3.7. The effective wake factor and thus the hull efficiency is slightly dependant on the viscous resistance and therefore on the vessels speed, however, the difference was deemed so small that a mean average is determined as a good estimation. Finally, for a conventional propeller, the relative-rotative efficiency should also be included and is usually estimated to be around 98%.

$$\eta_{hull} = \frac{1-t}{1-w} \tag{3.37}$$

	B/T_{aft}	C_8	T_{aft}/D	L/B	t	w	η_{hull}	$\eta_{rotation}$
Current PoA Vessel	5.93	29.78	0.78	4.66	0.24	0.38	1.23	0.98
New PoA Vessel	6.78	34.46	0.78	4.88	0.24	0.43	1.30	0.98

Table 3.7: Prediction of propulsion factors in PoA vessel.

3.2.3. Open water efficiency

In order to evaluate the propeller performance the open water efficiency is often used as defined in equation 3.38. Using the thrust factor K_T as defined in 3.40, the torque factor K_Q as defined in equation 3.43 and the advance ratio J as defined in equation 3.39.

$$\eta_{open} = \frac{J}{2\pi}\frac{K_T}{K_Q} \tag{3.38}$$

$$J = \frac{V_a}{n_p D_p} \tag{3.39}$$

$$K_T = \frac{T_p}{\rho n_p^2 D_p^4} \tag{3.40}$$

$$K_Q = \frac{Q}{\rho n_p^2 D_p^5} \tag{3.41}$$

Using these factor an open water diagram can be drawn as seen in figure 3.7. By defining the ship's thrust factor $K_{T,\,ship}$ as done in equation 3.52, the working point of the propeller can be determined with its corresponding efficiency. In this section different propellers will be modelled using the Wageningen B series and the optimal propeller will be chosen to determine the open water efficiency of the PoA vessel.

Wageningen B series
In 1974 M. Oosterveld and P. van Oossanen extensively tested a wide range of propellers and by using a linear regression method defined an empirical formula that describes the thrust and torque factors based on the advance ratio J, the pitch over diameter ratio (P/D), the effective blade area ratio (A_E/A_O) and the number of blades z. The factors can be determined using equation 3.42 and 3.43 where C is an extensive matrix containing the constants obtained by the analysis and can be found in their original work [50]. The result is an extensive polynomial that is implemented using Matlab to obtain specific open water diagrams, an example is given in figure 3.7 for the Wageningen B5-75 propeller.

$$K_T = \sum_{s,t,u,v} C^T_{s,t,u,v}\, J^s\, (P/D)^t\, (A_E/A_O)^u\, z^v \tag{3.42}$$

$$K_Q = \sum_{s,t,u,v} C^Q_{s,t,u,v}\, J^s\, (P/D)^t\, (A_E/A_O)^u\, z^v \tag{3.43}$$

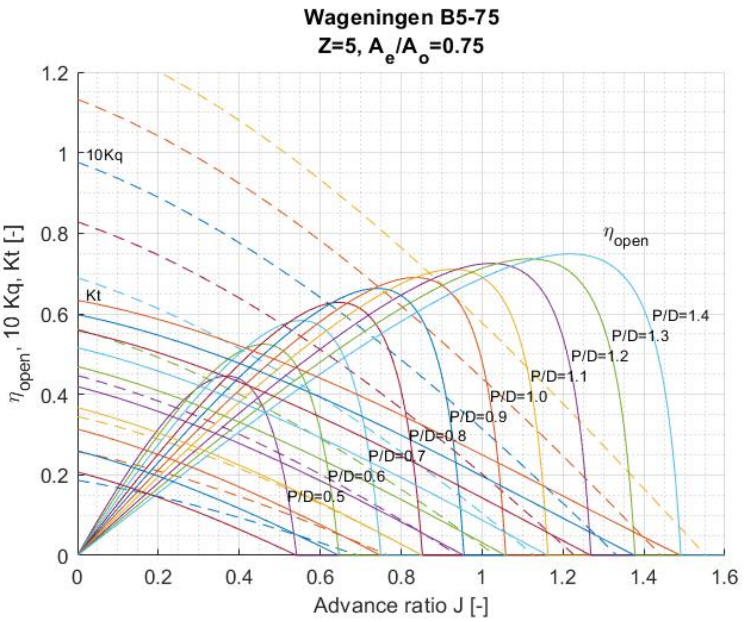

Figure 3.7: Typical open water diagram for a 5 bladed propeller from the Wageningen B series

The Wageningen B series is valid between the ranges for: (P/D)=0.5:1.4, (A_E/A_O)=0.3:1.05 and z=2:7. Other empirical methods based on tests are available such as the Gawn series and the AU series, however, the ranges and number of test samples are very limited so the Wageningen B series remains the most complete method and is, therefore, the preferred option.

Correction factors

The Wageningen series as tested in [50] is only valid for a Reynolds number of $2 \cdot 10^6$ and needs to be corrected for the specific Reynolds number and the roughness of the actual propeller. Holtrop and Mennen propose equations 3.44 and 3.45 in order to estimate the correction factor based on the ITTC-1978 method. Where Δ C_D is the difference in drag coefficient, P is the pitch, $c_{0.75}$ is the chord length at 0.75 percent, (t/c) is the thickness-chordlength ratio and k_p is the roughness factor estimated at 0.00003 for new build propellers. C_D, $c_{0.75}$ and (t/c) can be estimated using equations 3.46, 3.47 and 3.48 respectively [48].

$$K_{T-ship} = K_{T-B-series} + \Delta C_D 0.3 \frac{P c_{0.75} z}{D_p^2} \tag{3.44}$$

$$K_{Q-ship} = K_{Q-B-series} + \Delta C_D 0.25 \frac{c_{0.75} z}{D_p^2} \tag{3.45}$$

$$\Delta C_D = (2 + 4(t/c)_{0.75})(0.003605 - (1.89 + 1.62 log(c_{0.75}/k_p))^{-2.5}) \tag{3.46}$$

$$c_{0.75} = \frac{2.073(A_E/A_O)D_p}{z} \tag{3.47}$$

$$(t/c)_{0.75} = \frac{(0.0185 - 0.00125z)D_p}{c_{0.75}} \tag{3.48}$$

Cavitation
Besides efficiency, cavitation behaviour should also be taken into account. To find the minimum blade area ratio the Kellers formula is used as shown in 3.49. Where T_p is the propeller thrust, K is the 0.2 for single-screw ships and seawater at 15°C equation 3.50 can be used. In table 3.8 the minimum effective area ratio is given for the PoA vessel at 15 km/has a function of different blade numbers.

$$A_E/A_O = K + \frac{(1.3+0.3z)T_p}{D_p^2(p_0+\rho g h - p_v)} \tag{3.49}$$

$$\rho_0 - \rho_v = 99047 N/m^2 \tag{3.50}$$

	z=2	z=3	z=4	z=5	z=6	z=7
$A_E/A_{O min}$	0.56	0.62	0.68	0.73	0.79	0.85

Table 3.8: A_E/A_O ratio to prevent cavitation according to Kellers formula for the PoA vessel at 15 km/h

$K_{T,ship}$
In order to find the operating point of the propeller the $K_{T,ship}$ curve needs to be determined as a function of J, where the $K_{T,ship}$ curve intersects the $K_{T,p}$ curve is the operating point. The $K_{T,ship}$ is defined using the c_7 variable as defined in equation 3.51 and 3.52. For the PoA vessel three $K_{T,ship}$ curves are defined for the three design speeds of 6 km/h, 12 km/h and 15 km/h.

$$c7 = \frac{T_s}{\rho V_a^2 D_p^2} \tag{3.51}$$

$$K_{T,ship} = c_7 J^2 \tag{3.52}$$

Matching
The three $K_{T, ship}$ curves are plotted for all propeller types as tested in the Wageningen B series, taking in account the effective area limitation as defined by Keller's formula and the correction factor as defined bu Holtrop and Mennen. Then the efficiency at the three operating points was evaluated and optimised for the combined highest efficiency. In figure 3.8 the optimal configuration for each blade number is shown including the open water efficiencies.

Propeller selection
Figure 3.8 shows that the worst-performing propeller is the three-bladed propeller. The 2,3 and 7 bladed propellers scored average and the two best performing propellers are the 5 and 6 bladed propellers. Between these two the 5 bladed propellers performed better for the 12 km/h load and are therefore preferred since the energy efficiency becomes more important at high loads. Based on this conclusion, the B5-75 propeller with a P/D of 0.8 is selected for the modelling of the PoA vessel.

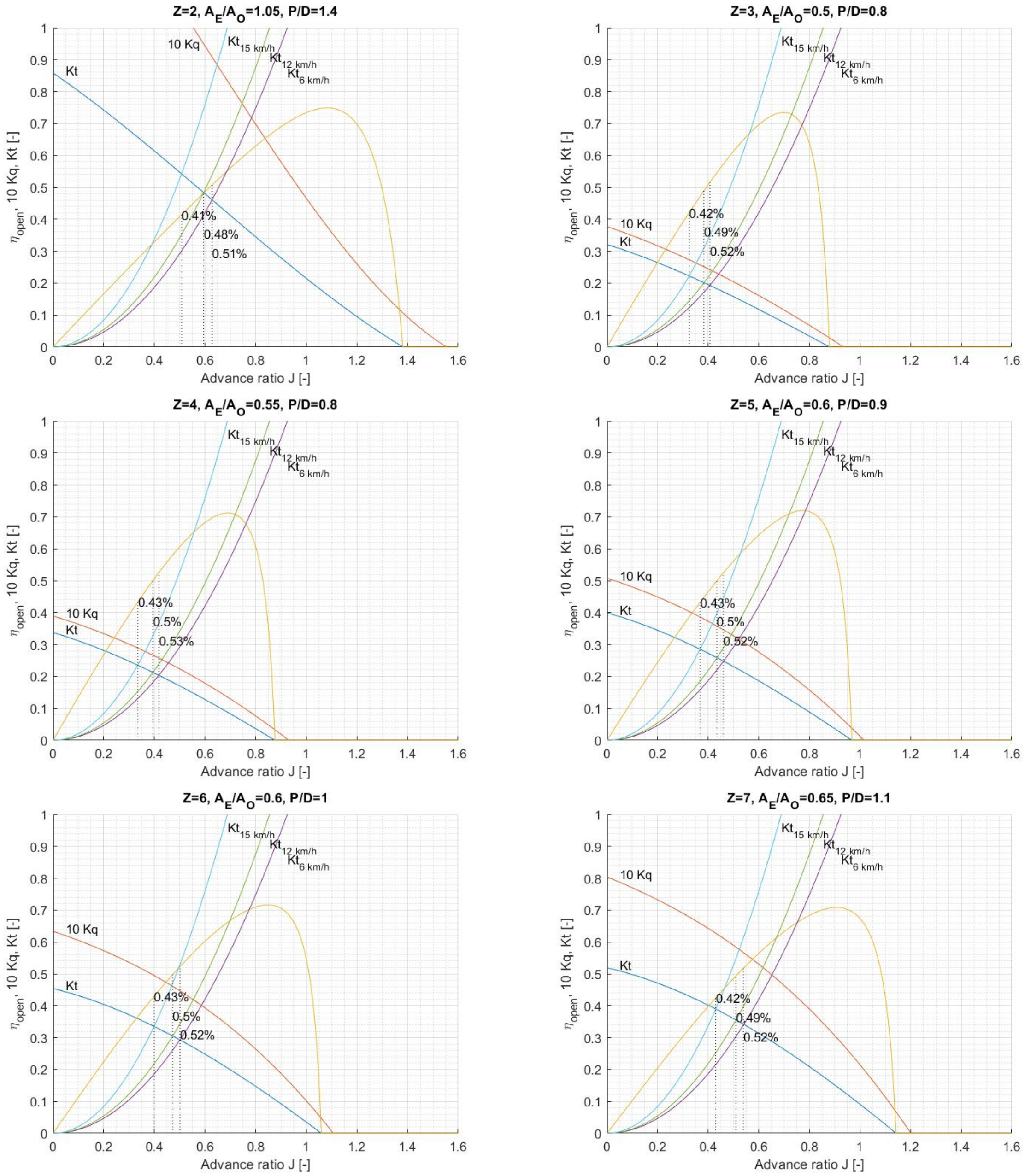

Figure 3.8: Optimal Wageningen B series propellers for the three working points of the PoA vessel

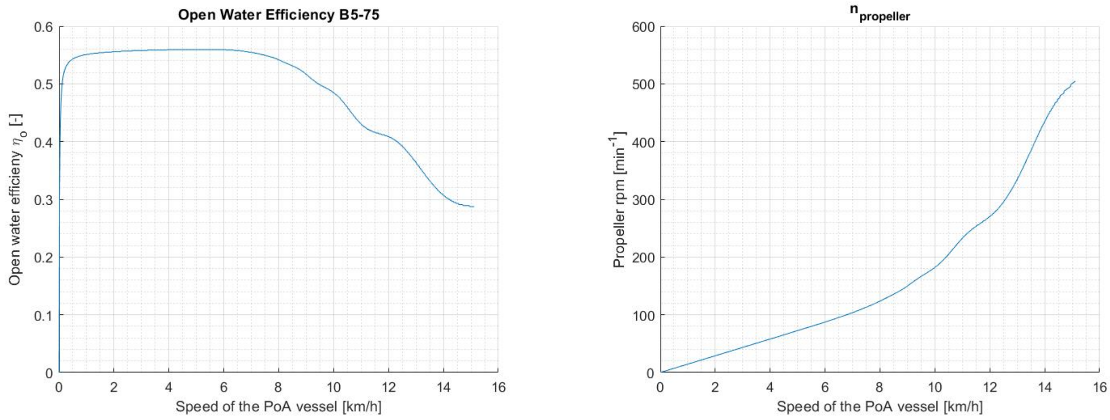

Figure 3.9: The open water efficiency and propeller rpm of the B5-75 propeller for he PoA vessel, as function of the vessel speed

In figure 3.9 the propeller performance is evaluated. By defining a wide range of c_7 variables for different loads according to the method described in 3.51, the open water efficiency could be plotted against the vessels speed. Also, the rpm of the propeller is evaluated using the obtained J values for different speeds and applying equation 3.53.

$$n_p = \frac{V_a}{D_p J} \tag{3.53}$$

3.2.4. Power Requirements

In figure 3.10 the different power curves for the PoA vessels is shown using the hull and open water efficiency as a function of speed. Then in picture 3.11 a comparison between the two power curves is shown. from this curve, it is clear that the power demand between the two vessels is quite similar. This can easily be explained since on the one hand the displacement is increased with the new PoA vessel but on the other hand, the length is increased, reducing the resistance due to the Froude effect. According to figure 3.11 this levels out pretty evenly in the up to 15 km/h with the new vessel even being more efficient for a large part of the operational range.

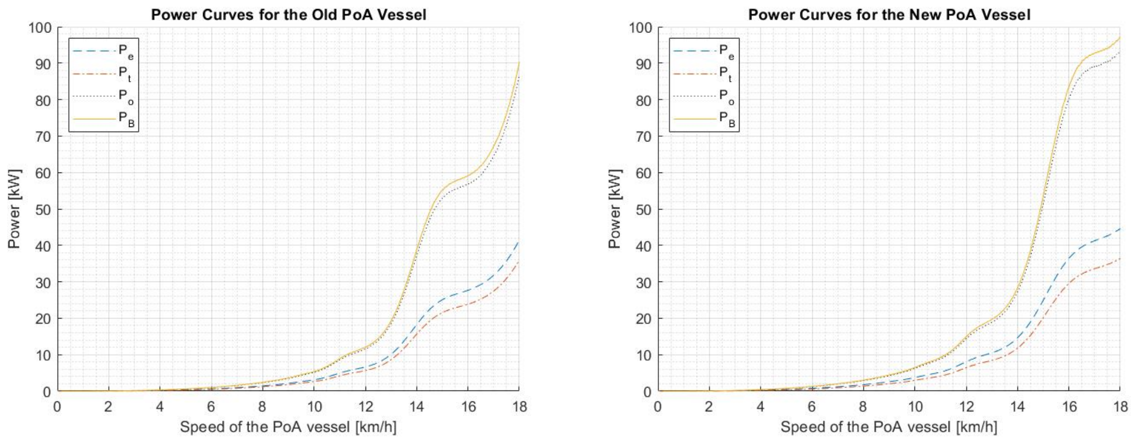

Figure 3.10: Different power curves for the PoA vessel

In table 3.9 the rotative, transmission and electric motor efficiencies determined in this chapter are summarised. Finally, the power around 17 km/h was considered to take advantage of the dip in resistance, including a service margin of 25 % leads to the conclusion that the PoA vessel will require an electric motor of kW, with consumption of kWe, assuming an electric induction motor with an efficiency of 84%.

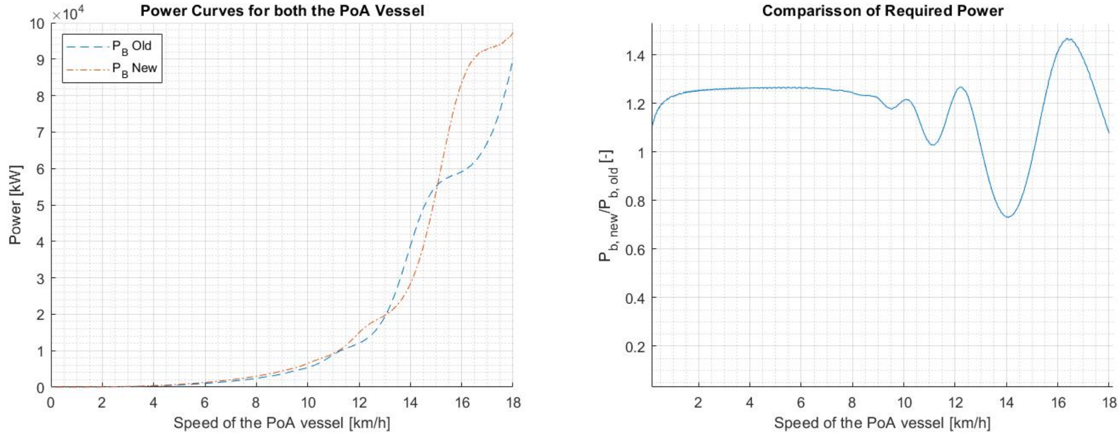

Figure 3.11: Comparison between the new and old power curves.

	η_h (avg.)	η_o (avg.)	η_r	η_{trm}	η_{EM} (avg.)	service factor	P_B (max)	$P_{installed}$ (mechanical)	$P_{installed}$ (electrical)
New PoA Vessel	1.30	0.43	0.98	0.98	0.87	0.25	100 kWm	127 kWm	146 kWe

Table 3.9: Summary of efficiencies and installed power for the PoA vessel as calculated in this chapter.

3.3. Operational Profiles

To determine the operational profile for the PoA vessel, the company Techno Fysica B.V. measured the performance of the current PoA vessel on an average operating day. The entire report including the sailing routes is included in appendix B. In figure **??** the measured mechanical power is plotted against the vessels speed, in table 3.10 and 3.13 the measurements are applied to the design vessel using the resistance calculations as defined in the previous sections. Finally, a sizing estimation for the required battery and hydrogen storage is made using the operational profiles during normal operations.

3.3.1. Techno Fysica B.V. Measurements

The measurements done by Techno Fysica that can be found in appendix B verified the calculated resistance from Holtrop and Mennen. However, the power output also differs strongly over any given speed. This difference in power output is mostly attributed to manoeuvring and this extra energy consumption adds to the overall profile. Therefore it is concluded that due to the extra energy consumption of manoeuvring, using just the resistance curve as calculated in chapter 3 is not enough basis for the operational profile. Instead, figure 3.11 is used, where the average energy consumption of the PoA measurements per speed range of 0.1 km/h is scaled based on the difference in resistance as calculated in chapter 3.2.

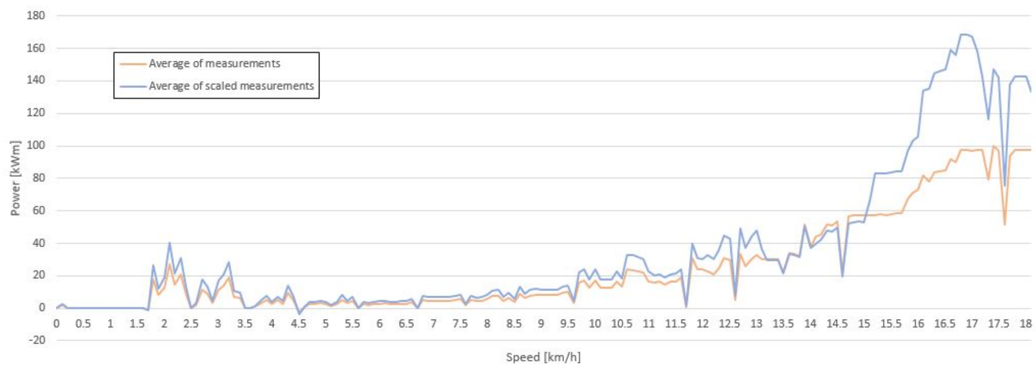

Figure 3.12: The average of the measured power consumption per 0.1 km/h and the scaled measurements according to figure 3.11

3.3.2. Cases

During normal operation of the vessel, three distinct modes of operations can be defined as illustrated in figure 3.13. Profile A1 and C are from sailing in the Amsterdam port area with an average speed of around 12.5 km/h. The B profile is sailing inside the Amsterdam canals with an average speed of around 7 km/h. And finally, the C profile is from sailing on in the port area at a maximum speed of 15 km/h. Based on the measurements, an average day consists of 50% sailing in the canals, 41 % sailing in the port area and 9% sailing at max speed. Furthermore, a hotel load is required, estimated at around 3 kWh for heating and 1 kWh for other onboard power consumption including pumps, based on a TNO research for electric shipping in Amsterdam for canal boats of roughly similar dimensions [52].

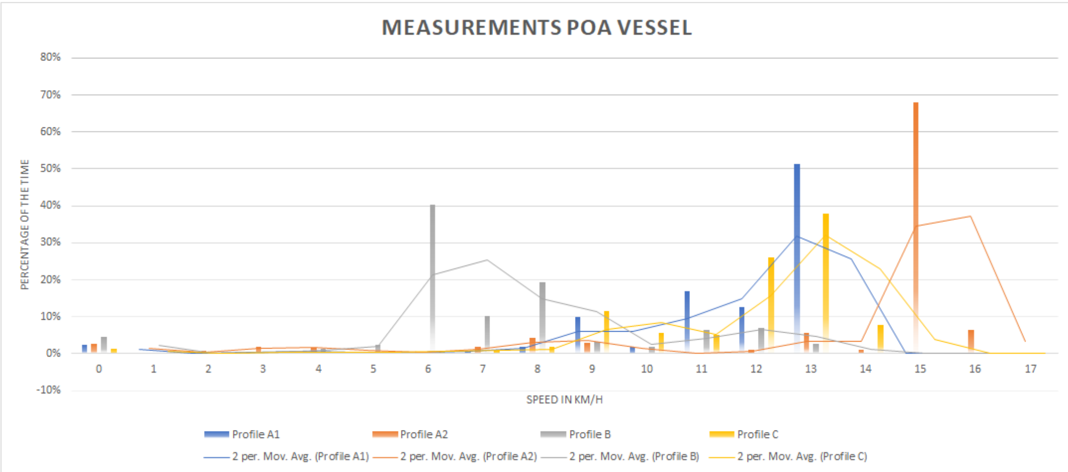

Figure 3.13: Different Operational modes for the PoA vessel as measured by Techno Fysica

Using the three modes as defined in figure 3.13 and the design requirements, four operational profiles are examined. The first one is an average day based on the measurements of the current vessel and scaled using figure 3.12 and 3.13, the second profile is a tour in the Amsterdam canals, thirdly is a work visit in the port area and the final scenario is a 10 hour trip to IJmuiden. The energy consumption of different operational profiles can be used to make an initial estimation for the sizing of the fuel cell and battery system. The electrical efficiency is also included, considering an 87% efficiency for the electric motor and a 95% efficiency for the transformer. This leads to a relation between break power and electric power as determined in equation 3.55.

$$P_{EM} = \frac{P_B}{0.826} \tag{3.54}$$

Case 0: An Average Day

The first case is completely based on the measurements by Techno Fysica B.V.. This operational profile starts with sailing from the dock to the pick-up point, then a tour through the Amsterdam canals is made, then a work visit is planned and finally, the vessel is returned to the dock. In table 3.10 the average energy consumption for an average day is calculated.

	Speed [km/h]	Power [kWe]	Time share [%]	Avg. Power [kWe]
Sailing in the Amsterdam canals	7	8.30	50%	4.15
Sailing in the Amsterdam port area	12.5	52.16	41%	21.39
Sailing at max speed	15	64.18	9%	5.78
Hotel loads	-	4.00	100%	4.00
Total				35.31

Table 3.10: Energy consumption for the design vessel for an average day, based on the scaled measurements

Case 1: Amsterdam Canals
The second case is an average tour of the Amsterdam canals. The day starts with the vessel sailing form the docks to the pick up point, as was done during the PoA measurements, with an average speed of 11.5 km/h, This takes the vessel 44 minutes. Then a tour of the city is organised, sailing at an average of 7 km/h for 2 hours and 59 minutes. Finally the captain decides to rush back to the dock at a maximum speeds of 15 km/h, taking 39 minutes. For the entire sailing time the hotel loads are also included. This operational profile is summarised in table 3.11.

	Speed [km/h]	Power [kWe]	Time [hr]	Energy [kWh]
Sailing from dock	11.5	25.62	0.44	18.79
Sailing in the Amsterdam canals	7	8.30	3.00	24.91
Sailing at max speed	15	64.18	0.39	41.72
Hotel loads	-	4.00	4.24	17.60
Total				103.02

Table 3.11: Average day: Tour in the Amsterdam canals

Case 2: Work Visit Port Area
The third case is an average work visit. Again the day starts with the vessel sailing from the docks to the pickup point, following the measurements at 11.5 km/h for 44 minutes. Then the vessel makes a tour around the port area, as was also executed during the measurements, sailing at an average of 12.5 km/h for 2 hours and 56 minutes. Finally, the captain decides to rush home again, sailing at 15 km/h for 39 minutes. This operational profile, including the hotel loads, is summarised in table 3.12.

	Speed [km/h]	Power [kWe]	Time [hr]	Energy [kWh]
Sailing from dock	11.5	25.62	0.44	18.79
Sailing in the Amsterdam canals	12.5	52.16	2.56	170.39
Sailing at max speed	15	64.18	0.39	41.72
Hotel loads	-	4.00	4.29	17.93
Total				248.83

Table 3.12: Average day: Work visit in the Port Area

Case 3: IJmuiden
Finally, an operational profile based on one of the design requirements is made. The requirement states that the vessel should be able to sail for 12.5 km/h for 10 hours to reach the city of IJmuiden. However, this profile was adjusted slightly to also include the high-speed part. The result is a trip that lasts 10 hours with an 8.5 hour trip to IJmuiden and back in between pickups.

	Speed [km/h]	Power [kWe]	Time [hr]	Energy [kWh]
Sailing from dock	11.5	25.62	0.44	18.79
Sailing in the Amsterdam canals	12.5	52.16	8.30	443.36
Sailing at max speed	15	64.18	0.39	41.72
Hotel loads	-	4.00	10.00	56.00
Total				559.87

Table 3.13: Energy consumption for the design vessel for the maximum range requirement, based on the scaled measurements

Conclusion
The highest power consumption is required during long transits to IJmuiden and back at an average speed of 12.5 km/h. Furthermore, the design requirements specify an operating range of 10 hours, thus the estimation for the required electrical energy on board of the vessel is at a minimum of 560 kWh. Taking into account a safety margin, it is recommended to design the vessel with an onboard energy storage of at least 600 kWh.

3.4. Initial Sizing

The mission of the PoA vessel is meant to be a battery-electric vessel, using a hydrogen-powered fuel cell as a range extender. Meaning that the energy storage will rely heavily on the batteries, only using the hydrogen for extra range when the system requires more energy than would normally be the case. Taking this into account, two average working days are defined using the resistance calculations and the measurements done by Techno Fysica B.V.. Then these two cases are compared and a decision is made for the size of the required battery system. The maximum range as determined using profile C is then used to determine the required $NaBH_4$ fuel on board. Then the installed fuel cell power is determined using the average power estimations.

Electric Motor

As determined in chapter 2 an induction motor will be used with an average efficiency of 87 %. It is also reasonable to assume that besides a motor a transformer is required, the efficiency of the transformer is estimated to have an average of 95 %. This leads to a relation between the break power and the electric power as defined in equation 3.55. In section 3.2 in table 3.9 it was determined that the electric motor should provide 127 kWm (mechanical power), taking into account a service factor of 0.25. Using the mentioned efficiencies this leads to a peak power load of 146 kWe for the electric motor.

$$P_{EM} = \frac{P_B}{0.826} \tag{3.55}$$

Fuel Cell

The fuel cell does not have to carry the maximum load of the vessel. Instead, the capability of providing the average load should be sufficient, in table 3.14 the average power per case is examined. The first two cases imply that a 40 kW fuel cell is sufficient, however, the average load for case two and three require a fuel cell of 60 kW to sustain the average load. However, since the fuel cell manufacturer Nedstack provides a maritime specific fuel cell of 40 kW, see appendix C, this option will first be evaluated.

	P_B avg. [kWm]	P_{EM} avg. [kWe]
Case 0	29.88	36.15
Case 1	20.75	25.10
Case 2	48.72	58.94
Case 3	47.10	56.98

Table 3.14: Average power requirements for the fuel cell per operational profile

Battery System

Case 1 and 2 for an average operational day require an energy capacity of 103 kWh and 249 kWh respectively. Since batteries are never completely discharged a maximum depth of discharge (DOD) also needs to be taken into account when estimating the batteries capacity and this is estimated at 70%. The required battery capacity is calculated in table 3.15, with a minimum requirement of 150 kWh for the Amsterdam tour and a maximum of 800 kWh if the entire vessel is to be battery-electric. It is concluded that if the design space allows, a battery capacity of 150 kWh should be installed to save operational costs. However, this is probably too expensive and due to the space limitations, undesirable. Thus instead a minimum capacity of 100 kWh should be used relying more on the energy-dense $NaBH_4$ storage.

	Energy [kWh]	DoD [%]	Battery [kWh]
Case 0	353.14	70%	504.49
Case 1	103.02	70%	147.17
Case 2	248.83	70%	355.47
Case 3	559.87	70%	799.81

Table 3.15: Required battery capacity for different operational profiles

$NaBH_4$ Storage

Total effective energy of 600 kWh is required for the PoA vessel. Since the vessel is hybrid the energy requirement is split over the batteries and the $NaBH_4$. Assuming a 100 kWh installed battery with a depth of discharge of 70% results in an energy requirement of 530 kWh electric. Applying a fuel cell efficiency of 50% and the required hydrogen is 1060 kWh LHV or roughly 32 kilograms of hydrogen. In table 3.16 the weight and volume of the required $NaBH_4$ and spent fuel is shown based on the results of chapter 2.

	kg	L
H_2	32	-
$NaBH_4$	150	139
Spent fuel	726	548

Table 3.16: Required NaBH4 capacity

On-board Restrictions

A few hydrogen vessels have already been build in the last decade and have also been certified by Germanischer Lloyd (GL). This means that there is already some framework concerning the safety risks and how to mitigate them in the design phase. The most important being the safe separation of areas as illustrated by the FC Alsterwasser vessel in figure 3.14. Other important design considerations include an air vent for the possible emergency discharge of the hydrogen. And sufficient air circulation to prevent hydrogen from building up in an area and creating an explosion risk. More guidelines can be found in the report and guidelines by GL such as "Guidelines for the use of fuel cell systems on board of ships and boats" - 2003, "Fuel cells in maritime applications challenges, chances and experiences" - 2010 [53] and from the H2Nemo vessel lessons learned report from 2011 [49]. A framework for the use of $NaBH_4$ and reforming it to H_2 does not exist and it is therefore recommended that the safety implications of the system are studied further in different research.

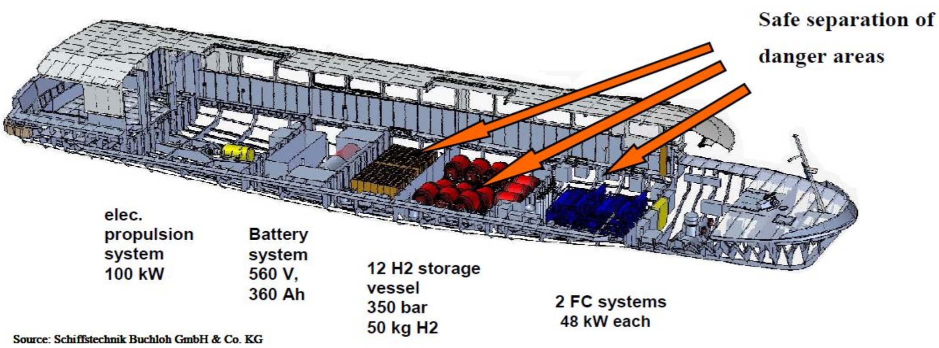

Figure 3.14: Safety concept of the FC Alsterwasser certified by Germanischer Lloyd [53]

Conclusion

The initial sizing of components for the new PoA vessel is summarised in table 3.17. The configuration will be verified using a Simulink model that is developed in chapter 4.

Component	Size
Electric motor	150 kWe
Fuel cell	40 kW
Li-ion	100 kWh
NaBH4	150 kg / 139 L
Spent fuel	726 kg / 550 L

Table 3.17: Initial sizing of components

4

Modelling of the System

This chapter will introduce the MATLAB/Simulink model used for the verification of the design parameters and the analysis of the dynamic behaviour of the power train system. The Simscape environment provided the battery and fuel cell model, modelling the electrical behaviour based on company-provided datasheets. The method of power conversion was proposed in the master thesis of F. Nievelt [21] and was also used in this model. The input for the model is defined in this report by using the hydrodynamic analysis and measurements from chapter 3. Finally the hydrogen generation, and the EMS subsystems are developed in this chapter.

4.1. Model Architecture

The model architecture is composed using five kinds of subsystems. The simulation input is based on the hydrodynamic analysis and measurements from 3 and provide the power demand that functions as the input for the simulation. This demand is then sent to the EMS where a decision is made on how much power is required from the fuel cell based on the SOC of the battery system. The power demand is also sent to the battery subsystem where the fuel cell power is subtracted so that the required power can always be delivered as long as there is sufficient charge in the battery system.

The required fuel cell power is then sent to the power transformation subsystem that converts the required current load to a required H_2 fuel flow rate. The pressure is another input that is used to increase the load and flow demand in case the pressure in the reactor gets to high. The hydrogen flow requirement is then sent to the hydrogen production subsystem where the hydrolysis reaction of $NaBH_4$ is modelled, including injection control, rinsing of the reactor and the flow control. The actual hydrogen flow is then sent to the fuel cell where it is converted into electrical power.

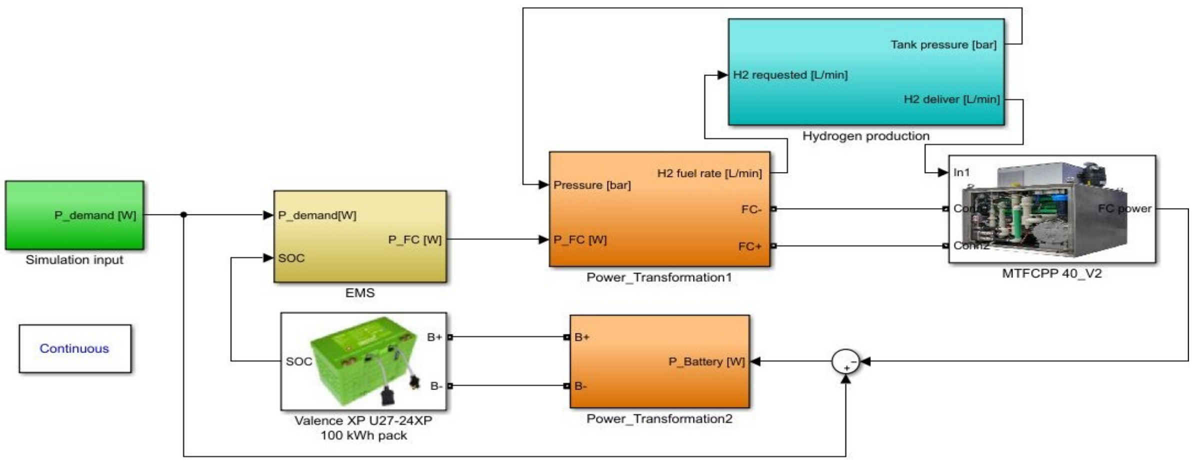

Figure 4.1: Overview of the model architecture and subsystems

4.2. Input

The input subsystem is shown in figure 4.3, first the measurements results are imported from the MATLAB workspace. The sample time is chosen at 10 seconds since the longest simulation will run for 10 hours and a larger sample time will speed up the simulation. Furthermore, the goal of the simulation is to analyse the energy demand of the vessel during a specific cycle and a 10 second sample time is sufficient for this purpose.

The current speed of the vessel is then used to determine the scaling factor as defined in chapter 3 and illustrated here again in figure 4.2. This factor is then used to scale the power demand gained from the measurements. The power is limited to 100 kW since this is the maximum installed power, and a hotel load of 4 kW is added as suggested by a TNO research of similar-sized canal boats [52], Finally the efficiency of the electric motor is assumed at 87% and is also taken into account.

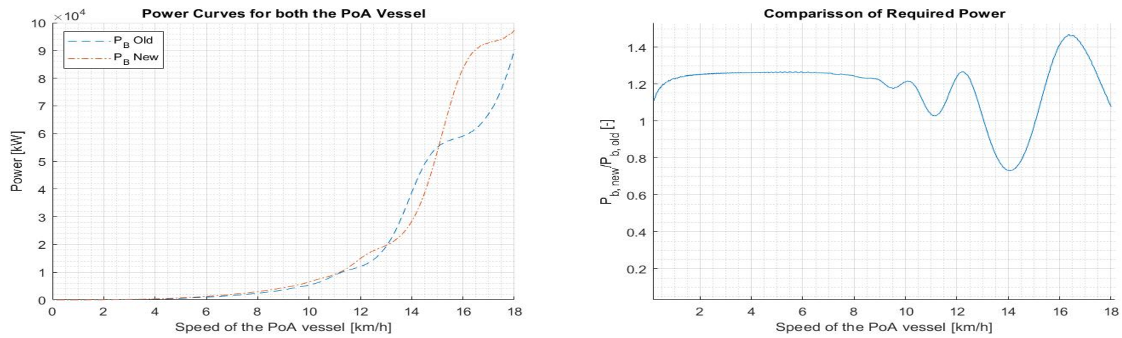

Figure 4.2: Comparison between the new and old power curves from chapter 3

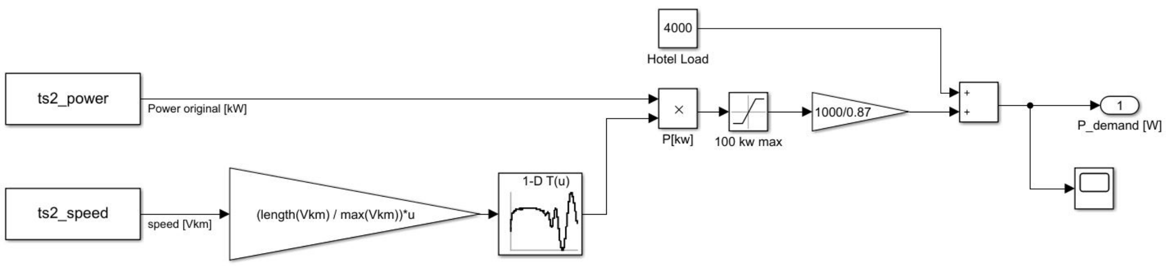

Figure 4.3: Input sub model converting the measured power output using the hydrodynamic analysis from chapter 3 based on the current speed of the vessel.

For the input of the simulation the measurements made by Techno Fysica B.V. are used together with input from the PoA in order to create three realistic test cases. in figure 4.4 the power demand for the operational profiles is shown.

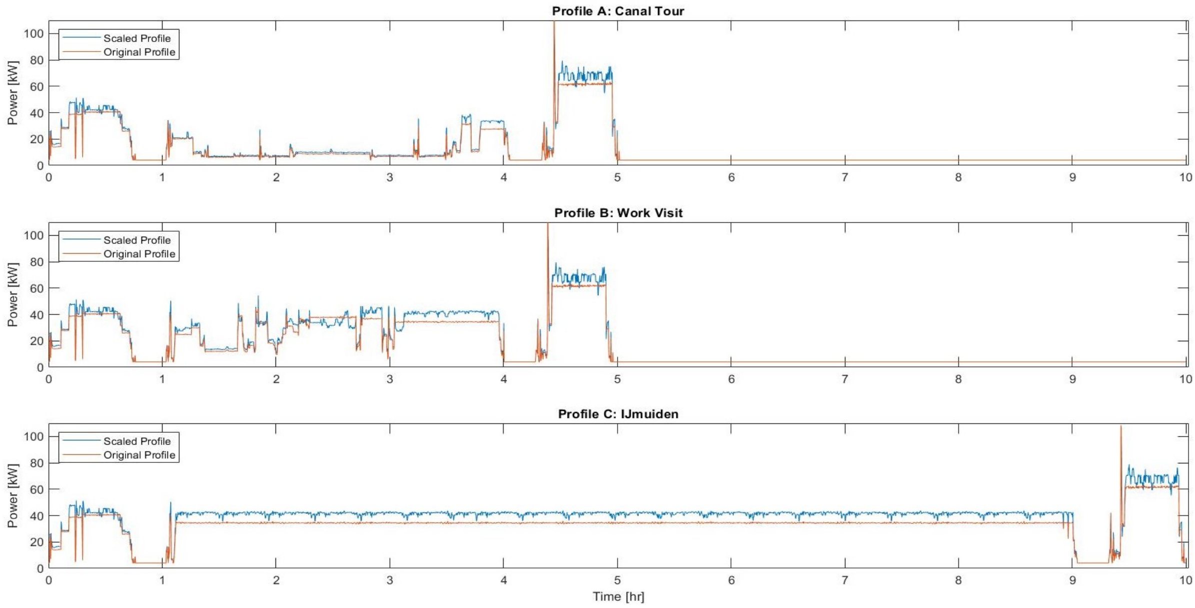

Figure 4.4: The three operational profiles scaled based on the hydrodynamic analysis.

4.3. EMS Models

The Energy Management Strategies determine the required fuel cell power. For the two rule based strategies, a MATLAB function was used following the rules as defined in equation 4.1 and 4.2. In figure 4.5 the application of EMS2, corresponding to equation 4.2 is shown.

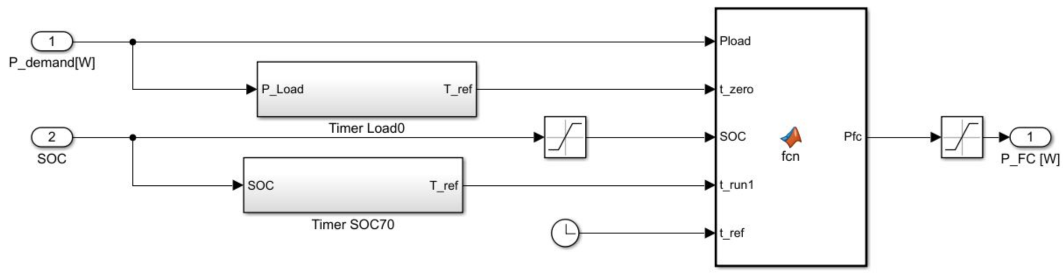

Figure 4.5: Energy Management Strategy sub model for EMS2, corresponding to equation 4.2

An extra timer is added that starts counting when the 70% SOC threshold is reached. This timer is then used so that the fuel cell runs for at least 20 minutes before being turned off. This prevents zero crossings in the algorithm but more importantly, it also increases the fuel cell lifetime by reducing the start/stop cycles of the cell. The t_0, and the t_{ref} timers are used so that the algorithm functions properly during the start-up and cool down of the simulation.

$$P_{FC} = \begin{cases} P_{FC,min} & \text{if } 50 < SOC \leq 70 \\ P_{FC,min} & \text{if } t_{run,1} < 1200s \\ P_{FC,max} & \text{if } SOC \leq 50 \\ P_{FC,max} & \text{if } t_{run,2} < 1200s \\ 0 & \text{else} \end{cases} \tag{4.1}$$

$$P_{FC} = \begin{cases} P_{FC,min} + \frac{SOC_H - SOC}{SOC_H - SOC_L} \cdot (P_{FC,max} - P_{FC,min}) & \text{if } 50 < SOC \leq 70 \\ P_{FC,min} + \frac{SOC_H - SOC}{SOC_H - SOC_L} \cdot (P_{FC,max} - P_{FC,min}) & \text{if } t_{run,1} < 1200s \\ P_{FC,max} & \text{if } SOC \leq 50 \\ 0 & \text{else} \end{cases} \tag{4.2}$$

For EMS3 a simple PI system using a back calculating anti-wind-up was implemented as illustrated in 4.6, the used setting are P=10, I=9, Kb=1 and the back-calculation saturation settings are between 0 and 40.000. According to the manufacturers, the fuel cell has a minimum power of 25 kW, so an extra filter is added that overrides the required power to zero whenever the value is lower than 25.000.

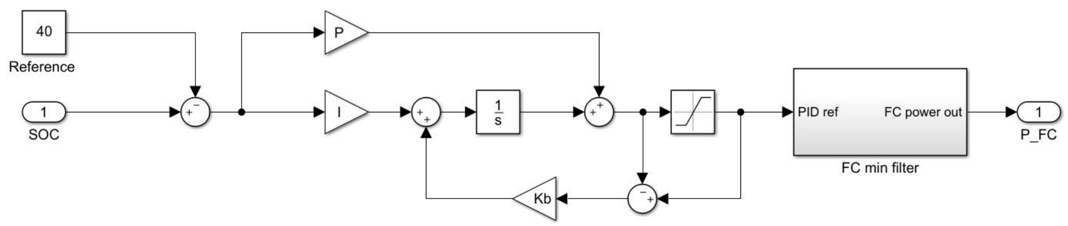

Figure 4.6: Energy Management Strategy submodel for EMS3

4.4. Power Transformation

Two power transformation blocks are used in the model to convert from a numerical value for power to the electrical grid used by Simscape. To achieve this the current-voltage is measured and equation 4.3 is applied. An efficiency for the transformer of 95% is assumed based on the results of chapter 2.

$$I = \frac{P}{V} \tag{4.3}$$

4.4.1. Battery

The power transformation from the required battery load $P_{battery}$ to the electrical grid is a simple application of equation 4.3. This transformation system uses a controlled ampere source and measures the voltage at the current time step as illustrated in figure 4.7.

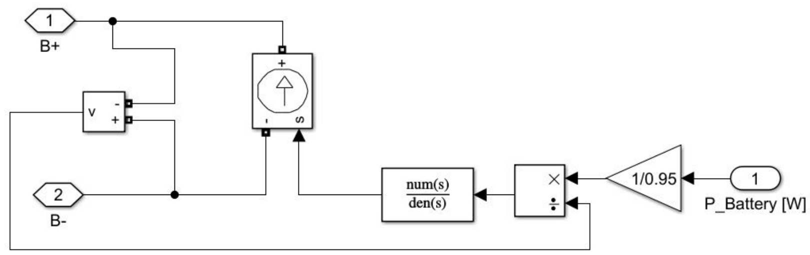

Figure 4.7: Power transformation subsystem for the battery

In reality, a DC/DC converter would be used between the systems, however, the correct modelling of such a converter can be complex and does not add to the analysis of the energy consumption of the vessel. So instead of dividing by the constant voltage of the DC grid, the actual voltage is measured and used for calculating a current. This current is then used as a negative current source, in effect draining the required power from the battery system. To prevent an algebraic loop in MATLAB, a transfer function is used to break the loop. A very small time derivative value is used so that the function does not affect the system, as illustrated in equation 4.4.

$$H = \frac{1}{0.0001s + 1} \tag{4.4}$$

Note that even though no DC/DC converter is used, the battery array has been chosen in such a way that it provides around 300 V, similar to the maximum 290 V output of the fuel cell, thus somewhat levelling the electric load for easy implementation of 300 Vdc bus.

4.4.2. Fuel Cell

The power transformation for the fuel cell is similar to figure 4.7 but a bit more complicated due to the pressure override that increases the load when required and the flow rate regulator that determines the hydrogen flow demand. Furthermore, some limits were added for the voltage and current based on the fuel cell requirements, the subsystem is illustrated in figure 4.8.

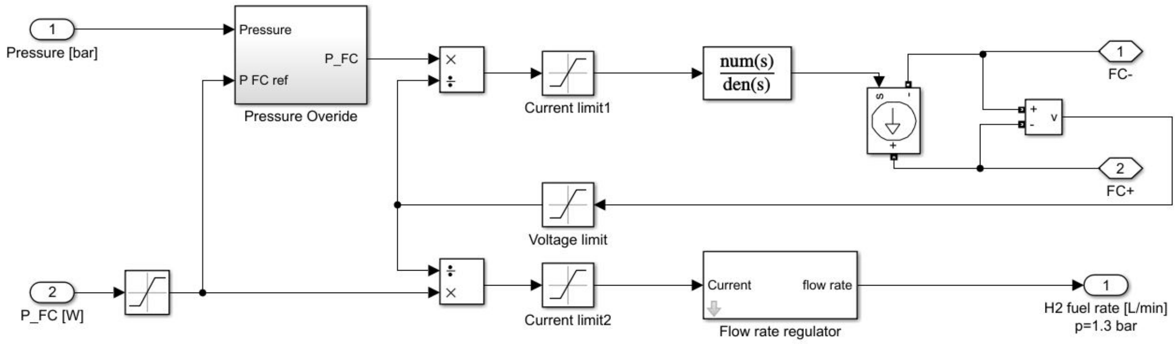

Figure 4.8: Power transformation subsystem for the fuel cell

Pressure Override

The maximum allowed pressure in the reactor is 100 bar. Under light load conditions, more hydrogen is produced than required, resulting in high pressure in the reactor. A safety measure is implemented that increases the fuel cell power if the pressure gets above 40 bar, the extra load is used to charge the battery. The load is increased proportional to the pressure, increasing to the maximum load of the fuel cell at 80 bars, as illustrated by equation 4.5. This method ensures safe operations for the reactor, the effectiveness of this system is evaluated and analysed in chapter 5.

$$P_{FC} = \begin{cases} \frac{p}{80} \cdot P_{FC,max} & p > 40 \\ P_{FC,ref} & else \end{cases} \tag{4.5}$$

Flow Rate Regulator

The relation between the current demand and the required flow rate can be determined using Faraday's law of electrolysis:

$$n = \frac{It}{Fz} \tag{4.6}$$

With n being the amount of substance liberated in moles, F as the Faraday constant of 96 485 C/mol, t is for the passed time in second, and z as the valance, which is one for hydrogen. By applying the ideal gas law as given in equation 4.7 the Faraday law can be written as equation 4.8 and then as 4.9 when also considering the utilisation rate of the hydrogen Uf_{H2}, as a function of the nominal LHV efficiency of the fuel cell, and the hydrogen content percentage x.

$$n = \frac{pV}{RT} \tag{4.7}$$

$$\frac{V}{t} = \frac{RTI}{Fp} \tag{4.8}$$

$$\frac{L}{min} = \frac{60000RT}{zFp_f Uf_{H2}x} \tag{4.9}$$

Finally adding all the constants and adding N_c for the number of cells equation 4.10 can be used in order to determine the required fuel flow for the model.

$$\frac{L}{min} = \frac{60000 \cdot 8.3145(273 + T) \cdot I \cdot N_c}{2 \cdot 96485 \cdot (101325 \cdot p_f) \cdot Uf_{H2} \cdot x} \tag{4.10}$$

4.5. Batch Reactor Model

The required hydrogen flow is first normalised to atmospheric pressure to NL/min since the pressure of the hydrogen flow towards the fuel cell and used in equation 4.10 is 1.3 bar. By assuming ideal gas law and using equation 4.7, the NL/min can be determined. Based on the flow demand, the fuel injection is controlled, then the $NaBH_4$ injected reacts in the half-life time subsystem. Next, the flow control determines the actual flow towards the fuel cell based on the hydrogen production and the reactor pressure. Finally, the hydrogen flow is converted to 1.3 bar and send to the fuel cell, the subsystem is illustrated in figure 2.7.

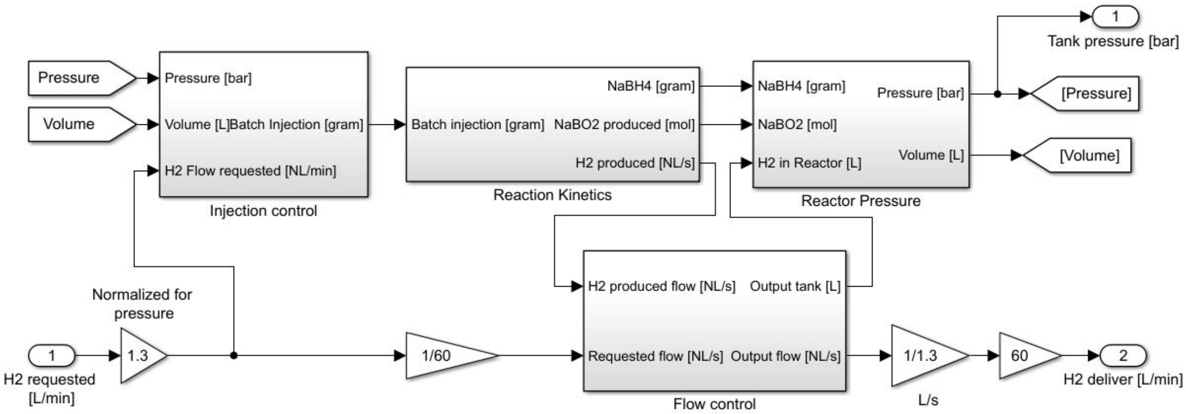

Figure 4.9: Model architecture of the hydrogen production subsystem, including the injection and flow control.

4.5.1. Injection

The fuel is injected using a pulse signal multiplied with an amount of $NaBH_4$ as illustrated in figure 4.10. The pressure in the reactor is used to determine if an injection is required, when the pressure comes below the 15 bar, fuel is injected. Furthermore, if the level indicator shows that the reactor tank is too full and needs to be emptied, the injection is stopped. The settings for how much fuel is injected and at what interval are further explored and analysed in chapter 5 and will prove to be important for the start-up time of the hydrogen production system.

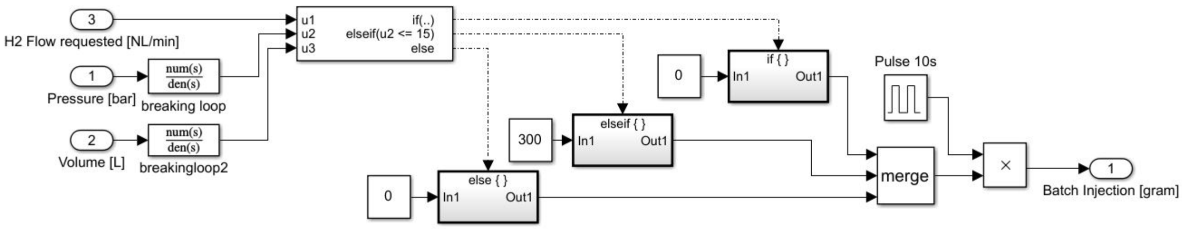

Figure 4.10: Model of the injection Subsystem

4.5.2. Reaction Kinetics

The pulse signal of the $NaBH_4$ injection is converted to a steady signal using a sample and hold block as illustrated in figure 4.11. These blocks are also used to reset the system whenever a new injection takes place. A value is sampled so that the accumulation of $NaBH_4$ in the reactor is taken into account, a value is also sampled after the integration step to reset the $NaBH_4$ dynamics every cycle, preventing the accumulation of "lost" $NaBH_4$.

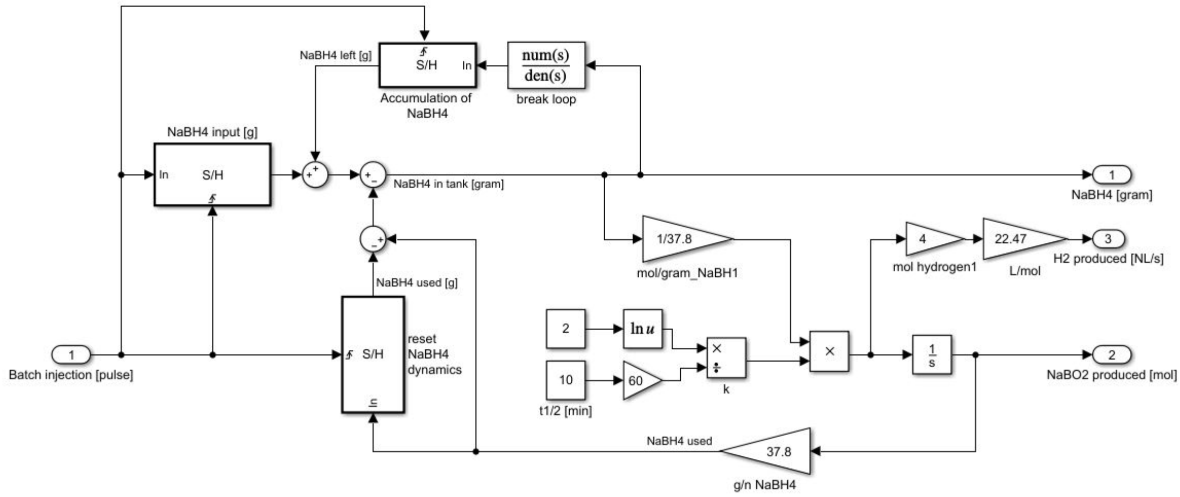

Figure 4.11: Model for the subsytem for the reaction kinetics of the hydrolysis reaction.

Reaction rate

According to [18] the reaction rate of the catalytic hydrolysis reaction of $NaBH_4$ can be described using a first-order reaction rate. On the other hand [25] state that the first part of the reaction can be estimated using a 'quasi zero-order reaction', however it should be noted that the experiments from [25] were carried out at a temperature of 30°C. Both these conclusions seem to match well with the results from the University of Gent that were discussed in section 2.2.3 from [17].

From those experiments, it was concluded that at low temperatures the reaction rate was almost zero-order, however, at higher temperatures the rate increased dramatically. Since the reactor will reach temperatures of around 90 °C, it is concluded that the reaction rate is of the first order. Furthermore, since it is the intention to evaluate the system for different half-life times, to take into account varying circumstances of the catalyst. The change of reactants for a first-order equation is redefined as 4.11, this is then integrated to achieve the amount of $NaBH_4$ that reacted, and this can be used to calculate the amount of $NaBO_2$ and H_2 produced since the mole ratio is 1:1 and 1:4 respectively.

$$-\frac{d[A]}{dt} = \frac{ln(2)}{t_{1/2}}[A] \tag{4.11}$$

Verification

The simulation results of two, 300 gram of solved NaBH4 injections is modelled with an injection window of 600 seconds and a half-life time of 10 minutes, or 600 seconds over 5000 seconds. Figure 4.12 shows the behaviour as would be expected from a first-order model, as well as the accumulation of $NaBH_4$ in the reactor over multiple reactions.

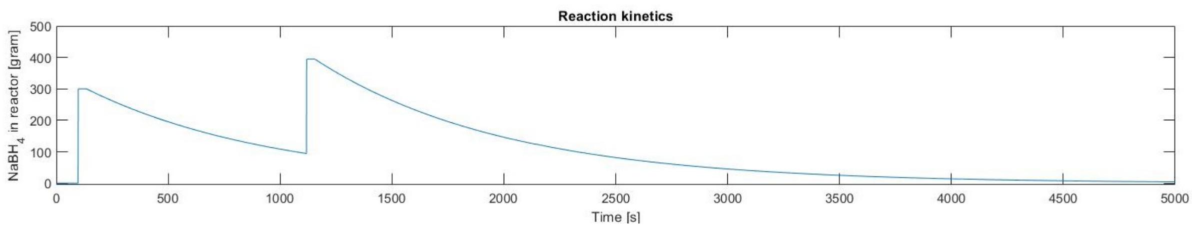

Figure 4.12: Simulation of a first order reaction of 300 gram $NaBH_4$ with a half-life time of 10 minutes and an injection window of 5000 seconds.

4.5.3. Flow control

There is not always enough hydrogen produced to meet the hydrogen demand of the system. To manage the hydrogen flows some kind of flow control needs to be implemented that controls the outflow of the reactor. This is modelled by using if statements as illustrated in figure 4.13. When integrated, the difference between produced flow and delivered flow results in the accumulation or depletion of hydrogen in the reactor. In reality, the flow doesn't increase or decrease instantly, so to simulate a smoother transition a transfer function was also implemented.

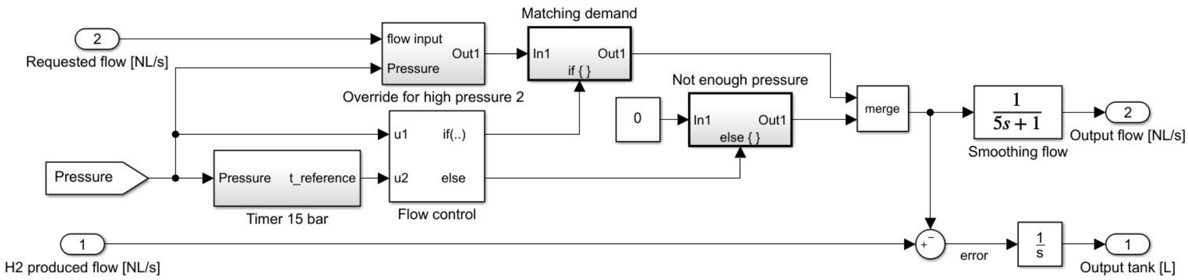

Figure 4.13: Subsystem for the flow control and the accumulation of hydrogen in the reactor.

Output Flow

The flow settings are chosen so that the pressure in the reactor remains 15 bar. With 15 bar the system proved resilient to sudden changes in the hydrogen demand and proved capable of continues operation. A buffer in the tank provides some extra time for the injection system to react and for the hydrolysis reaction to take place. A timer was also used to prevent zero crossings at the if statement, basically ensuring that a change in flow is sustained for at least 100 seconds, the system is illustrated in equation 4.12.

$$\dot{V}_{H2} = \begin{cases} \dot{V}_{H2,ref} & p > 15\ bar \\ \dot{V}_{H2,ref} & t_{15} < 100s \\ 0 & else \end{cases} \tag{4.12}$$

Override Pressure

The override for high pressure is already mentioned in section 4.4.2 and is there to ensure that the pressure in the reactor remains below 100 bar. When the pressure is above 40 bars the load is increased, the extra load is used to charge the battery and ensures safe operations for the reactor. The load is increased proportional to the pressure, increasing to the maximum load of the fuel cell at 80 bars, as illustrated by equation 4.13.

$$\dot{V}_{H2} = \begin{cases} \frac{p}{80} \cdot \dot{V}_{H2,max} & p > 40\ bar \\ \frac{p}{80} \cdot \dot{V}_{H2,max} & t_{40} < 100s \\ \dot{V}_{H2,ref} & else \end{cases} \tag{4.13}$$

Emptying Reactor

When there is no load and there is still hydrogen in the reactor, the reactor needs to be emptied. This is done according to equation 4.14, if the pressure is above 15 bars the minimum hydrogen flow is given and the fuel cell works at max efficiency. When the pressure is above 40 bar the override safety mechanism takes over. Once activated, the hydrogen flow continues for at least 100 seconds, resulting in a pulsing flow that slowly empties the reactor.

$$\dot{V}_{H2} = \begin{cases} \frac{p}{80} \cdot \dot{V}_{H2,max} & p > 40\ bar \\ \frac{p}{80} \cdot \dot{V}_{H2,max} & t_{40} < 100s \\ \dot{V}_{H2,min} & p > 15\ bar \\ \dot{V}_{H2,min} & t_{15} < 100s \\ 0 & else \end{cases} \tag{4.14}$$

4.5.4. Reactor Pressure

The ideal gas law is used to calculate the pressure inside the reactor and a constant temperature of 90°Celsius is assumed. Then the available volume for the hydrogen gas is calculated by subtracting the $NaBH_4$ and spent fuel solutions in the tank from the tank volume of 38 L, the subsystem is illustrated in figure 4.14.

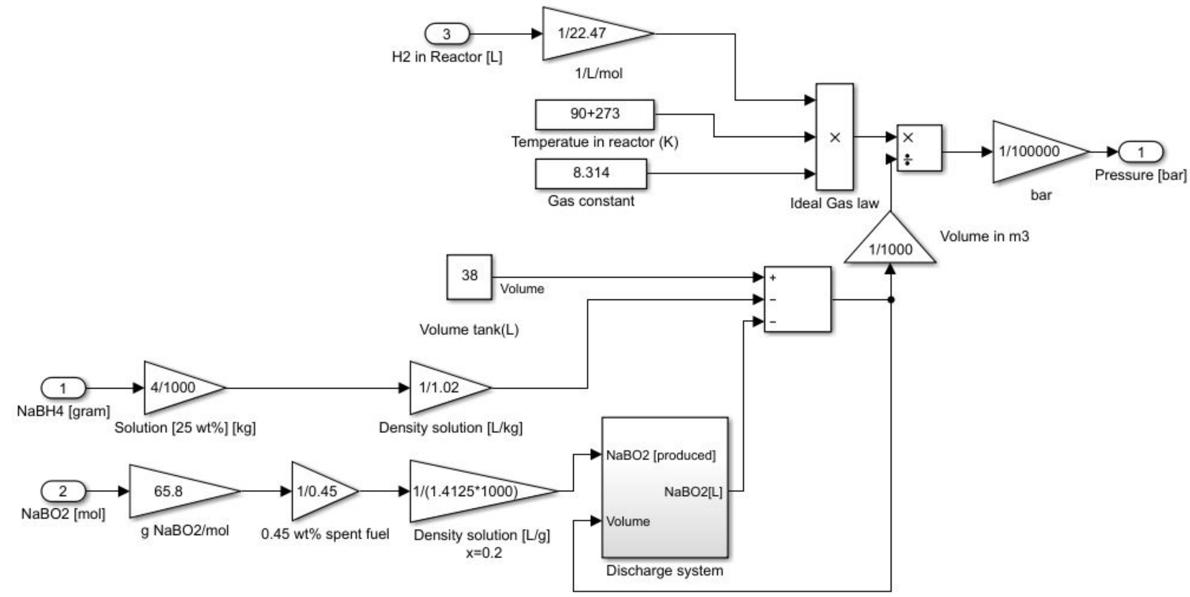

Figure 4.14: Model for the pressure calculating subsystem, also including the discharge of the reactor.

Discharge

The discharge system is originally modelled by assuming that the system will be rinsed when a certain threshold is reached by the level indicator. In the model this means that when the available gas volume is less than 10 litres, the spent fuel and remaining $NaBH_4$ solution is discharged and thus lost, this is simulated by using a sample and hold block.

During analyses in chapter 5 the lost of $NaBH_4$ proved to be substantial, since the level indicator would be triggered right after the fuel injection. Therefore another discharge system was developed to be used during the simulation from section 5.3 onwards.

The new rinse cycle starts after 30 injections of 300 gram $NaBH_4$. In the injection system, a trigger subsystem is used that after 30 injection triggers a timer. The injection is then stopped for 20 minutes, during 15 minutes of which the reaction continues producing hydrogen. At 15 minutes the reactor is discharged and the spent fuel and remaining $NaBH_4$ solution is lost. An additional 5 minutes are used to simulate a realist rinse cycle during which the reactor is completely offline. In figure 4.15 the trigger subsystem as implemented in the injection subsystem is illustrated.

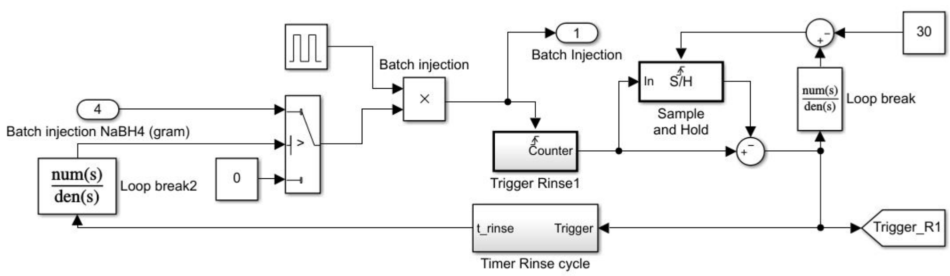

Figure 4.15: model for the subsystem in the injection subsystem used for the discharge system from section 5.3 onwards.

4.6. Fuel Cell model

The MATLAB/Simulink, Simscape environment has an integrated model for the fuel cell dynamics. This model emulates the electrical behaviour as provided in the product data-sheet and is thus easy to implement without needing any additional measurements or assumptions. In Appendix C the product sheet of the MT-FCPP-40 fuel cell developed by Nedstack is provided. Since it also states that the 40 kW fuel cell is based on four FCS 10-XXL fuel cells this product sheet is also included. Together these data sheet provided enough data for the modelling of the fuel cell. In figure 4.16a the electrical specifications of the FCS 10-XXL from the data-sheet is illustrated. In figure 4.16b the simulation results for the collective of four FCS 10-XXL is shown. The fuel cell model itself is further explained in the 2009 paper of Njoya et al. ”A generic fuel-cell model for the simulation of fuel cell vehicles” [44].

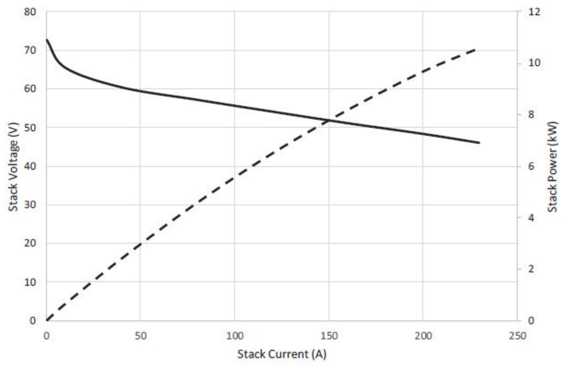

(a) Electrical specification of the Nedstack FCS 10-XXL, Appendix C

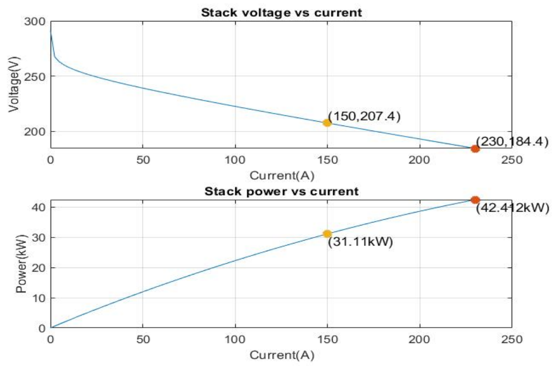

(b) Simulation of the Nedstack MT-FCPP-40 fuel cell

Figure 4.16: Data sheet information and simulated results.

Efficiency

According to the product sheet of the MT-FCPP-40 from Nedstack, the peak consumption is 2.5 kg/h at 40 kWe. This results in efficiency at peak load of 48%. Integrating this into the Simulink model leads to the following estimation of the efficiency curve.

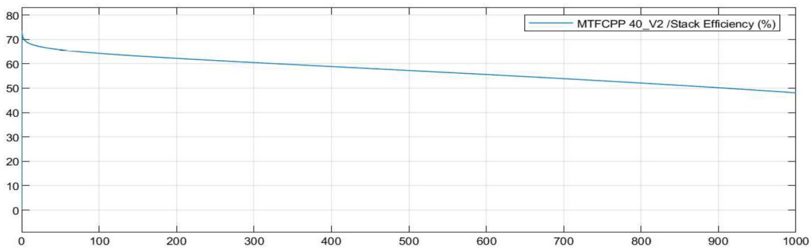

Figure 4.17: Efficiency curve of the MT-FCPP-40 simulink model

The lower the load, the more efficient the fuel cell operates. For the 10-XXL fuel cell, a minimum flow is defined of 56 L/min and since the MT-FCPP-40 consists of 4 10-XXL modules it is assumed that a minimum flow of 224 L/min is the limitations for the fuel cells max efficiency. Thus 230 L/min and 25 kW is used as minimal fuel cell power and the maximum is 4 times 120 nL/min thus 480 L/min max, resulting in 40 kW.

4.7. Battery Model

Similar to the fuel cell model, the MATLAB/Simulink, Simscape environment also has a built-in model for batteries that work very similar to the fuel cell model. The model requires input from a data sheet provided by a manufacturer and then mimics its behaviour. The battery type chosen was the LPF type lithium-ion battery that is capable of high power and is well known for its safety due to the high thermal runaway temperature making it ideal for maritime applications. A battery pack developed by LithiumWerks from the Valence series was selected and the product data-sheet is included in appendix D. In figure 4.18 the characteristics of the battery module is shown including the behaviour at different discharge currents.

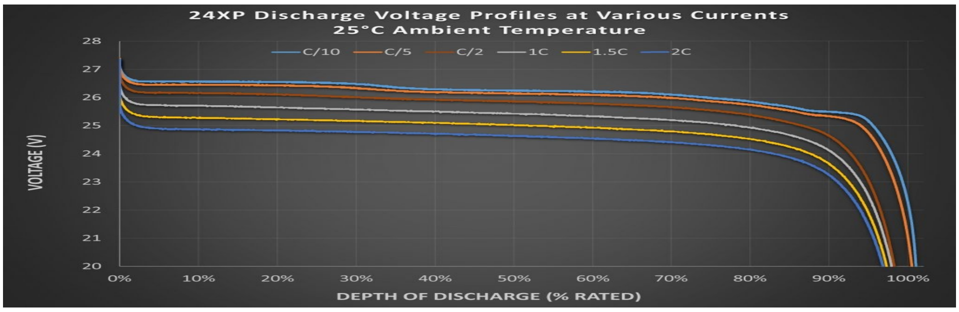

Figure 4.18: Characteristics of the Valence U-Charge U27-24XP LFP Battery, appendix D

Assuming a DC-bus voltage of 300V, a battery module of 13 parallels results in 299V. With 5 modules in series will result in 360A, resulting in energy storage 107 kWh. 1C thus results in only 107 kW of power, but the system can go to 2C according to figure 4.18 thus providing over 200 kW of power which is sufficient for the max power of the EM at 150kWe. The results of the MATLAB simulation for the battery module and the battery pack are illustrated in figure 4.19.

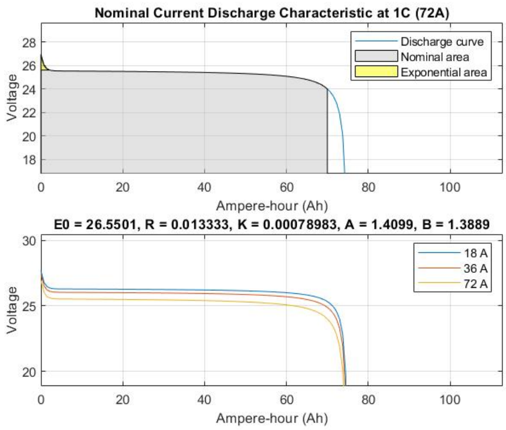

(a) The model of one single U27-24XP battery module

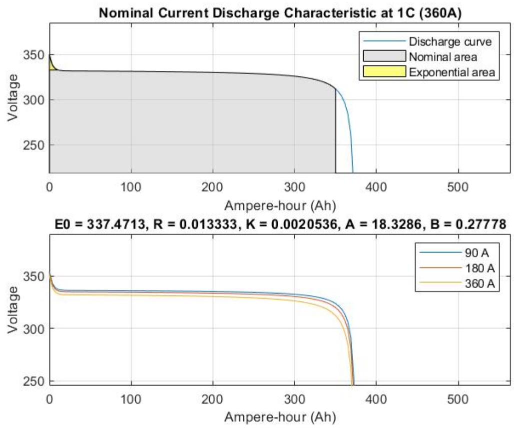

(b) The model of the combined U27-24XP battery package

Figure 4.19: The simulation of a single module and the 100 kWh battery pack

5
Analysis of Results

This chapter will evaluate and analyse the system using the developed model. This chapter is divided into four sections, First, the reactor and hydrogen production process using $NaBH_4$ is analysed, resulting in secondary control settings for fuel injection and a pressure safety mechanism. Then a sensitivity analysis is done on the half-life time of the reaction and the reactor size to asses if a deviation from the assumed ten minutes and 37L results in a significant change in the system dynamics.

Secondly, the Energy Management Strategies are evaluated and optimised for three operational profiles based on the measurements on a similar vessel and hydrodynamic analyses of the vessel. In this section a continuous hydrogen flow is assumed to evaluate the EMS system, assuming that the hydrogen production process works as required.

The third section integrates the hydrogen production process and the EMS and analyses different configurations for the propulsion system, varying the number of reactors and the use of a possible hydrogen buffer. Finally, the $NaBH_4$ system will be compared to other zero-emission alternatives such as compressed hydrogen and full battery electric so that the performance of the developed system can be discussed.

5.1. Hydrogen Production Process

In this chapter, the reactor performance is evaluated. First, the simulation method is defined by defining a test profile to test various characteristics of the reactor performance, assuming a half-life time of 10 minutes. Then the chosen control strategy for the reactor is evaluated based on varying the injection parameters to understand the effect that the control strategy has on the system. Then the effect of different reaction rates is evaluated since the reaction rate can vary depending on factors such as the amount of catalyst, reactor design, and temperature. Finally, the effect of the tank volume will shortly be discussed to understand the impact of changing reactor tank volumes.

5.1.1. Simulating method

The model that is used and the separate subsystems are described in chapter 4, this section will discuss the input used for the model as well as the different elements used for this simulation. The input used simulates various step function from and to a 40 and 20 kW demand. This is meant to simulate the most extreme behaviour of the reactor and will thus give a good indication on how the design will operate under various conditions, the input signal is given in 5.1.

The subsystems used for the reactor model are the power transformation block, the hydrogen production block and the fuel cell block. The green input block is also used to create the defined input, the model layout can be seen in figure 5.2. The fuel cell block is also used to help understand the system better, one of the reasons is because not all hydrogen delivered to the fuel cell will be used, another reason is that integrating the fuel cell block will help to determine the efficiency of the different settings.

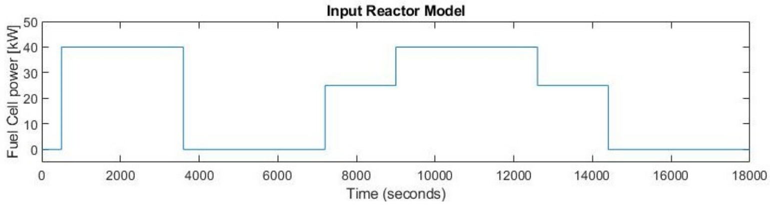

Figure 5.1: Test profile used for evaluation of the reactor model

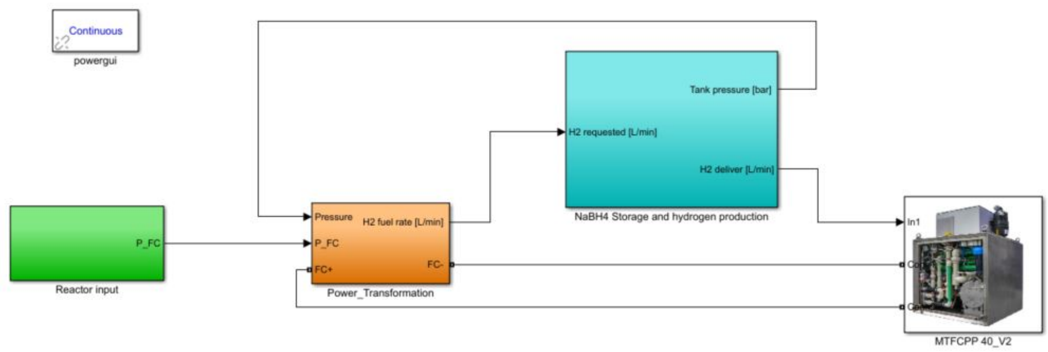

Figure 5.2: Lay out of the different subsystems used for simulating and evaluating the reactor performance.

5.1.2. Control Strategy

The reactor is controlled in three ways, first, the injection control determines how much fuel is added to the reactor, this determines in a large part the rise time of the system. Secondly is the flow control, when the pressure reaches a certain threshold, the system will release extra hydrogen to lower the pressure in the reactor, this leads to an excess of hydrogen production. Finally, there is the $NaBO_2$ discharge control, this system empties the reactor to prevent it from flooding. This section will discuss and illustrate the effects of these control systems as well as determine the optimal injection settings for a catalyst with an assumed half-life time of 10 minutes.

Injection Control

The fuel injection system determines at what interval and how much fuel should be added to the reactor to full fill the hydrogen demand and this determines the rise time. In figure 5.3 the third graph shows the injection time, the rise time can be found in the fourth graph and is realised when the H_2 supply flow has reached 99% of the H_2 demand flow.

Flow control

Second is the flow control, here the system determines how much hydrogen should flow to the fuel cell. If the pressure in the reactor gets too high, the flow control will also release hydrogen to the fuel cell, first at a steady flow at maximum efficiency, and if the pressure gets too low, in short burst so that the reactor slowly empties over time. This is done because the fuel cell has a rather high minimum power of 20 kW and thus small amounts of hydrogen would be wasted if channelled to the fuel cell, an example of these bursts can be seen in the fourth graph in figure 5.3. If the pressure gets even high on the other hand, the hydrogen flow increases as a function of the pressure, an example of this behaviour can be seen in figure 5.4. At around t=4000 a large increase in the H_2 delivered graph is caused by the high pressure in the reactor, as the pressure goes down, so does the hydrogen flow. As a result of this safety system in the flow control, there is an excess amount of hydrogen being produced. That is to say, more hydrogen is delivered to the fuel cell then it demands, this results in more power being delivered as well. There is no preventing this excess production due to the slow nature of the system and the unpredictability of the load. This excess power does not need to be a problem since it can be used to charge batteries, but it is something that the designer should be aware of when integrating the systems.

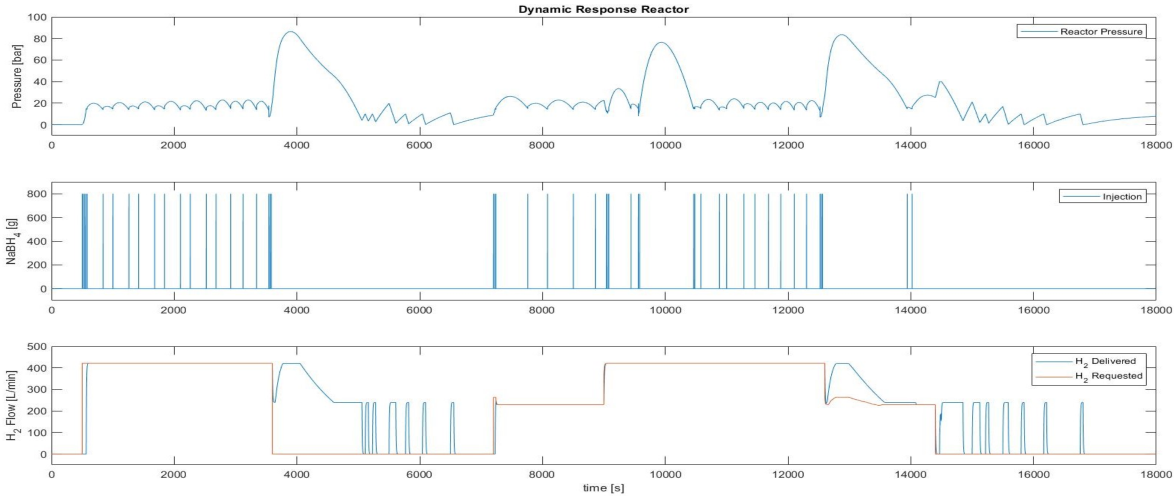

Figure 5.3: Dynamic response of the reactor system, using 800 grams of $NaBH_4$ injections with a 20 second interval.

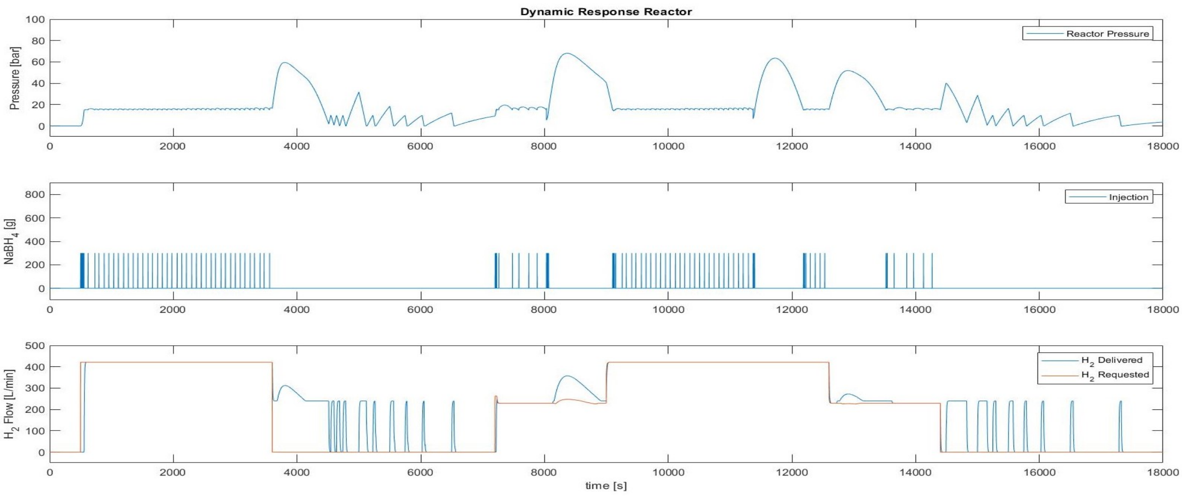

Figure 5.4: Dynamic response of the reactor system, using 300 grams of $NaBH_4$ injections with a 5 second interval.

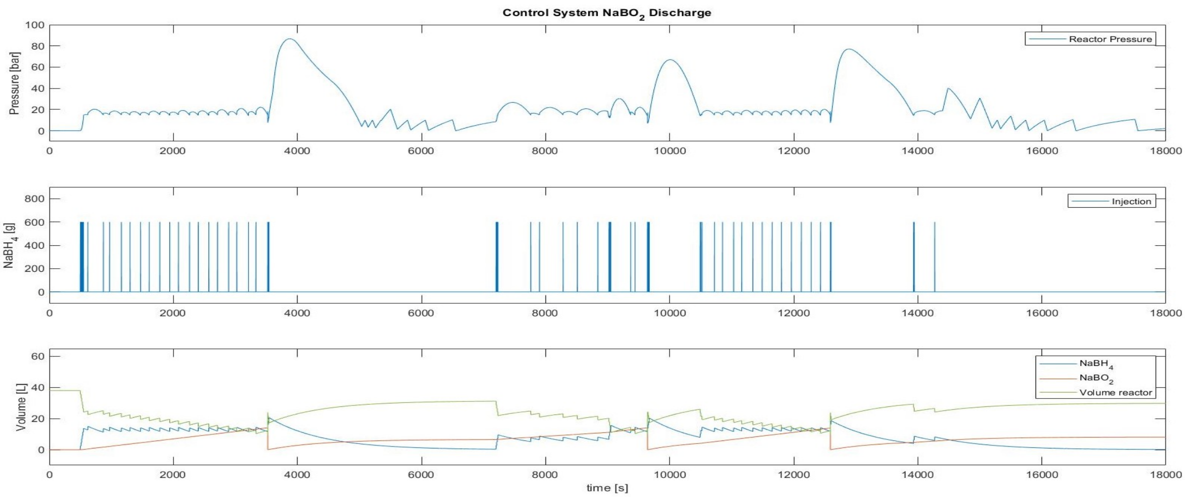

Figure 5.5: The change in volumes for the $NaBH_4$ and $NaBO_2$ solutions in the reactor during operations, injection is 600 gram with 10 seconds interval.

NaBO2 Discharge

As the hydrolysis reaction progresses, $NaBH_4$ becomes $NaBO_2$ and over time more $NaBH_4$ solution is added to the reactor chamber as well. Together this increases the liquid reactants in the chamber, leading to a decrease in volume for the H2 in gas form. To prevent flooding a simple discharge control system is implemented, if the solutions mixture has a volume of 20 litres, the amount of liquid coinciding with the amount of produced spent fuel is discharged through a valve. It is acknowledged that there is a risk of flushing usable $NaBH_4$ as well, however since $NaBO_2$ is much heavier it is assumed that it will gather at the bottom of the reactor. For the simulation, it is therefore assumed that no $NaBH_4$ is lost during discharge. It is however recommended that such a discharge system is further developed since it can impact the efficiency of the system quite drastically. The working of this discharge control system is illustrated in figure 5.5, in the third graph the different volumes can be seen, as well as the available gas volume for the hydrogen.

Optimising Injection Control

The injection control has two major parameters namely, the amount of $NaBH_4$ being injected and the interval of injection. The control algorithm automatically stops the injection as well based on the pressure in the reactor, however, this parameter was kept constant and is not further evaluated. Furthermore, the half-life time of the reaction was also assumed constant at 10 minutes, the effects of the half-life time will be evaluated in section 5.1.3. The goal of the optimisation was to evaluate the effect that the injection has on the system and to find the fastest rise time t_r. Three metrics are used to evaluate the behaviour, namely the rise time, the maximum pressure and the excess amount of hydrogen produced as a percentage of the requested amount. 28 simulations were executed and the results are shown in table 5.1.

		5 s			10 s			20 s			30 s	
	t_r	**Pressure**	**Excess**	**t_r**	**Pressure**	**Excess**	**t_r**	**Pressure**	**Excess**	**t_r**	**Pressure**	**Excess**
NaBH4 **200 g**	97 s	61 bar	15.9%	132 s	59 bar	14.2%	181 s	56 bar	12.3%	228 s	60 bar	9.7%
300 g	80 s	68 bar	16.1%	108 s	61 bar	15.4%	146 s	58 bar	13.5%	185 s	56 bar	12.6%
400 g	70 s	83 bar	20.1%	95 s	61 bar	15.3%	126 s	59 bar	14.2%	160 s	56 bar	12.9%
500 g	65 s	93 bar	20.2%	85 s	79 bar	18.7%	113 s	70 bar	17.2%	145 s	52 bar	15.4%
600 g	60 s	96 bar	23.6%	77 s	87 bar	22.2%	105 s	66 bar	16.9%	131 s	65 bar	15.2%
700 g	56 s	100 bar	23.4%	74 s	93 bar	21.4%	95 s	64 bar	15.6%	125 s	59 bar	15.7%
800 g	54 s	127 bar	24.2%	68 s	85 bar	21.9%	88 s	86 bar	21.9%	115 s	61 bar	15.3%

Table 5.1: Simulation results for various injection setting, the timing interval is tested for 5, 10, 20 and 30 seconds and the injection size is varied for 200-800 grams of $NaBH_4$ solved in water

Conclusion

The goal of the evaluation was to determine the effect of the control strategy on the dynamic performance of the reactor model. It became apparent that it is inevitable that an excess amount of hydrogen is produced due to the slow and unpredictable nature of the system. The amount of excess hydrogen is affected by the amount of $NaBH_4$ injected and the interval, the excess production increases with large injection input and small injection intervals. The excess production can be expected to be around between the 15% and 20% of the requested hydrogen flow. The excess production is a direct result from the safety system that increases the hydrogen flow when the reactor pressure reaches critical limits. From the simulation results, it can be concluded that in most cases the safety system works and the pressure does not reach higher than 100 bar. The only exceptions being the 700 and 800 gram injections with a 5 seconds interval, this is attributed to the huge increase in water and fuel in the tank, leading to a small volume for the hydrogen to be compressed in. Finally, the rise time is affected by the injection systems and can be increased to 80 seconds using a 5 second interval and a 300 gram $NaBH_4$ injection. This leads to a relatively small excess in hydrogen production of 16.1% and a maximum pressure of 68 bar. These settings will be used as the default for further analysis of the system.

5.1.3. Reaction Kinetics

As discussed in chapter 2.2.3 many factors can influence the half-life time of the reaction, therefore a half-life time of 10 minutes is assumed deviations are evaluated by running 8 simulations. The simulations used the 300 gram with 5 seconds interval setting as determined in 5.1.2. The results of these simulations can be seen in table 5.2, the same metrics of rise-time, maximum pressure and excess H_2 production are used as in section 5.1.2.

From the results, it can be concluded that the half life-time has a small impact on the rise time and a large impact on excess hydrogen production. This point is further illustrated in figure 5.6, 5.7 and 5.8, where system behaviour of an half-life time of 5, 10 and 15 minute is shown. The differences become especially apparent during the excess H_2 production at t=3600 to t= 7200 and from t = 12600 when the demand jumps from 40 kW to 25 kW.

Half life times [min]	Rise time	Max pressure	Excess production
2.5	55 s	75 bar	3.7%
5.0	66 s	76 bar	7.4%
7.5	75 s	60 bar	11.8%
10.0	80 s	68 bar	16.1%
12.5	85 s	63 bar	17.0%
15.0	90 s	83 bar	22.6%
17.5	95 s	64 bar	25.1%
20.0	97 s	92 bar	27.9%

Table 5.2: Simulation result for half life times from 2.5 to 20 minutes, using a 300 gram injection at a 5 seconds interval.

5.1.4. Reactor Volume

The reactor is still being developed and is therefore not optimised for the operations onboard the PoA vessel. In this section, the effects of changing the reactor volume are evaluated by simulating at 75% and 125% of the original 38 L reactor volume. From the results in table 5.3 and figures 5.9, 5.10 and 5.11 the result of these simulations are shown.

Enlarging the volume seems to have little advantages except for decreasing the excess production. Negative effects such as higher rise times are attributed due to the flow control settings that first create a buffer before allowing flow to ensure the correct functioning of the fuel cell. This buffer is based on reactor pressure so higher rise times are likely a result of a slow rise in pressure. The negative effect of reducing the reactor volume is the increase in required $NaBO_2$ discharges, this can lead to loss of $NaBH_4$ as discussed in section 5.1.2. Since volume is limited in ship design it is recommended that the reactor volume is further optimised for the required operations on board.

	Rise time	Pressure	Excess production	NaBO2 discharges
75%	78 s	58 bar	16.0%	6
100%	80 s	68 bar	16.1%	2
125%	89 s	84 bar	14.4%	2

Table 5.3: Simulation results for the effects of varying the reactor volume.

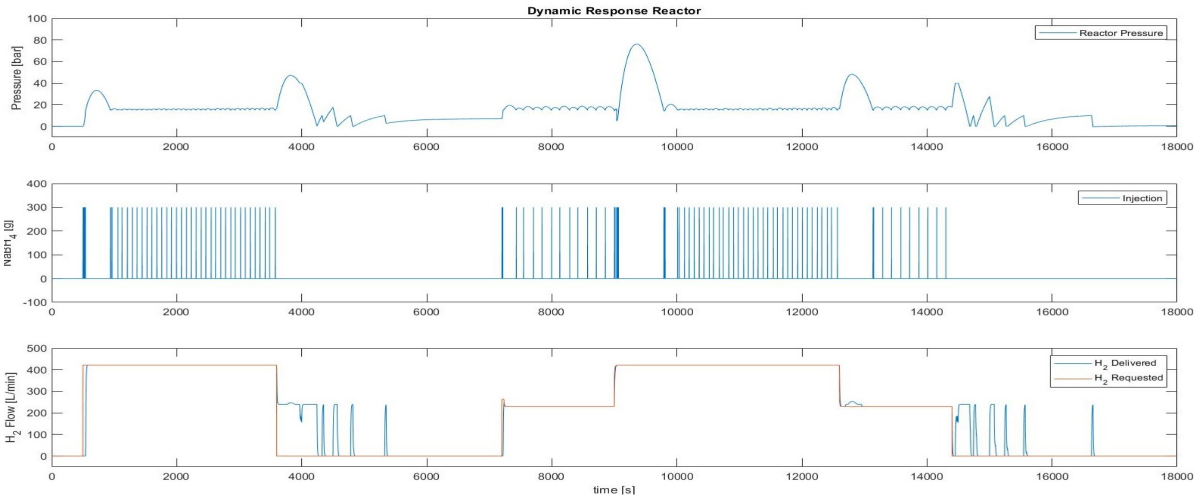

Figure 5.6: Dynamic response of the reactor system with a half life time of 5 minutes

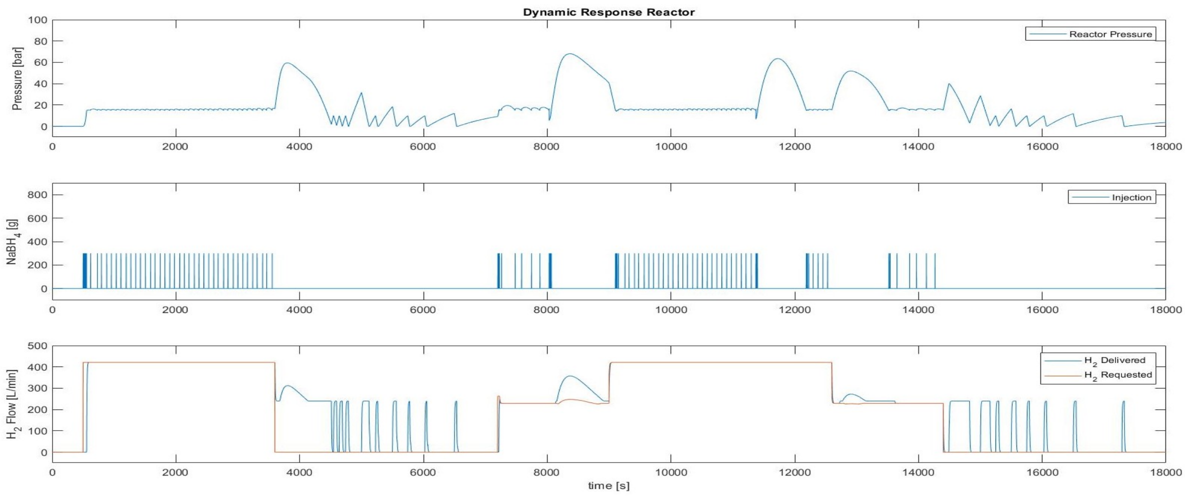

Figure 5.7: Dynamic response of the reactor system with a half life time of 10 minutes

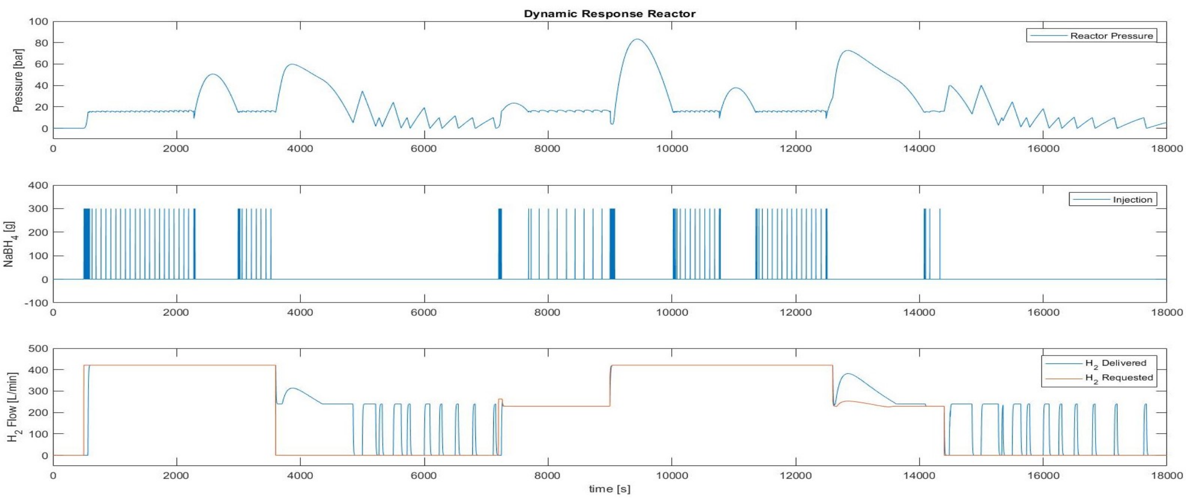

Figure 5.8: Dynamic response of the reactor system with a half life time of 15 minutes

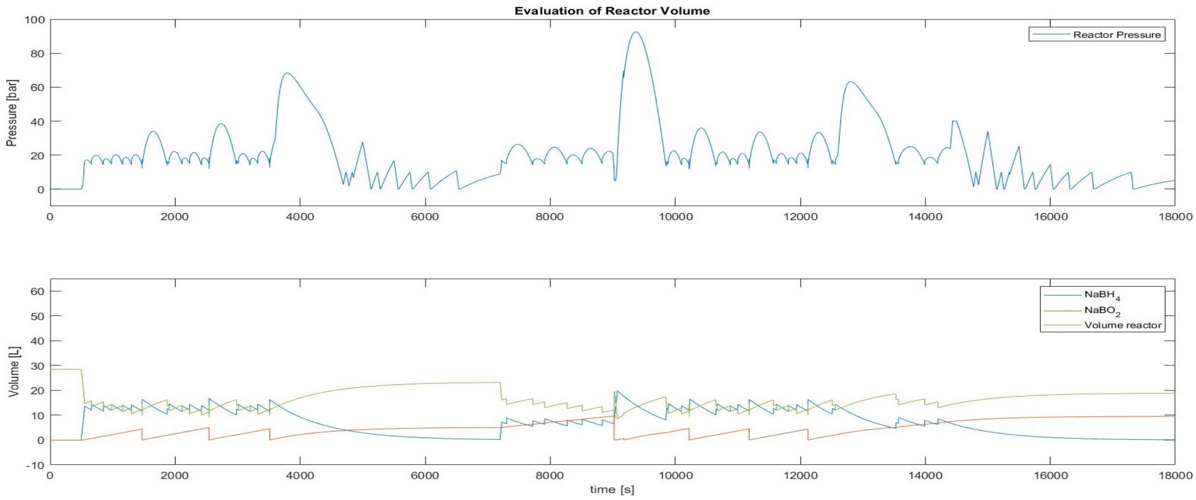

Figure 5.9: Simulation result for the effects of changing the reactor volume to 75%.

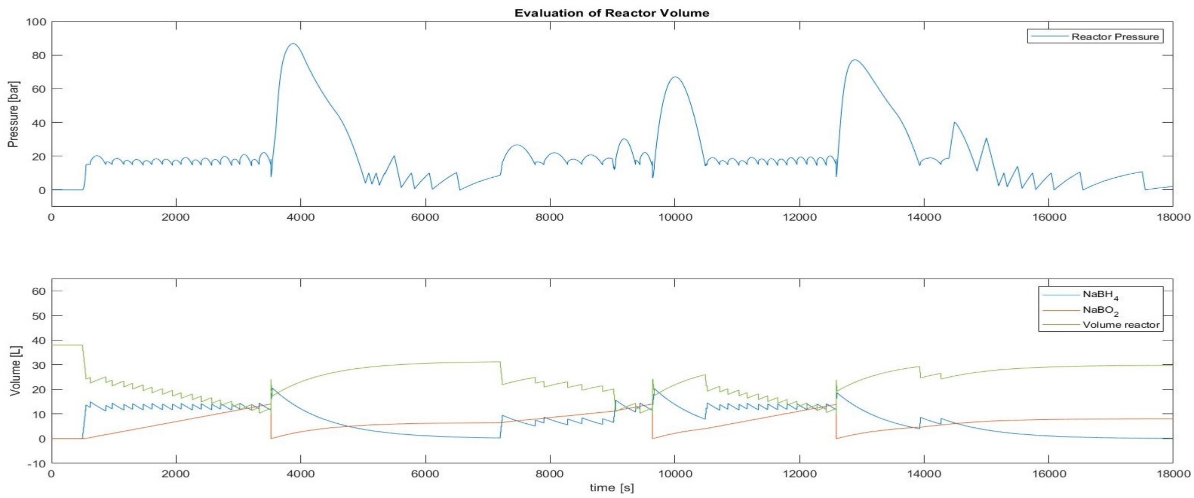

Figure 5.10: Simulation result for the original reactor volume of 38 L.

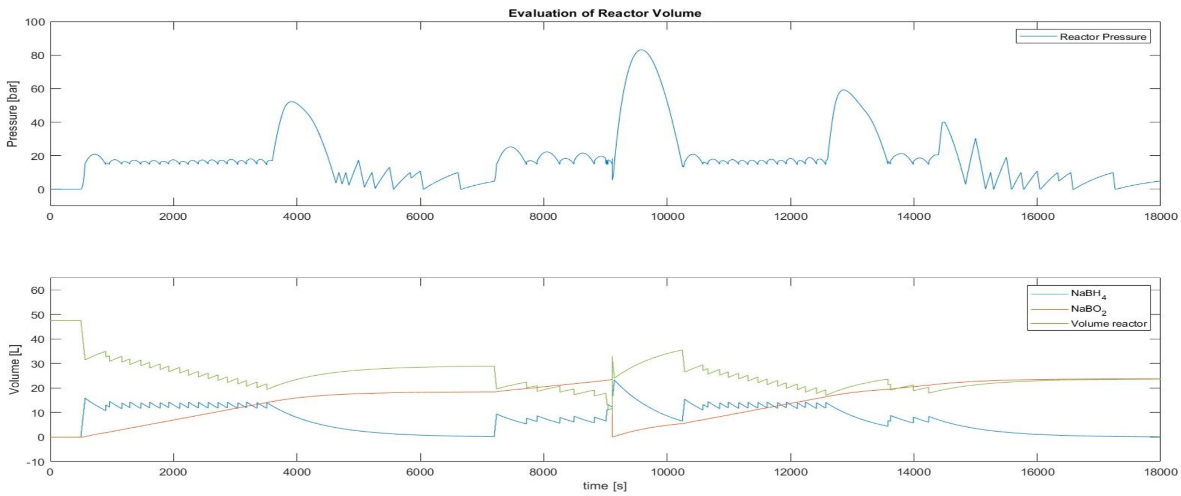

Figure 5.11: Simulation result for the effects of changing the reactor volume to 125%.

5.1.5. Conclusions

In this section, the hydrogen production model has been evaluated based on a generic power demand designed to test the limits of the system. As a result, the optimal settings for fuel injection were determined and are summarised in table 5.4. The effects of variables such as the half-life time and the reactor volume were evaluated. Also, the various graphs in the section illustrated the behaviour of the hydrogen production system and its' subsystems such as the flow control for safety and the discharge of the spent fuel. From these evaluations the following conclusions can be made:

- Injection control has a large impact on the rise time of the system.
- When properly tuned rise times of between one and two minutes can be expected for the hydrogen production.
- $NaBO_2$ discharge is required quite often and a suitable control system needs to be developed so that a minimum amount of $NaBH_4$ is lost when flushing the spent fuel, and normal operation is not disturbed significantly.
- A safety system in the flow control is required to ensure low pressure and will result in an excess H_2 production.
- A half-life time of 10 minutes is assumed, however, lower half-life times are expected. deviations in half-life time will have a large impact on the excess H_2 production and a small impact on the rise time. With lower half-life times leading to smaller rise times and excess production, and high half-life times leading to larger rise times and excess production.
- Reactor volume and thus system volume could be reduced without too many negative effects.

Variable	Explanation	Setting
NaBH4 injecction	The injection of NaBH4 determines for a large part the start up time of the reactor.	300 g, 10 sec
Min pressure for start flow	The pressure is kept at a constant level in order to deal with sudden load changes.	15 bar
Pressure relieve window	When the pressure becomes too high the load is increased from minimum to maximum fuel cell power depending on the pressure window.	40-80 bar

Table 5.4: Control setting used for the batch reactor model

5.2. Energy Management Strategy

This section will evaluate the hybrid behaviour of the PoA vessel under different energy management strategies (EMS). A continues supply of hydrogen is assumed and a configuration using a 60 kW fuel cell and a 100 kWh battery pack is used. Based on the analyses a suitable EMS is chosen and the fuel cell and battery are sized for the integrated model in section 5.3.

5.2.1. Simulation Method

The three different Energy Management Systems that are simulated have also been explained in chapter 2 and 4 but will be shortly summarized here. EMS 1 and 2 are state-based strategies using rules based on the SOC state of the battery as defined in table 5.5. EMS 1 is a discrete function using either the maximum efficiency or maximum power setting of the FC. EMS 2 uses a function inspired by the penalty coefficient of the ECMS as found in the literature and is defined in equation 5.1. EMS 3 uses a PI controller with an anti-windup and a reference value of 40 % SOC.

	State based Discrete		State based continuous	
	Pbatt	Pfc	Pbatt	Pfc
SOC >= 40	Pload	0	Pload	0
30 <SOC <40	Pload - Pfc_min	Pfc_min	Pload - Pfc(SOC)	Pfc(SOC)
SOC <= 30	Pload - Pfc_max	Pfc_max	Pload - Pfc(SOC)	Pfc(SOC)

Table 5.5: Heuristic rules for EMS 1 and EMS 2

$$P_{FC}(SOC) = P_{FC,min} + \frac{SOC_{high} - SOC}{SOC_{high} - SOC_{low}} \cdot (P_{FC,max} - P_{FC,min}) \tag{5.1}$$

In figure 5.12 the different subsystems used in the EMS simulation are shown. These subsystems include the fuel cell block, the battery block, three different EMS systems, two different power transformation blocks and the input block. The battery output is put in series with the fuel cell so that the required load will always be delivered, even if the fuel cell produces more or less power then required. The workings of the different blocks and the underlying assumptions and methods are elaborated on in chapter 4.

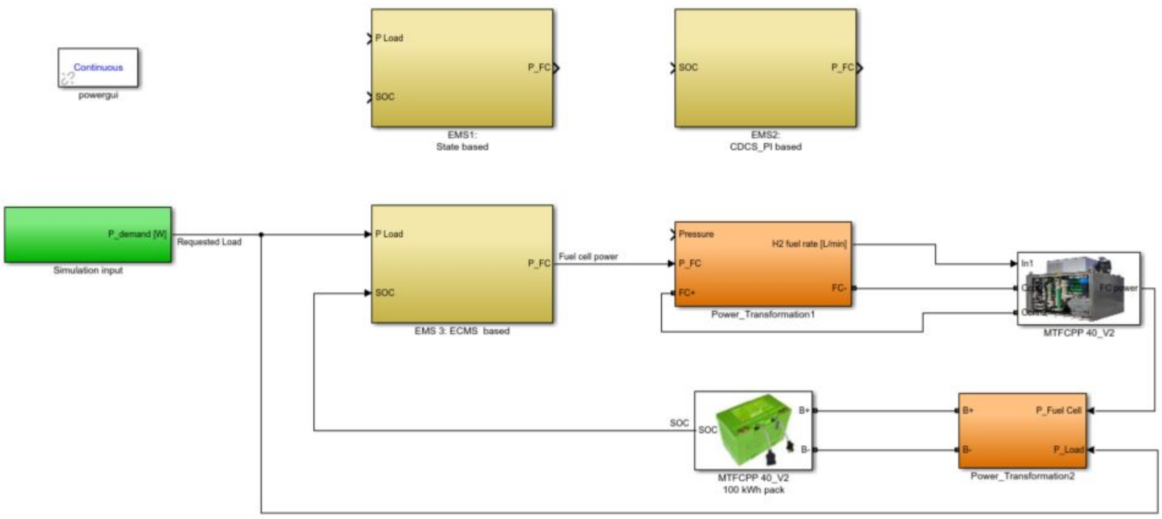

Figure 5.12: Lay out of the different subsystems used for evaluating the Energy Management Strategies

5.2.2. Comparison EMS

The three EMS systems are simulated using the three operational profiles an evaluated on H_2 consumption, FC efficiency, minimum SOC, maximum C-rate and the start/stop cycles of the fuel cell. The different behaviour of the three systems is illustrated in figure 5.14 and the simulation results are summarised in table 5.6.

The classical PI strategy performed poorly over all three profiles with low efficiency and the highest hydrogen consumption. The two state-based strategies performed similar to the discrete system being more efficient on profile A and B, and the continuous system being more efficient on Profile C.

Overall three profiles the continuous system provided the lowest fuel consumption. The discrete system had one less stop cycle but does have very sudden changes in the fuel cell power that could also potentially harm the fuel cycles lifetime. Therefore it is concluded that the continuous EMS system is the best suitable option.

		State based continuous	State based discrete	Classical PI
Profile A	H2 consumption [kg]	1.84	1.72	3.11
	Average FC efficiency	54.04%	54.71%	48.23%
	Min SOC	35.40%	34.87%	25.77%
	C-rate max	0.70	0.70	1.03
	Start/stop	2	2	1
Profile B	H2 consumption [kg]	5.32	5.19	3.49
	Average FC efficiency	53.97%	54.69%	49.50%
	Min SOC	33.86%	30.02%	31.43%
	C-rate max	0.64	0.69	0.7
	Start/stop	2	2	2
Profile C	H2 consumption [kg]	19.96	20.55	21.33
	Average FC efficiency	52.52%	51.41%	49.80%
	Min SOC	31.38%	29.06%	23.36%
	C-rate max	0.78	0.69	1.03
	Start/stop	2	1	6

Table 5.6: simulation results with a 100 kWh battery and a 60 kW fuel cell.

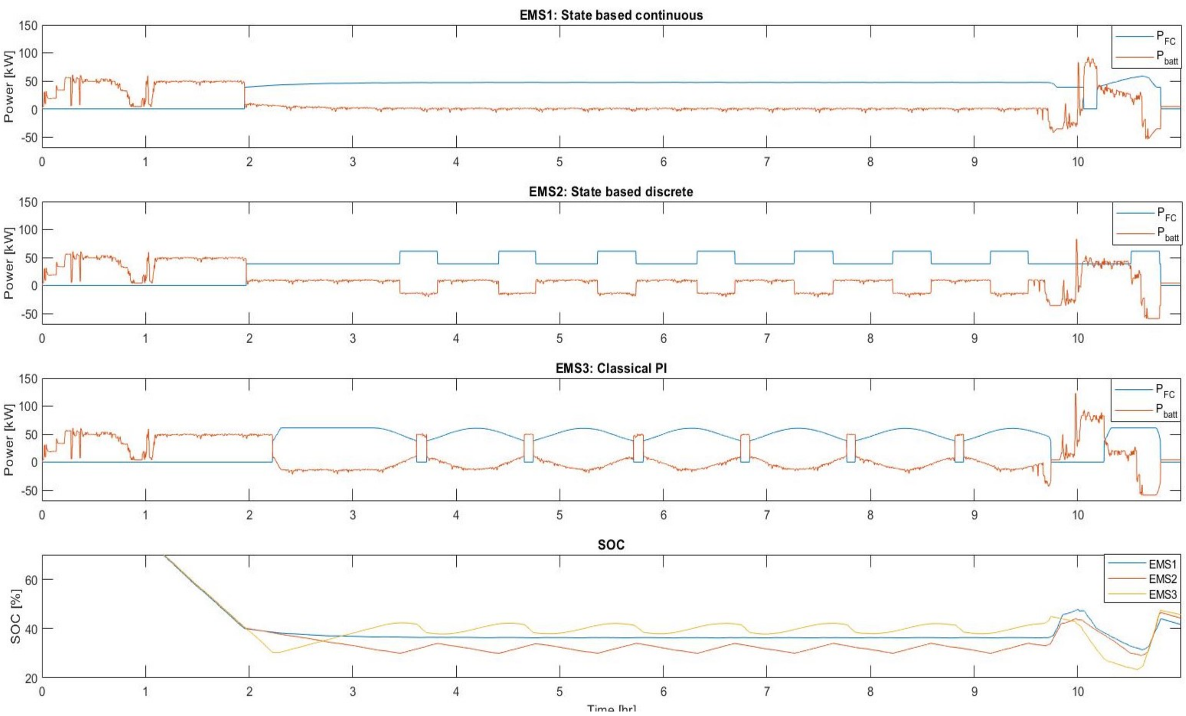

Figure 5.13: Simulation results for operational profile C using a 100 kWh battery pack and a 60 kW fuel cell.

5.2.3. Configuration

Different configurations of battery capacity and fuel cell power are considered. The state-based continuous EMS system is used. The SOC settings of this EMS system, the window between SOC high and SOC low, is adapted to maintain sufficient SOC, especially during operational profile C. In table 5.7 the simulation results for four configurations are shown. The first configuration uses a 60 kW fuel cell and analyses the effect of a smaller battery pack, the other three configurations use a 40 kW fuel cell with varying battery packs. Configuration 4 assumes some a-priori knowledge about the route that allows the EMS system to be turned off to sail solely on the battery power, called 'Battery mode'.

The results show that a smaller battery pack is feasible but only if a 60 kW fuel cell is used. In this configuration more hydrogen thus $NaBH_4$ is required, resulting in more operational costs. Configuration 2 and 3 show that a 100 kWh battery pack is insufficient for operational profile C when a 40 kW fuel cell is used, even with the SOC setting up to 70 and 50%. A 150 kWh battery pack, however, is sufficient, but for feasible operations, the EMS settings need to be very high.

To prevent unnecessary consumption of hydrogen a 'Battery mode' is proposed in configuration 4. When the captain is aware of the route beforehand, he/she can engage a battery-only mode and turn the fuel cell and hydrogen production process off. The battery pack, in this case, is sufficient for a tour around the Amsterdam canals and the EMS settings can be optimised for maximum range.

		Configuration 1	Configuration 2	Configuration 3	Configuration 4
	Battery / Fuel cell	50 kWh / 60 kW	100 kWh / 40 kW	150 kWh / 40 kW	150 kWh / 40 kW
	EMS SOC settings	40-30	70-50	70-50	70-50 and 0
Profile A	H2 consumption [kg]	4.99	3.88	3.06	0
	Average FC efficiency	52.36%	52.46%	52.58%	0
	Min SOC	20.72	54.56%	58.69%	27.95%
	C-rate max	2.62	1.03	1.02	1.02
	Start/stop	5	5	3	0
Profile B	H2 consumption [kg]	8.22	7.07	6.085	6.085
	Average FC efficiency	53.26%	51.09%	51.35%	51.35%
	Min SOC	23.26%	48.25%	52.84%	52.84%
	C-rate max	2.61	0.75	0.74	0.74
	Start/stop	5	2	1	1
Profile C	H2 consumption [kg]	22.39	20.61	19.59	19.59
	Average FC efficiency	52.32%	48.06%	48.28%	48.28%
	Min SOC	23.43%	15.00%	29.74%	29.74%
	C-rate max	2.61	0.67	0.67	0.67
	Start/stop	3	1	1	1

Table 5.7: Simulation results for different configurations and EMS settings

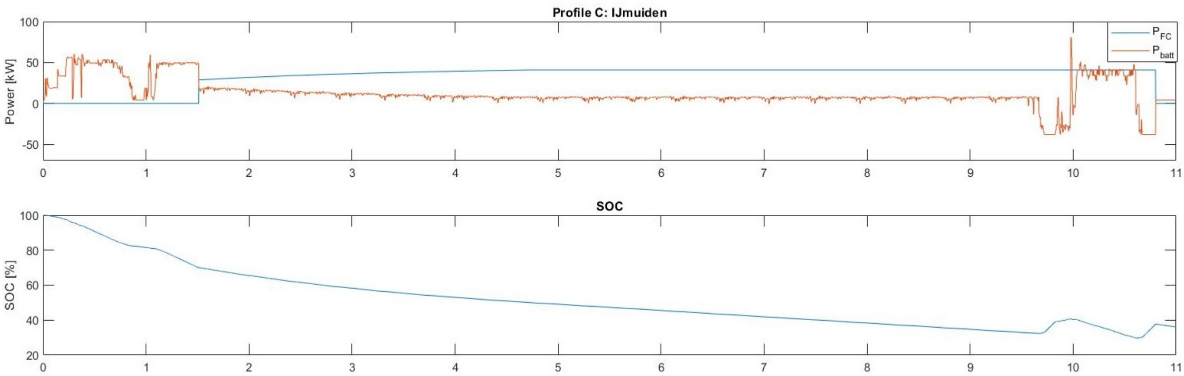

Figure 5.14: Simulation results for operational profile C using a 150 kWh battery pack and a 40 kW fuel cell.

5.2.4. Conclusions

In this section different Energy Management Strategies (EMS) have been evaluated based on three real-life operational profiles. As a result, an EMS was chosen and tuned for the required operational profiles leading to the desired EMS behaviour over all three profiles by minimising the fuel cell start/stop cycles and maintaining a minimum SOC level of 30 %. Also, various graphs show the behaviour of the EMS systems and the ability of these systems to follow the requested loads without reaching dangerous C-rate levels.

Different configurations for the fuel cell and battery pack were also considered, resulting in a 150 kWh battery pack and a 40 kW fuel cell. Also, a 'Battery mode' is suggested that allows the vessel to sail on batteries only when the route is known beforehand by the captain. From the evaluation of various operational profiles and the EMS systems the following conclusions can be made:

- A 150 kWh battery system is sufficient for a battery-electric tour of the canals in Amsterdam.
- A fuel cell of 60 kW would be ideal to sustain the battery charge, however, 40 kW is sufficient when an appropriate EMS is used.
- The state base continuous EMS is capable of delivering the requested loads and maintaining a minimum SOC of 30% over the given operational profiles.
- Some a priori knowledge needs to be provided using human-machine interaction to use the battery hydrogen system effectively when operating in a small range.
- C rates have stayed between the acceptable norms with mostly staying below the 1 C requirement of low power batteries, only under configuration 1, a maximum of 2.6 C was observed.
- Between bunkering trips a minimum of 20-25 kg H_2 is required depending on the configuration.

Because the power density of the fuel cell and hydrogen reactor is low, a 40 kW fuel cell is preferred over a 60 kW fuel cell. It is therefore recommended that configuration 4 is implemented for the Port of Amsterdam's vessel, using a 150 kWh battery pack, a 40 kW fuel cell and introducing a 'Battery mode' for short trips with low power requirements.

5.3. Integrated Design

In this section the results and conclusions from the previous two models are used to design and evaluate two setups for the complete $NaBH_4$ fueled propulsion system. The most important conclusion from section 5.1 and 5.2 is that a better system is required for rinsing the reactor from spent fuel. The previous system of simply emptying the tank when a certain level is reached results in significant loss of $NaBH_4$ since typically the injection of new $NaBH_4$ solution would trigger the level indicator and thus flush out the solution without giving it time to react and release hydrogen.

To combat this problem four configurations are evaluated, the first configuration is using one reactor and expanding the control system of the reactor so that a more elaborate rinse cycle is included, the second configuration adds a hydrogen buffer to equalize the hydrogen output. The third configuration uses two reactors so that the hydrogen production can be shared and a more continues process is realised. Finally, a configuration using two reactors and an extra hydrogen buffer was used to give the reaction more time and thus utilise more $NaBH_4$ during the rinse cycle.

5.3.1. Configuration A: Single Reactor

First, the feasibility of a configuration using one reactor and an elaborate rinse cycle is evaluated. The rinse cycle starts after 30 injections of 300 grams $NaBH_4$ and the matching amount of water, at this point there will be a maximum of 20 L of spent fuel in the 37 L reactor tank. The rinse cycle starts with 10 minutes of reaction time where the $NaBH_4$ left in the reactor has time to react, during this time the fuel cell works at maximum efficiency, only rising when the pressure in the tank is above 60 bar. The second part of the rinse cycle starts with discharging the leftover $NaBH_4$ solution and the spent fuel, followed by 5 minutes of actual rinsing and cleaning the reactor. The rinse cycle is illustrated in figure 5.15 where the integrated system is simulated over 2.5 hours while under a 40 kW load. The control settings as introduced in section 2.2 are elaborated with the rinse cycle settings as in table 5.8

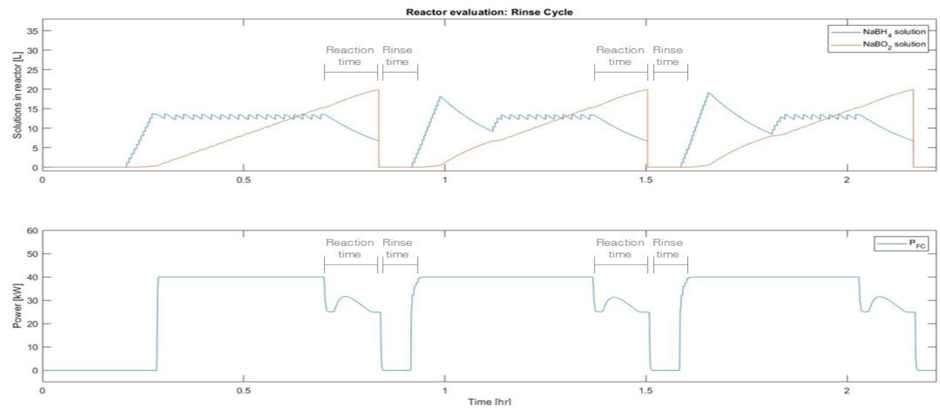

Figure 5.15: Overview of the 15 minute rinse cycle while under a 40 kW load.

Variable	Explanation	Setting
NaBH4 injecction	The injection of NaBH4 determines for a large part the start up time of the reactor.	300 g, 10 sec
Min pressure for start flow	The pressure is kept at a constant level in order to deal with sudden load changes.	15 bar
Pressure relieve window	When the pressure becomes too high the load is increased from minimum to maximum fuel cell power depending on the pressure window.	40-80 bar
Start rinse cycle	The rinse cycle for cleaning starts when the reactor is almost full.	30 injections
Reaction time rinse cycle	After the rinse cycle starts, some time is given for the left over NaBH4 to react.	10 min
Cleaning time rinse cycle	Some time is required for cleaning the inside of the reactor after all the spent fuel is flushed out.	5 min

Table 5.8: Control setting used for the batch reactor model with integrated rinse cycle.

		Profile A	Profile B	Profile C
Config A	NaBH4 Consumption [kg]	0.00	34.20	113.10
	Spent Fuel [L]	0.00	81.00	254.80
	Water required [L]	0.00	77.00	242.40
	Lost NaBH4 [%]	0.00%	11.40%	17.39%
	Min SOC [%]	27.95%	49.76%	18.44%
	Start/ Stop Cycles FC	0	4	15
		Profile A	Profile B	Profile C
Config A2	NaBH4 Consumption [kg]	0.00	45.00	146.90
	Spent Fuel [L]	0.00	106.00	339.00
	Water required [L]	0.00	100.80	322.40
	Lost NaBH4 [%]	0.00%	12.01%	14.03%
	Min SOC [%]	27.95%	50.43%	28.38%
	Start/ Stop Cycles FC	0	1	1

Table 5.9: Simulation results for configuration A, using one reactor and a rinse cycle, and A2 using a 200L hydrogen buffer.

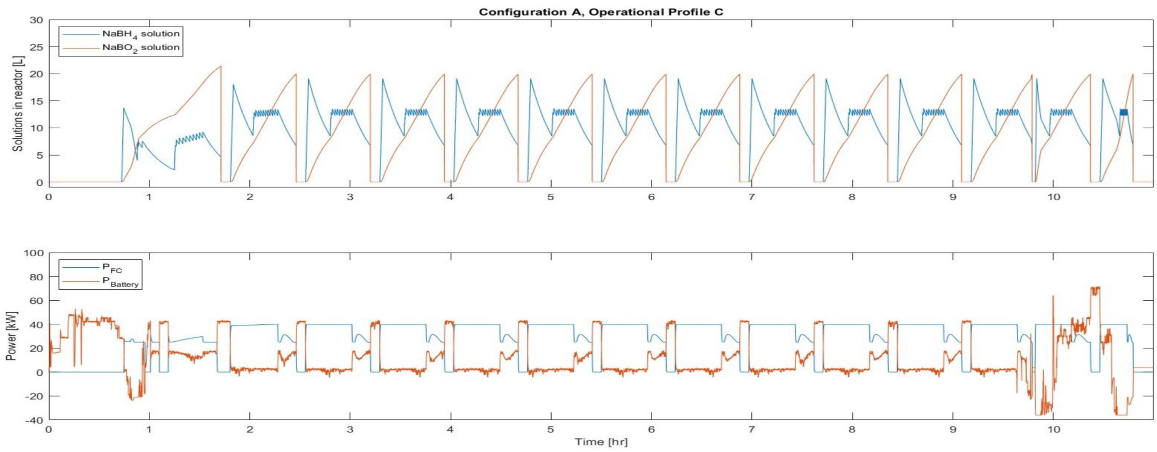

Figure 5.16: Simulation results of configuration A, with operational profile C

Hydrogen buffer

To overcome the offline periods as a result of the rinse cycle, a 200 L hydrogen buffer was used. In table 5.9 the simulation results for this configuration is shown. The injection controls were adapted to obtain more hydrogen in the buffer during the offline periods. Now, all the $NaBH_4$ is injected at once and the reaction time was optimised to be as long as possible without interrupting the hydrogen supply. Also, the flow control is no longer on the reactor, instead, it is on the buffer with all the hydrogen from the reactor being pumped into the buffer immediately. The control settings used are summarised in table 5.10

The results show that a configuration with one reactor and a buffer is feasible and can achieve an acceptable minimum SOC level. On the other hand, the percentage of lost $NaBH_4$ is still significant at around 14%, furthermore, the pressure becomes pretty high as illustrated in figure 5.17 and this might result in a large high-pressure vessel. Simulations with a smaller half lifetime of 5 minutes instead of 10 show that the reaction has enough time and only 2% of $NaBH_4$ is lost. The high-pressure problem could be mitigated with better control but pressures of around 80 bar are still required to maintain enough hydrogen though. Shortening the rinse cycle time of 5 minutes could result in a lower hydrogen demand and therefore result in a lower pressure in the buffer.

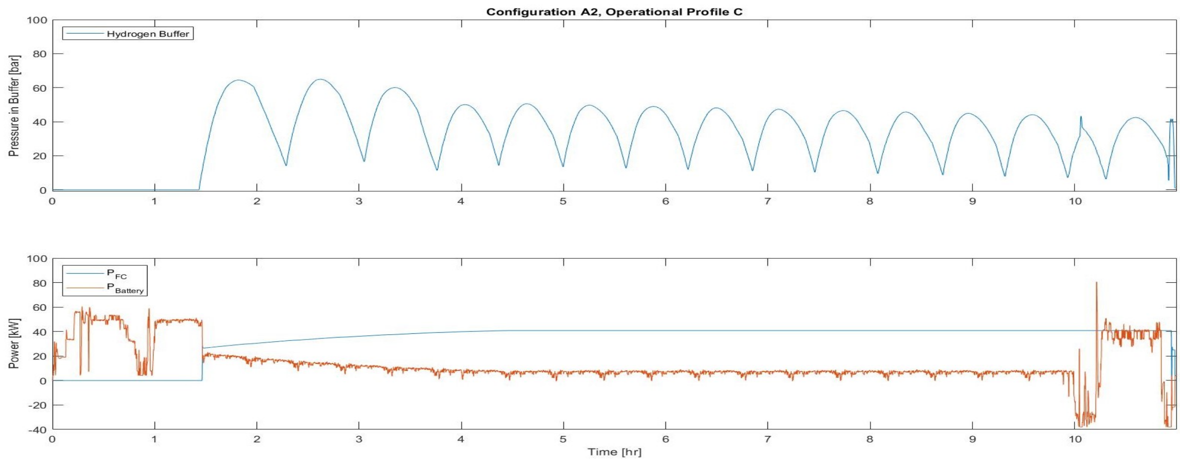

Figure 5.17: Simulation results of configuration A2 for operational profile C with a 200L hydrogen buffer

Variable	Explanation	Setting
NaBH4 injecction	The injection of NaBH4 determines for a large part the start up time of the reactor.	9 kg
Min pressure for start flow	The pressure is kept at a constant level in order to deal with sudden load changes.	10 bar
Start rinse cycle	The rinse cycle for cleaning starts when the reactor is almost full.	1 injection
Reaction time rinse cycle	After the rinse cycle starts, some time is given for the left over NaBH4 to react.	27.5 min
Cleaning time rinse cycle	Some time is required for cleaning the inside of the reactor after all the spent fuel is flushed out.	5 min

Table 5.10: Control setting used for the batch reactor model when using a hydrogen buffer and one reactor

5.3.2. Configuration B: Multiple Reactors

In the previous section, it became apparent that utilising one reactor for the H_2 production from $NaBH_4$ is unfeasible unless the fuel cell and reactor installed power is increased. So instead, a configuration using two reactors is examined so that a semi-continues flow can be realised and the EMS can function as tested in section 5.2.

Combining Flows

When using two reactors the two flows need to be combined and some additional control rules need to be made to ensure safe operation of the reactor vessel, and the leftover reactants of the $NaBH_4$ solution need to be used efficiently. To achieve these goals the reactor on/off control dictates that a second reactor goes online when the first reactor fails to meet 90% of the hydrogen flow demand. Since the first reactor is then still producing hydrogen, this flow is subtracted from the second reactor to ensure efficient use of the hydrogen. However, if the pressure becomes too high in the second reactor, this subtraction is overruled by the original safety mechanism of increasing the hydrogen flow to ensure safe pressure.

The behaviour as described can be seen in figure 5.18, where the hydrogen flow of the first reactor slowly decreases as a function of the reactor's pressure, and the second reactor's hydrogen flow slowly increases until it is overruled and a 'hump' is seen as a result of the high pressure in the reactor. The second graph of the figure shows the combined flow and the irregularities that result from the slightly delayed operations and the safety mechanism. At the 'humps' the hydrogen flow exceeds the maximum capacity of the fuel cell and thus some hydrogen is lost. On the other hand, the reaction time part of the rinse cycle could be increased from 10 minutes to 15 minutes, resulting in less loss of $NaBH_4$ during the discharge cycle. The simulations results for this configuration are shown in table 5.11

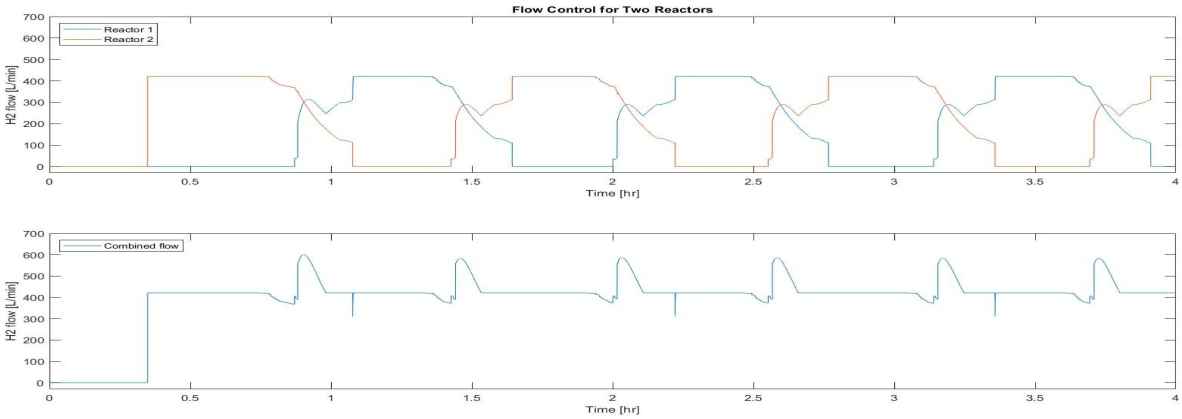

Figure 5.18: Flow control for configuration B under a 40 kW load

		Profile A	Profile B	Profile C
Config B	NaBH4 Consumption [kg]	0.00	51.60	186.30
	Spent Fuel [L]	0.00	127.50	443.30
	Water required [L]	0.00	155.30	560.00
	Lost NaBH4 [%]	0.00%	9.49%	13.01%
	Min SOC [%]	27.95%	53.46%	36.53%
	Start/ Stop Cycles FC	0	2	2
Config B2	NaBH4 Consumption [kg]	0.00	42.60	126.00
	H2 in buffer left [kg]	0.00	0.78	0.80
	Spent Fuel [L]	0.00	114.20	336.80
	Water required [L]	0.00	128.00	379.10
	Lost NaBH4 [%]	0.00%	1.70%	2.40%
	Min SOC [%]	27.95%	51.25%	27.75%
	Start/ Stop Cycles FC	0	3	3

Table 5.11: Simulation results for configuration B, using two reactors, and B2, using two reactors and a 100L buffer

Hydrogen Buffer

To smooth out the irregularities caused by the flow management between two reactors and to utilise the otherwise lost overproduction of hydrogen due to the safety mechanism, a hydrogen buffer is proposed. A hydrogen tank of 100 L is assumed, in figure 5.19 the effect of the hydrogen buffer on the hydrogen flow is shown. Only during the first cycle, when the buffer is still empty, the hydrogen supply drops, during the following cycles the buffer ensures constant flow. Furthermore, due to the efficient use of overproduced hydrogen, the reaction time of the rinse cycle can be increased further to 40 minutes, ensuring a very low loss of $NaBH_4$ during the rinse cycle. If the half-life time of the catalytic reactors is lower then the now assumed 10 minutes, a near-complete reaction might be even possible. The results for configuration B2, including the hydrogen buffer is shown in table 5.11 and for operational profile C in figure 5.20. The control settings used for this configuration are summarised in table 5.12.

Variable	Explanation	Setting
NaBH4 injecction	The injection of NaBH4 determines for a large part the start up time of the reactor.	300 g, 10 sec
Min pressure for start flow	The pressure is kept at a constant level in order to deal with sudden load changes.	15 bar
Pressure relieve window	When the pressure becomes too high the load is increased from minimum to maximum fuel cell power depending on the pressure window.	40-80 bar
Start rinse cycle	The rinse cycle for cleaning starts when the reactor is almost full.	30 injections
Reaction time rinse cycle	After the rinse cycle starts, some time is given for the left over NaBH4 to react.	40 min
Cleaning time rinse cycle	Some time is required for cleaning the inside of the reactor after all the spent fuel is flushed out.	5 min

Table 5.12: Control setting used for the batch reactor model when using two reactors and a buffer

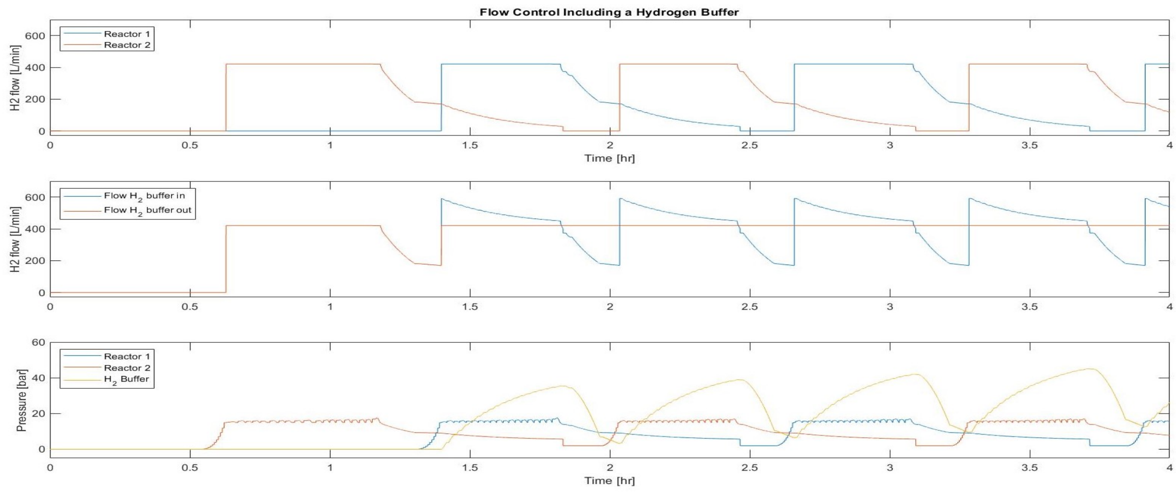

Figure 5.19: Flow control for configuration B2 under a 40 kW load, and including a 100 L hydrogen buffer

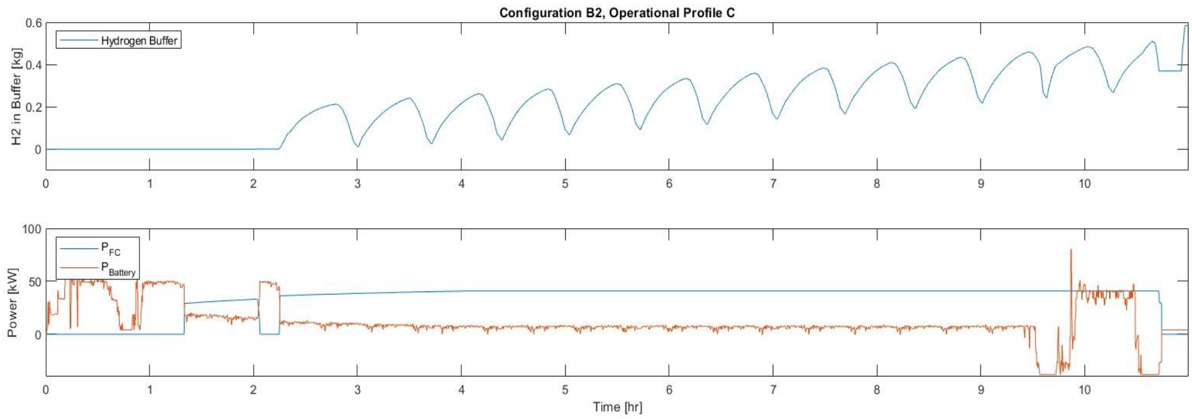

Figure 5.20: Simulation results for profile C, configuration B2 with a 100 L hydrogen buffer, a 150 kWh battery and 40 kW FC

5.3.3. Conclusion

In this section, various configurations for the $NaBH_4$ powered propulsion system has been evaluated using Simulink modelling aiming to find a feasible solution for the three operational profiles of the Port of Amsterdam's vessel. It was found that even though some $NaBH_4$ was lost, a configuration using one reactor and a low-pressure hydrogen buffer of 200 L is a feasible solution for the PoA vessel.

- When using two reactors, the safety measures that regulate the pressure in the reactors results in an excess hydrogen production that has to be discarded if no buffer is used.
- A hydrogen buffer is required to ensure a continues flow, furthermore, the use of a buffer can increase the efficiency since more time is available for the completion of the hydrolysis reaction of the $NaBH_4$ solution.
- A configuration with one reactor and a buffer minimises volume but due to the slow reaction speed, some fuel is lost.
- Between bunkering trips a minimum of 130 kg of $NaBH_4$ is required and a minimum spent fuel tank of 350 L.
- During operational profile C a total of 380 L water needs to be produced, adding an estimated 3.8 kWh to the energy balance, assuming 0.01 kWh per L using reverse osmosis [30].

5.4. Comparison Alternatives

In the previous section, a feasible configuration for the $NaBH_4$ system was realised using a small hydrogen tank, one reactor, a fuel cell, and a battery pack. In this section, the configuration is compared to alternative zero-emission options such as conventional hydrogen storage under pressure and a full battery-electric system. The volume and weight estimation of the system components can be found in table 5.14 and in figure 5.21 the total system requirements for three systems are compared.

Furthermore, in table 5.13 the gravimetric and volumetric, power and energy densities are summarised. It is clear that the energy density of the $NaBH_4$ system is very high, however, the power density is low, resulting in a low overall system density of 103 Wh/L and 114 Wh/kg. This is still in line with other fully developed alternatives such as battery and compressed hydrogen systems. This scenario, however, is based on a maximum range of one trip to IJmuiden of around 10 hours. When refuelling between trips is not desired, the range can easily be increased. For a 100 hour range, for example, the system density could be as high as 555 Wh/L and 577 Wh/kg. In figure 5.22 the different systems are compared when a 100h range is desirable, it can be concluded that in this case the $NaBH_4$ solution has a significant advantage over traditional solutions.

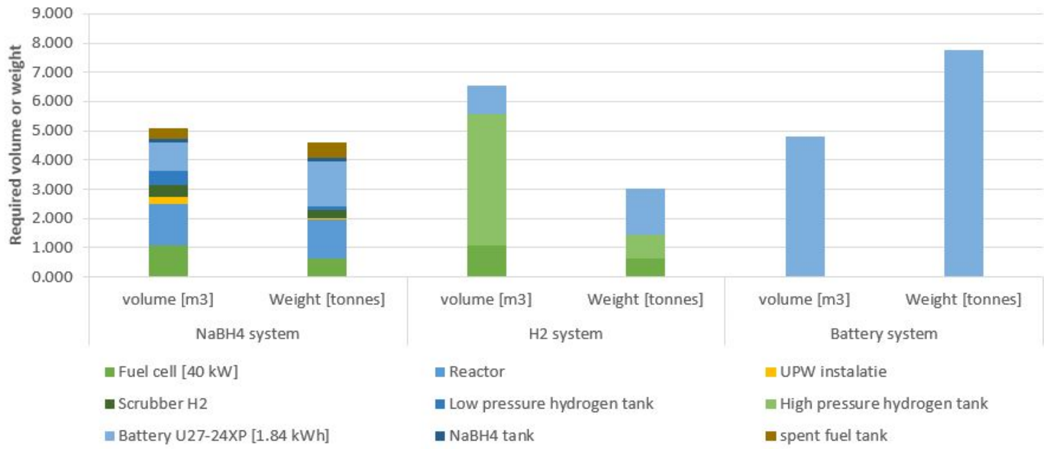

Figure 5.21: Volume and weight estimations for different zero emission systems for a 10 hour range.

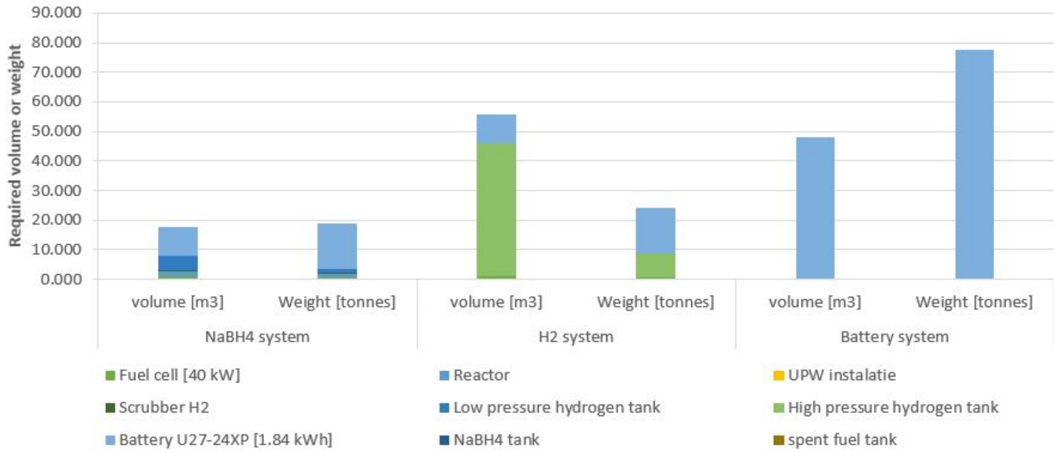

Figure 5.22: Volume and weight estimations for different zero emission systems for a 100 hour range.

	Volumetric densities [W/L]			Gravimetric densities [W/kg]		
	$NaBH_4$ System	H_2 System	Battery System	$NaBH_4$ System	H_2 System	Battery System
Power density	33	74	31	39	68	19
Energy density	1086	116	109	842	644	67
Total	103	80	109	114	173	67

Table 5.13: Volumetric and gravimetric densities of different zero emission systems.

System Components	volume [L]	Weight [kg]	$NaBH_4$ System	H_2 System	Battery System
Fuel cell [40 kW]	1066	650	1	1	0
Reactor	720	650	2	0	0
UPW installation	250	60	1	0	0
Scrubber H2	375	300	1	0	0
$NaBH_4$ tank	123	125	1	0	0
Spent fuel tank	350	494	1	0	0
High pressure hydrogen tank 500 L / 9 kg	1504	270	0.00	3	0
Low pressure hydrogen tank 100 L	250	50	2	0	0
Battery U27-24XP [1.84 kWh]	12	19.2	81	81	404

Table 5.14: Estimation for components sizing fr 10h range

5.5. Discussion

This research has examined different configurations for a $NaBH_4$ fuelled hydrogen systems and analysed the dynamic behaviour of the propulsion system under different loading conditions. In these sections, the analysis and results will be discussed. The limitations and assumptions of the Simulink model will be evaluated and the results of this research will be compared to the literature and conflicting explanations will be discussed.

Accuracy of MATLAB model

To model the dynamic behaviour and gain more insight into the sizing of different components a MATLAB/Simulink model was developed. The fuel cell and battery components in this model are based on a built-in model from the Simscape package that uses factory provided data sheets to model the electric behaviour. The results are compared to the datasheets and show similar behaviour, however, actual validation of the components is not possible without measuring the components themselves.

The electric behaviour of the system is also not included in the model since the electrical system such as grid distribution and voltage control is outside the scope of this research. Furthermore, the efficiency of the electric motor and the transformers are assumed constant, while in reality, this is highly dependant on the load fluctuations and the control of the motor. Other factors that increase the load are the balance of plant component, the hydrogen production system, the fuel cell system and the battery system. These systems require ventilation in the rooms for safety, cooling systems and pumps that all contribute to the complete load of the system. These balance of plants components are also beyond the scope of this research but together with the electrical losses will surely increase the load of the system.

The measured resistance of the old vessel was used to build three simulation cases by scaling the measured power with a factor. This scaling factor is a function of the current speed of the vessel and is obtained by creating two hydrodynamic models, one for the old vessel and one for the new vessel. This way, deviations in speed due to manoeuvring, or increased resistance due to weather conditions can be taken into account, resulting in a more accurate load profile. The hydrodynamic model used is based on Holtrop and Mennen and showed similar results when compared to the measurements. However, the research institute of MARIN also created a power curve based on Holtrop and Mennen and tuned the curve to fit a bit better with the measurements. They could do so because of their experience in the field and vast database on ship resistance, the difference is more resistance at lower speeds. Furthermore, MARIN also expects lower resistance due to a better selection of the propeller, arguing based on the rotation speed of the drive axis that a more efficient propeller can be used. The resistance calculations of MARIN would result in a lower scaling factor and thus smaller loads. However, since the scaling factor is based on the fraction of the two modelled resistances, it is argued that a small inaccuracy in the resistance curve is not a problem. As long as the same method is used for calculating the old resistance as the new resistance, the interest is in the difference of resistances not necessarily in the accuracy of the resistance curve.

In conclusion, the resistance calculations of MARIN suggests lower loads then used in the research. On the other hand, the addition of electrical systems and balance of plant components would result in higher loads then tested in the system. Without validation the model can not be taken as an accurate view of reality, instead, it functions as a design tool to understand the limitations and implications of different system configurations to come to a feasible design configuration.

Discussion on Energy Management System

The state-based EMS that is implemented scaled the fuel cell power based on the battery SOC between from minimum to maximum in a window from 70 -50%. This EMS system proved to be effective and more importantly flexible, being easily adaptable to different configurations by changing the window. The simulation with a 60 kW fuel cell also demonstrated the load following properties of this EMS system perfectly. Where other systems would oscillate around a certain SOC, the continuous state-based EMS would match the load and sustain charge with constant fuel cell power.

In the literature, however, a lot of references are made to the Equivalent Consumption Minimisation Strategy or ECMS, especially in the automotive industry. Good results for shipping systems are also found using the ECMS by Grimmelius et al. and Bassam et al. in [54] and [43]. However, the ECMS also fluctuates a lot as a result of the constant change in cost function resulting in heavy fluctuating fuel cell loads, as also illustrated by Motapon et al. in [44] and fluctuating fuel cell loads decrease the lifetime of the fuel cell. This can be mitigated by adding another level of control to prevent the fluctuation and subsequent on/off operations, as is done by Geng et al. in [55]. However Motapon et al. also compared different EMS systems including a rule-based strategy using fuzzy logic and state-based strategy that showed similar results and less load on the fuel cell. The use of ECMS on hybrid systems with an internal combustion engine has traditionally been preferred, but when using a fuel cell system the penalty on the fuel cell lifetime becomes undesirable and other systems such as state-based lead to better results.

The results from section 2.4.2 suggest that using the most efficient EMS for long-range might not be the most desirable EMS for short tours that could sail on battery only. A solution would be a Multi scheme EMS that can interact with the end-user and thus prioritise different objectives, eg range, power, battery usage, and can create a system that optimises performance for specific requirements.

Discussion on Configurations

The density used for different spent fuel concentrations are based on literature and are interpolated and information on viscosity is very rare. Better research into the spent fuel densities and viscosity properties are required, with extra attention to the formation of $NaBO_2$ crystal over time and the effect this can have ion the system in terms of viscosity.

To maintain a steady flow of hydrogen to the fuel cell system, two reactors and a hydrogen buffer were eventually required. This has a huge impact on the energy density of the system and is mostly the result of the batch input nature of the reactor and the slow reaction time. Resulting in a long cooling down period for the reactor to use all the available $NaBH_4$. The half-life time is assumed to be around 10 minutes but higher half-life times are to be expected as the research done by the University of Gent suggests [17]. If this is the case it might be possible to work with smaller reactors or maybe even one reactor. Using a continuous flow reactor instead of a batch reactor as is suggested by Kim et al. [13] could also improve the power density of the system, although the loss of $NaBh_4$ might be more substantial.

The energy density of the entire system was estimated to be 120 Wh/kg and 45 Wh/l. For ship design, the volumetric energy density is more interesting but to compare this design with other applications the gravimetric energy density is used. A battery system has an energy density of between the 60-200 kWh/kg depending on the type of batteries used, it is worth noting that the 200 Wh/kg batteries do not provide high power and can be dangerous. Other $NaBH_4$ systems have energy densities of 114 Wh/kg [13], 165 Wh/kg [12] and even 463 Wh/kg by using a cartridge system [14]. The designed system in this comparison looks pretty low with 120 Wh/kg but this can be increased dramatically up to 500-650 Wh/kg if the range is increased because the gravimetric energy density of the system is now mostly determined by the low power density of the reactors.

6 Conclusion

The research question and subquestion that were answered in this report are repeated and this chapter summarises the answers to these questions in different sections. The first section concludes the maritime application of a $NaBH_4$ system and answers subquestion one. The reactor model section and the EMS section answer questions three and four and question two and five are answered in the sections discussing the sizing for the Port of Amsterdam's vessel and the comparison of alternatives. The main research question and its subquestions are:

What is a suitable design for a $NaBH_4$ hybrid propulsion system for a small inland vessel and how can the design and different control strategies be improved using dynamic modelling?

1. *What are the possibilities and limitations of the subsystem components, and how can a $NaBH_4$ system be integrated into a maritime application?*
2. *What is the correct sizing of components for the Port of Amsterdam new build vessel?*
3. *How can the batch reactor be modelled and what other models can be used to validate the initial design?*
4. *What is an effective energy management system for the power distribution of the Port of Amsterdam's vessel and how can the hydrogen production system be integrated?*
5. *How does the final design perform when compared to traditional (zero-emission) alternatives?*

Maritime application

The application of a $NaBH_4$ hydrogen storage system for a maritime vessel has an advantage over traditional solutions since less water needs to be transported on-board. The implications of such a system on board of a ship are investigated in section 2.2. It was concluded that a maritime application can achieve higher energy densities compared to land or air-based applications by producing clean water directly from the marine environment.

The energy cost for filtering and producing clean water on board is low compared to the amount of energy produced by hydrogen. For producing 1 kg of hydrogen, 15 L water is required. The hydrogen has an LHV of around 33 kWh and a fuel cell has an efficiency of around 50%, this means that one litre of water is required in the system for producing around 1 kWh of electric energy. The energy cost of a reverse osmosis plant that can filter fresh and saltwater is estimated, conservatively, at 10 kWh per cubic meter [30] or 0.01 kWh/L. This means that only around 1% of energy is lost to the production of water on-board.

The theoretical maximum hydrogen storage capacity is increased by using water from the outside environment compared to land-based solutions. Assuming a spent fuel concentration with a 0.2 mole fraction of $NaBO_2$, a traditional system with water on board would result in a hydrogen storage capacity of 2.65 wt%. A maritime system that uses water from the outside environment can result in hydrogen storage capacity of 4.38 wt%. This is a 1.65 fold increase over the traditional $NaBH_4$ systems proposed for cars and UAVs. This percentage is still limited by the mole fraction of $NaBO_2$ in the spent fuel. More research needs to verify what safe and practical conditions for spent fuel concentrations are to further optimise the hydrogen storage.

Reactor model

After studying the behaviour of the cobalt catalyst developed by the University of Gent [17] and that of similar cobalt-based catalysts in the literature, the reaction will likely behave as a first-order chemical reaction when under temperatures of around 90°Celsius. The actual reaction rate, however, is difficult to define because many factors can influence the reaction kinetics of a batch reactor, including increasing the amount of catalyst and increasing the flow over the catalyst inside the reactor. The reaction rate is expressed as a function of the half-life time and the effects of different half-life times are evaluated in section 5.1.3. It was found that the start-up time of the system was not affected in any major way. Faster reaction kinetics did, however, result in lower pressures and better load following capabilities for the batch reactor. It is also expected that less $NaBH_4$ will be lost during the cleaning of the reactor if the half-life time is low.

For the reactor to be integrated into the system a set of control settings needed to be developed. These mechanisms were incorporated in the model and some viable settings were selected for the operation of the reactor in the propulsion system.

Variable	Explanation	Setting
NaBH4 injection	The injection of NaBH4 determines for a large part the start up time of the reactor.	9 kg
Min pressure for start flow	The pressure is kept at a constant level in order to deal with sudden load changes.	10 bar
Start rinse cycle	The rinse cycle for cleaning starts when the reactor is almost full.	1 injection
Reaction time rinse cycle	After the rinse cycle starts, some time is given for the left over NaBH4 to react.	27.5 min
Cleaning time rinse cycle	Some time is required for cleaning the inside of the reactor after all the spent fuel is flushed out.	5 min

Table 6.1: Control setting used for the batch reactor model when using a hydrogen buffer and one reactor

The reactor was integrated into the model and it became apparent that one reactor cannot provide a continuous flow of hydrogen. The reactor needs to be stopped to flush out the spent fuel and clean the system. When applying a buffer after the reactor the amount of hydrogen stored can be enough for continuous operation, but with a half-life time of 10 minutes, not all the $NaBH_4$ can react. Faster reaction kinetics can help to shorten the reaction time of the rinse cycle and possibly create a viable system with one reactor and a buffer without loss of fuel.

EMS system and Integration

The Port of Amsterdam's vessel is designed to be a plug-in hybrid vessel with significant energy storage in the battery system that can be charged when in the dock. So to efficiently use the battery system an EMS that prioritises the battery is required. The charge deplete charge sustain (CDCS) is a suitable method but the method of sustaining charge was further investigated.

The tested state-based strategies performed better than the traditional PI strategy over all three profiles. Of the two, the continuous SOC state-based strategy was slightly more efficient. Another advantage is that there are no sudden jumps in power for the fuel cell and instead the fuel cell power changes smoothly based on the SOC. The state-based also proved to be adaptable to a different configuration, by changing the SOC level where the strategy enables the fuel cell it was possible to maintain a 30% minimum SOC for different configurations for the PoA vessel.

The EMS and hydrogen system was integrated and it proved essential to maintain a continuous flow of hydrogen to maintain the right minimum SOC and to prevent excessive start/stop cycles. A feasible configuration consisted of two reactors and a buffer to maintain a continuous flow. However, the reactor volume was kept constant and the reactor control settings were not optimised for a configuration using one reactor and a buffer. By developing the reactor further a better configuration capable of delivering a continuous flow should be possible with either a larger reactor and a buffer or two small reactors.

Sizing of electrical systems for the Port of Amsterdam's vessel
Three configurations of battery and fuel cell size were evaluated in section 2.4.2. The configuration using a 60 kW fuel cell and a 50 kWh battery pack could sustain the battery charge and allow for increased power during acceleration and maximum speed. In this configuration, a larger fuel cell and reactor installation would be required resulting in a low power density and because of the small battery more fuel is required.

A configuration using a 40 kW fuel cell and a 100 kWh battery pack proved insufficient for operational profile C, trip to IJmuiden, and resulted in low SOC levels at the end of the trip. This is a result of the 40 kW fuel cell not being sufficient for sustaining the charge. Instead, a 150 kWh battery pack was found to be sufficient of the fuel cell starts to assist on time, in this case, the load was shared starting from 70 % SOC. Besides 150 kWh is also enough for operational profile A, tour in the canals, to be executed on batteries only. It is therefore suggested that a 'battery only' mode is used for short, low power demand trips. This will safe on $NaBH_4$ costs by sailing on battery power only during small trips.

Comparison alternatives
The newest generation hydrogen tanks used in the comparison in section 5.4 store under 500 bar and weigh 279.5 kg for 9.5 kg of hydrogen storage, resulting in a gravimetric energy density of 3.6 wt%. Taking into account the energy density of hydrogen and efficiency of the fuel cell this equals to 566 Wh/kg of electric energy. The thick walls required for safe pressure however result in a density of 158 L/kg_{H2} and by including the energy content and efficiency of the fuel cell this results in only 105 Wh/L of usable electric energy.

The battery system used in the comparison has a density of 0.625 L/kg and a gravimetric energy density of 96 Wh/kg, however, to maintain a 30% SOC on the battery and increase the half-life time this results in 67 Wh/kg of effective electric energy. This results in 107 Wh/L of effective electric energy.

The maritime $NaBH_4$ application has a maximum theoretical hydrogen storage capacity of 4.38 wt%. Taking in account the fuel cell efficiency, a reaction efficiency of 100% conversion, and the energy density of hydrogen, this results in a gravimetric energy density of 730 Wh/kg and volumetric energy density of 968 Wh/L. These numbers are theoretical maximums for a $NaBH_4$ system but show a significant increase in energy storage potential when compared to batteries and compressed hydrogen. In terms of volumetric energy density specifically, the $NaBH_4$ storage solution shows the possibility of a 7 fold increase compared to traditional zero-emission alternatives.

On the other hand, the power density of the configuration as implemented for the Port of Amsterdam is relatively poor due to the relative large size of the reactors. This is a scaling effect caused by the relatively low storage amount of energy on board. A better design for the reactors that optimises for continues flow and reactor volume can also result in better overall system densities.

Recommendations

A system using one reactor and a 200 L hydrogen buffer was found to be feasible. However, if the reaction can be controlled better a smaller hydrogen buffer could also be feasible. Further investigation on possible control systems and development of the reactor and the catalyst is, therefore, a natural next step.

The energy density of the system is determined for a large part by the allowable molar concentration of the spent fuel. The literature has provided a phase diagram but further investigation on the behaviour of different concentrations of spent fuel is required. How the spent fuel will form over time and at what molar concentrations the liquid is still safe to pump through the system requires more attention.

The efficiency of the fuel cell is now purely based on the information provided by the Nedstack datasheets. The actual system will also include balance of plant components such as pumps, cooling and water production. These parts will require power and this will negatively impact the efficiency of the entire system. If the reactor is further developed an analysis of the required balance of plant components and their energy consumption can be made.

The $NaBH_4$ is only a carrier for hydrogen. The process of recycling the spent fuel and creating a circular system that results in new $NaBH_4$ needs to be developed further. The efficiency of the recycling reactions needs to be increased or a source of inexpensive energy needs to be found to obtain competitive fuel prices. Besides the chemical recycling process of the $NaBH_4$ the logistics process of resupplying and delivering a solid based fuel both on shore as well as within the system also poses some challenges.

A

Measurements for inland vessels

(1) **Koninkrijk der Nederlanden** - **N.**

(2) Bureau van meting: Rotterdam

3 Onderscheidingsletters van het bureau: HN

(4) Meetbrief No.: 4879

(5) Ingeschreven de 7 maart 1995

(6) **METINGSMERK** HN 4879

(7) **Naam of kenspreuk van het vaartuig:**

HAVENBEHEER

Invulling door
bevoegde autoriteit

8 **Nieuwe naam of kenspreuk**____________________

(9) Te________________, de____________________

(10) De ambtenaar van de Scheepsmetingsdienst,

(11)

8 **Nieuwe naam of kenspreuk**____________________

(9) Te________________, de____________________

(10) De ambtenaar van de Scheepsmetingsdienst,

(11)

8 **Nieuwe naam of kenspreuk**____________________

(9) Te________________, de____________________

(10) De ambtenaar van de Scheepsmetingsdienst,

(11)

HOOFD SCHEEPSMETINGSDIENST ROTTERDAM NEDERLAND

(12) **Afmetingen van het schip voor het passeren van kunstwerken.**

a. Lengte	16.75	m.
b. Breedte	3.98	m.
c. Diepgang bij de grootste inzinking	1.45	m.
d. Hoogte boven water tot het vlak van ledige diepgang	1.90	m.

Opmerkingen:

OMSCHRIJVING VAN HET VAARTUIG

(13) Soort van vaartuig: directievaartuig

(14) Materiaal:
a. Van de romp : staal
b. Van de bovenbouwen *): staal
c. Van de luiken *) : -----

(15) Nadere gegevens over de bouw:
met dek

(16) Werf van aanbouw: Molenaar's Scheepswerf B.V.
te Zaandam
(17) Bouwjaar: februari 1995

(18) **Grootste lengte van de romp :** 16.75 m.
(19) **Grootste breedte van de romp:** 3.82 m.

(20) Aard, identificatiemerken en vermogen van het voortstuwingswerktuig *): dieselmotor
fabrikant: FORD-SABRE
type : 185 L
motorno. : 826 F 1 J 23A
vermogen : 185 pk

(21) Gemiddelde inzinking van het ledige schip: 63 cm.
(in zoetwater)

22 Laadvermogen hier niet van toepassing.
Zie rubriek 34 en 36.

(23) Vertikale afstand van het vlak van de grootste toegelaten diepgang tot het dek c.q. gangboord:
a. Op het midden van de lengte van de romp 57 cm.
b. Op het laagste punt van het dek c.q. 55 cm.

GEWICHTEN AAN BOORD DIE BEHOREN BIJ DE LEDIGE INZINKING

(24) Plaats en omschrijving van de vaste ballast *)

600 kg. beton in voor- en achterpiek

(25) Werktuigen, ketels, pijpleidingen of andere installaties die water, olie of andere vloeistoffen, welke nodig zijn voor de goede werking ervan, bevatten *)

-----

26 Bij benadering vastgesteld gewicht van het water dat met de gebruikelijke middelen niet uit het ruim kan worden verwijderd *)

-----

27 Uitrusting:
a) Omschrijving en bij benadering vastgesteld gewicht van de ankers en de ankerkettingen 30kg
b) Bij benadering vastgesteld gewicht van andere verplaatsbare uitrusting en reservedelen 50kg
c) Bij benadering vastgesteld gewicht van het meubilair 80kg
d) Bij benadering vastgesteld gewicht van de aan boord zijnde reddingboot of reddingboten ----kg

Proviand:
a) Bij benadering vastgesteld gewicht van het zoetwater 500kg
b) Bij benadering vastgesteld gewicht van de andere proviand 50kg

IJKMERKEN

(28) **Het vlak van de grootste toegelaten diepgang wordt aan weerszijden van het vaartuig aangegeven door twee gecenterde lijnen.**

	Bakboord(L)			Stuurboord(R)		
Merken v.h. vooreinde v.h. vaartuig afgerekend.	1 (voor)	2	3	1 (voor)	2	3
(29) **Horizontale afstanden in m.**						
a) Van de vertikale lijn v.h. voorste merk tot het vooreinde v.h. vaartuig.	5.70			5.70		
b) Tussen de vertikale lijnen v.d. merken onderling.		6.20			6.20	
c) Van de vertikale lijn v.h. achterste merk tot het achtereinde v.h. vaartuig.		4.85			4.85	
(30) **Vertikale afstand ter plaatse van ieder ijkmerk in cm:**						
a) Tussen het merk en het dek c.q. gangboord.	61	55		61	55	
b) Tussen het merk en het vlak parallel aan het vlak v.d. grootste diepgang waarboven het schip niet geacht wordt waterdicht te zijn.		70			70	
c) Tussen het merk en het vlak van ledige inzinking.	10	10		10	10	
d) Tussen het vlak van ledige inzinking en de onderkant v.h. vaartuig.	76	49		76	49	
e) Tussen het merk en de onderkant v.h. vaartuig (som v.h. onder c. en d. ingevulde).	86	59		86	59	

Noot. De ijkplaten of de ijkmerken op de zijden van het vaartuig moeten door de schipper steeds duidelijk zichtbaar worden onderhouden. Bij gebreke hiervan wordt de meetbrief niet erkend.

METINGSMERKEN

31 Ter aanvulling van de plaatsing bij de ijkmerken, wordt het metingsmerk ook aangebracht op het achterschip aan BB-zijde in het berghout

0.00 m uit hekplaat, 0.25 m uit lengteas,
0.01 m boven dek.

32 Een ijkschaal is niet aangebracht onder elk ijkmerk.

(33) Is hier niet van toepassing

II. Meting volgens artikel 5 van de bijlage van de Overeenkomst (vaartuig, niet bestemd voor het vervoer van goederen).

34 **Maximum toelaatbare waterverplaatsing** 35.547 m3.

35 **Waterverplaatsing in ledige toestand** 30.778 m3.

36 **Verplaatsing** 4.769 m3.

(37)-(59) **Opmerkingen.**

(37) Vaargebieden.
(Bij de toekenning van een vaargebied blijft de sterkte van de scheepsromp buiten beschouwing).

Vaargebied A B C

Vervolg (37) Opmerkingen:

Overzicht vaarwegen in Nederland

Vaargebied A:

Dollard
Eems
Waddenzee, met inbegrip van de verbindingen naar de Noordzee
IJsselmeer, met inbegrip van Markermeer en IJmeer, met uitzondering van Gouwzee
Rotterdamse Waterweg en het Scheur
Hollands Diep
Haringvliet en Vuile Gat, met inbegrip van alle vaarwateren tussen Goeree-Overflakkee enerzijds en Voorne-Putten en de Hoekse Waard anderzijds.
Hellegat
Volkerak
Krammer
Grevelingen en Brouwershavense Gat, met inbegrip van alle vaarwateren tussen Schouwen-Duiveland enerzijds en Goeree-Overflakkee anderzijds.
Keten, Mastgat, Zijpe
Oosterschelde en Roompot, met inbegrip van de vaarwateren tussen Walcheren, Noord- en Zuid-Beveland enerzijds en Schouwen-Duiveland en Tholen anderzijds, met uitzondering van het Schelde-Rijnkanaal.
Schelde en Westerschelde en zijn uitmonding naar Zee, met inbegrip van de vaarwateren tussen Zeeuws-Vlaanderen enerzijds en Walcheren en Zuid-Beveland anderzijds met uitzondering van het Schelde-Rijnkanaal.

Vaargebied B:

Sneekermeer, Koevordermeer, Heegermeer, Fluessen, Slotermeer, Tjeukemeer, Beulakerwijde, Belterwijde, Ramsdiep, Ketelmeer, Zwartemeer, Veluwemeer, Eemmeer, Gooimeer, Alkmaardermeer, Gouwzee, Buiten IJ, afgesloten IJ, Noordzeekanaal, haven van IJmuiden, havengebied van Rotterdam, Nieuwe Maas, Noord, Oude Maas, Beneden Merwede, Nieuwe Merwede, Dordtsche Kil, Boven Merwede, Waal, Bijlandsch Kanaal, Boven Rijn, Pannerdensch Kanaal, Geldersche IJssel, Neder Rijn, Lek, Amsterdam-Rijnkanaal, Veerse Meer, Schelde-Rijnkanaal tot uitmonding in Volkerak, Amer, Bergsche Maas, Maas beneden Venlo.

Vaargebied C:

B

Measurements Techno Fysica B.V.

TECHNO FYSICA B.V.

TECHNICAL PHYSICS DEPARTMENT

Meetrapport	:	17106
Ons order nr.	:	119417
Inkoop opdracht nr.	:	28361
Installatie	:	Directievaartuig PA 20 "Havenbeheer"
Gevraagd onderzoek	:	Vermogensprofiel voortstuwing
Onderzoek besteld door	:	Dhr. H. van der Boom Havenbedrijf Amsterdam NV
Adres	:	De Ruijterkade 7 1013 AA Amsterdam

Datum besteld	:	19 september 2019
Datum onderzoek	:	4 oktober 2019
Meetrapport opgesteld door	:	A. Dubbeldam
Datum rapport	:	Barendrecht, 10 oktober 2019
Handtekening	:	ing. M.A. van der Heijde

Techno Fysica B.V.
Aalborg 5
2993 LP Barendrecht
The Netherlands

Phone +31(0)180-620211
Fax +31(0)180-620705
E-mail info@technofysica.nl
Internet www.technofysica.nl

Inhoud

Inleiding 4
Doel van het onderzoek 4
Algemene gegevens 5
Instrumentatie en meetprogramma 6
Meetprogramma 6
Meetmethode 7
Koppelmetingen 7
Toerental 7
Snelheid en positie 7
Registratie en analyse 7
Meetresultaten 8
Bijlage A 9
Foto's meetlocatie. 9
Bijlage B 11
Vaarprofiel geplot in Google Earth. 11
Vaarprofiel A: varen Technisch Centrum naar Hoofdgebouw 12
Vaarprofiel B: Varen op de grachten 13
Vaarprofiel C: Varen door het havengebied 14
Vaarprofiel D: Varen van Hoofdgebouw naar Technisch centrum 15
Vaarprofiel E & F: Varen op het Noordzeekanaal 16
Bijlage C 17
Grafieken vaarprofiel vermogen & snelheid tegen de tijd 17

Inleiding

De heer H. van der Boom van Havenbedrijf Amsterdam verstrekte Techno Fysica b.v. de opdracht voor het vastleggen van het vermogensprofiel van de voortstuwinginstallatie aan boord van het directievaartuig “Havenbeheer” te Amsterdam. Dit in combinatie met het registreren van de scheepssnelheid en locatie.

Doel van het onderzoek

Het directievaartuig “Havenbeheer” heeft een diesel gedreven voortstuwingsinstallatie. Op termijn wordt het schip vervangen door een nieuw directievaartuig wat elektrisch op waterstof gaat varen. Het doel van dit onderzoek is het vastleggen van het vermogen/ vaarprofiel wanneer met potentiële klanten of genodigden de haven en de stad wordt bekeken.

Algemene gegevens

Schip

Naam	:	PA20 “Havenbeheer”	
Bouwjaar	:	-	
Type	:	Directievaartuig	
Lengte	:	15	m
Breedte	:	3	m

Motor

Merk	:	John Deere	
Type	:	6068TFM75 – 6.8L	
Rating	:	M3	
Vermogen	:	150	kW (204 pk)
Toerental	:	2600	omw/m.
Serie nr.	:	CD6068G145179	

Tandwielkast

Merk	:	PRM Marine LTD
Type	:	1000D3
Reductieverhouding	:	3 : 1
Serie nr	:	2007199 M01340

Schroef

Merk	:	-	
Aantal bladen	:	4	
Diameter	:	-	mm

Instrumentatie en meetprogramma

Instrumentatie a/b "Havenbeheer"

- Koppel schroefas
- Toerental schroefas
- Scheepssnelheid d.m.v. GPS

Meetprogramma

Om zoveel mogelijk inzicht te krijgen in het vermogens vaarprofiel van het directievaartuig "Havenbeheer" is het volgende, door Havenbedrijf Amsterdam & Marin opgestelde meetprogramma uitgevoerd:

A. Varen van Technisch Centrum ADM-Werkhaven naar Havengebouw steiger IJ De Ruyterkade West 2 (IJ RW2).
B. Varen van Havengebouw IJ RW2 door de grachten voor 3 uur en terug naar Havengebouw IJ RW2.
C. Varen van Havengebouw IJ RW2 door het havengebied voor 3 uur en terug naar het Havengebouw IJ RW2.
D. Varen Havengebouw IJ RW2 terug naar Technisch centrum ADM-Werkhaven.

De volgende 2 meting zijn uitgevoerd om het schroef toerental, het vermogen en de snelheid vast te leggen.

E. Toeren stappen varend op het Noordzeekanaal richting IJmuiden.
F. Toeren stappen varend op het Noordzeekanaal terug richting ADM-Werkhaven.

Meetmethode

Koppelmetingen

De koppelmetingen zijn verricht door op de schroefas rekstroken aan te brengen. Door vervormen van de as levert deze brug van Wheatstone een signaal. Dit signaal wordt gemoduleerd en draadloos naar een ontvanger gezonden. Na demodulatie is het signaal proportioneel aan het statisch koppel in de as. De meetnauwkeurigheid bedraagt >98%.

Toerental

Het toerental van de schroefas is bepaald met een infrarood zender / ontvanger in combinatie met een reflector op de as. Dit systeem genereert een puls per omwenteling en een toerental in toeren per minuut.

Snelheid en positie

Een GPS datalogger is gebruikt om de positie en snelheid tijdens de proefvaart vast te leggen.

Registratie en analyse

De signalen zijn opgenomen met behulp van een 16 kanaals IMC data acquisitie systeem met 10 Hz samplerate.

De data is verwerkt met de softwareprogramma’s Diadem & Excel. Voor de presentatie in Excel is de data gereduceerd naar 1 Hz.

Meetresultaten

Foto's van de locatie voor koppelmeter & toerental op de schroefas, GPS-ontvanger en registratie appratuur zijn in bijlage A opgenomen

In bijlage B zijn de routes geplot in Google Earth.

Alle data van de vaarprofielen zijn in Excel formaat verwerkt in grafiekvorm en gepresenteerd in bijlage C. In deze grafieken is de snelheid van het schip met bijhorend berekend schroefas vermogen (gemeten toerental en koppel van de schroefas) tegen de tijd weergegeven.

In geval verder bewerking of presentaties gewenst zijn dan is dit uiteraard mogelijk en zo gewenst kunnen ook de Excel gegevens worden gestuurd.

Bijlage A

Foto’s meetlocatie.

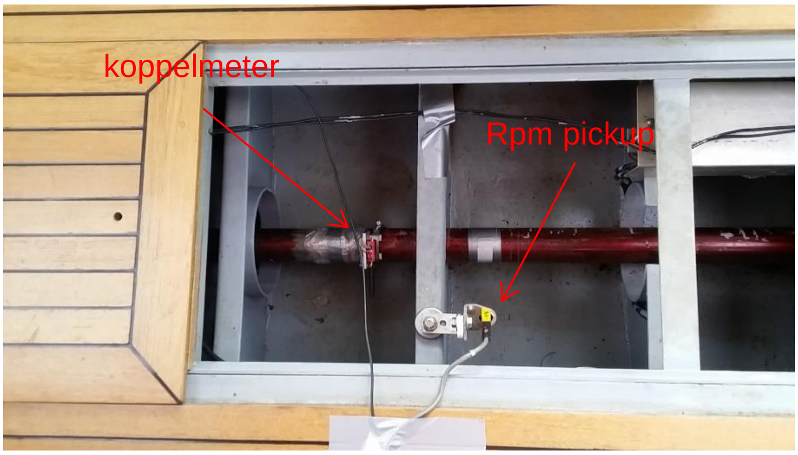

Foto 1: koppelmeter op de schroefas

Foto 2: locatie gps-ontvanger

Foto 3: Registratieapparatuur

Bijlage B

Route geplot in Google Earth.

Vaarprofiel A: varen Technisch Centrum naar Hoofdgebouw

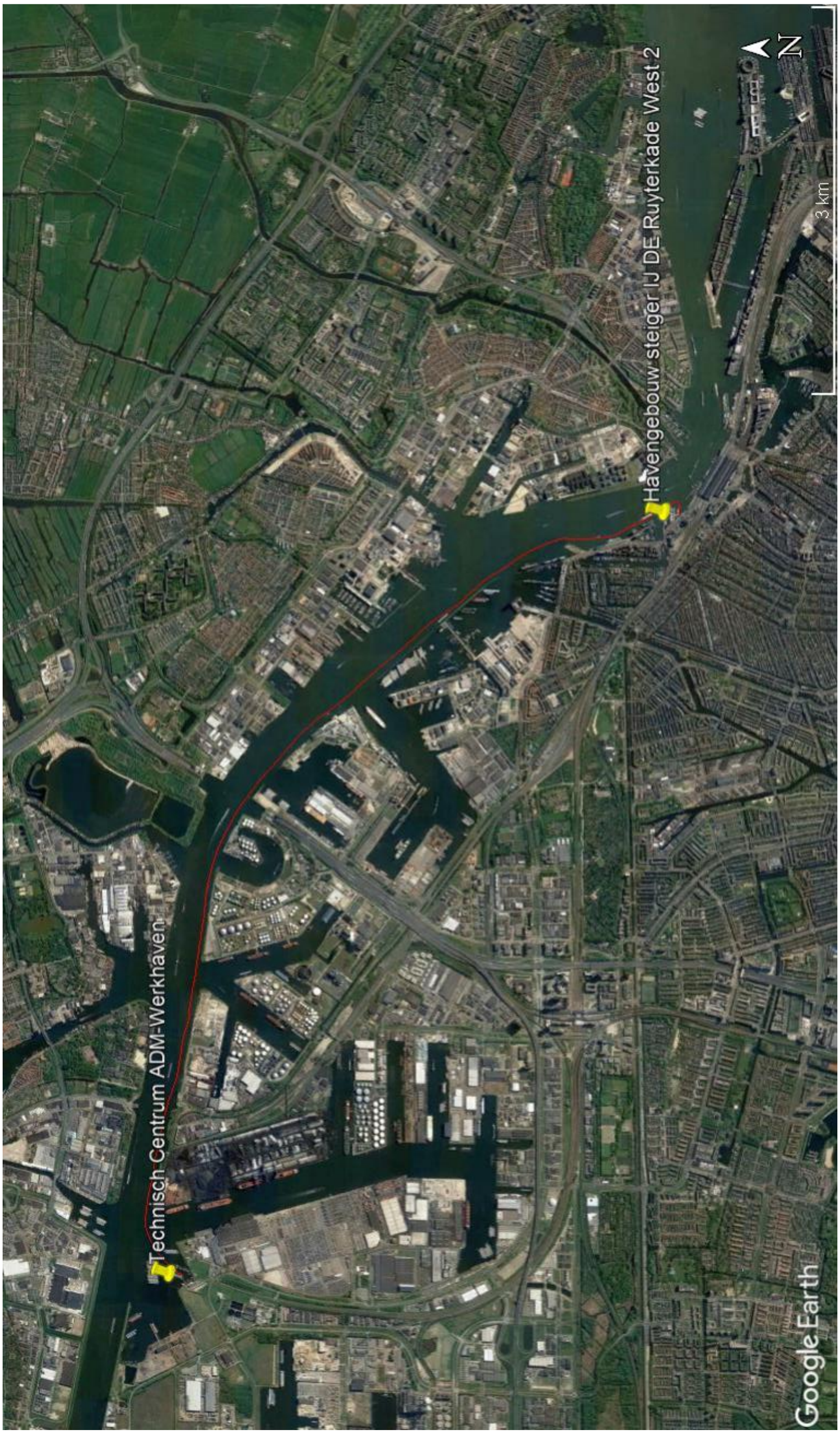

Vaarprofiel B: Varen door de grachten

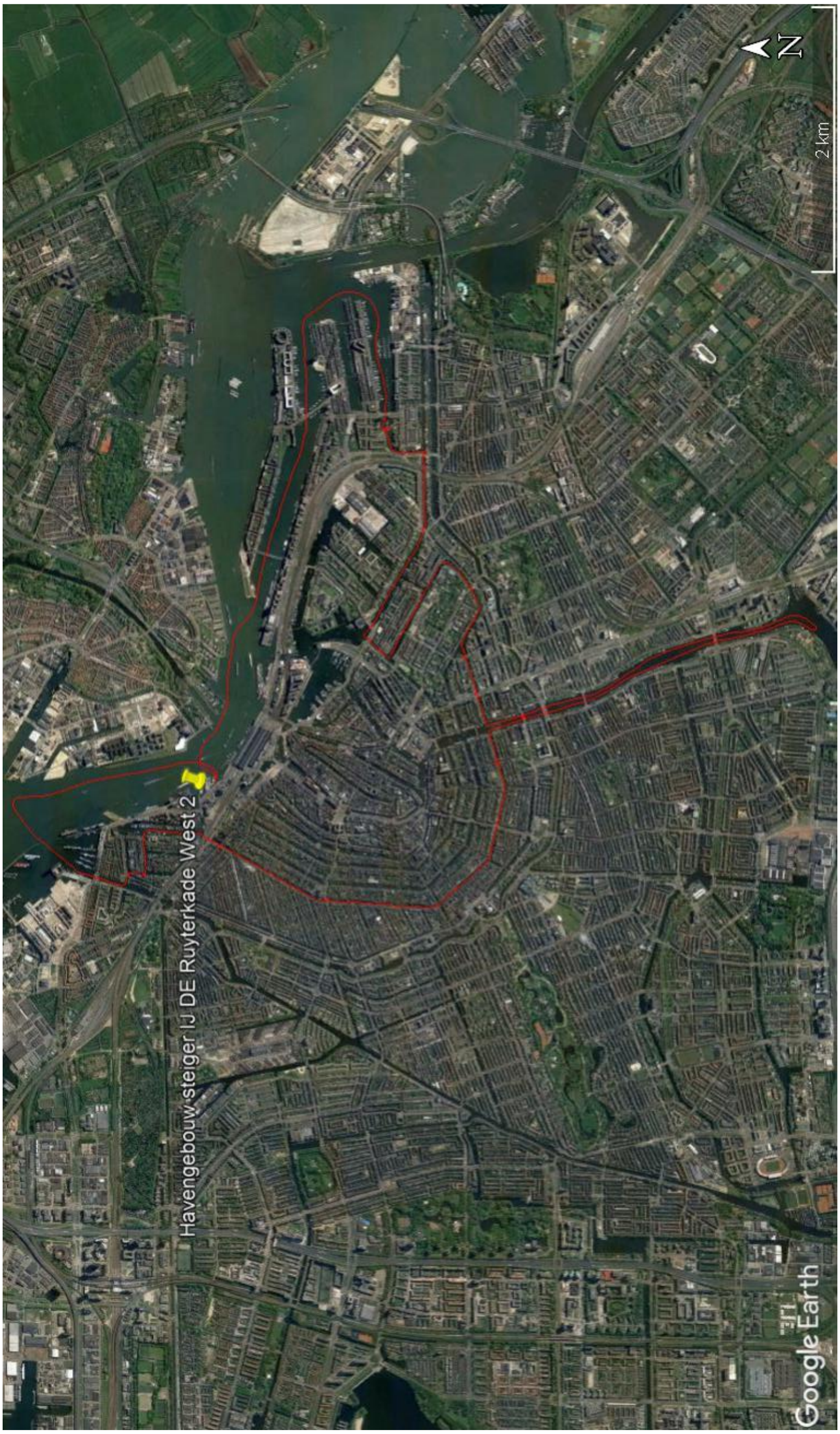

Vaarprofiel C: Varen door het havengebied

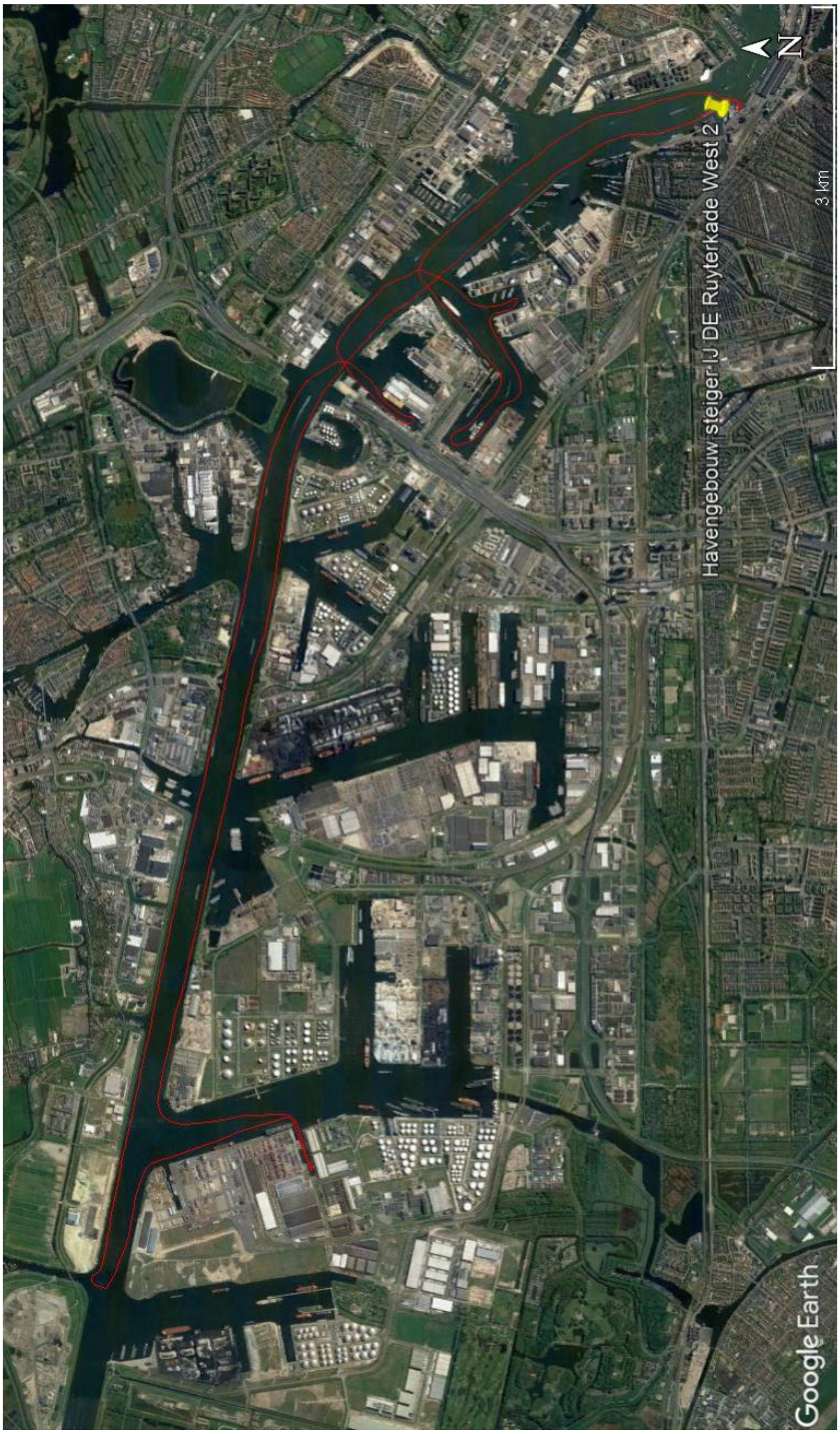

Vaarprofiel D: Varen van Hoofdgebouw naar Technisch centrum

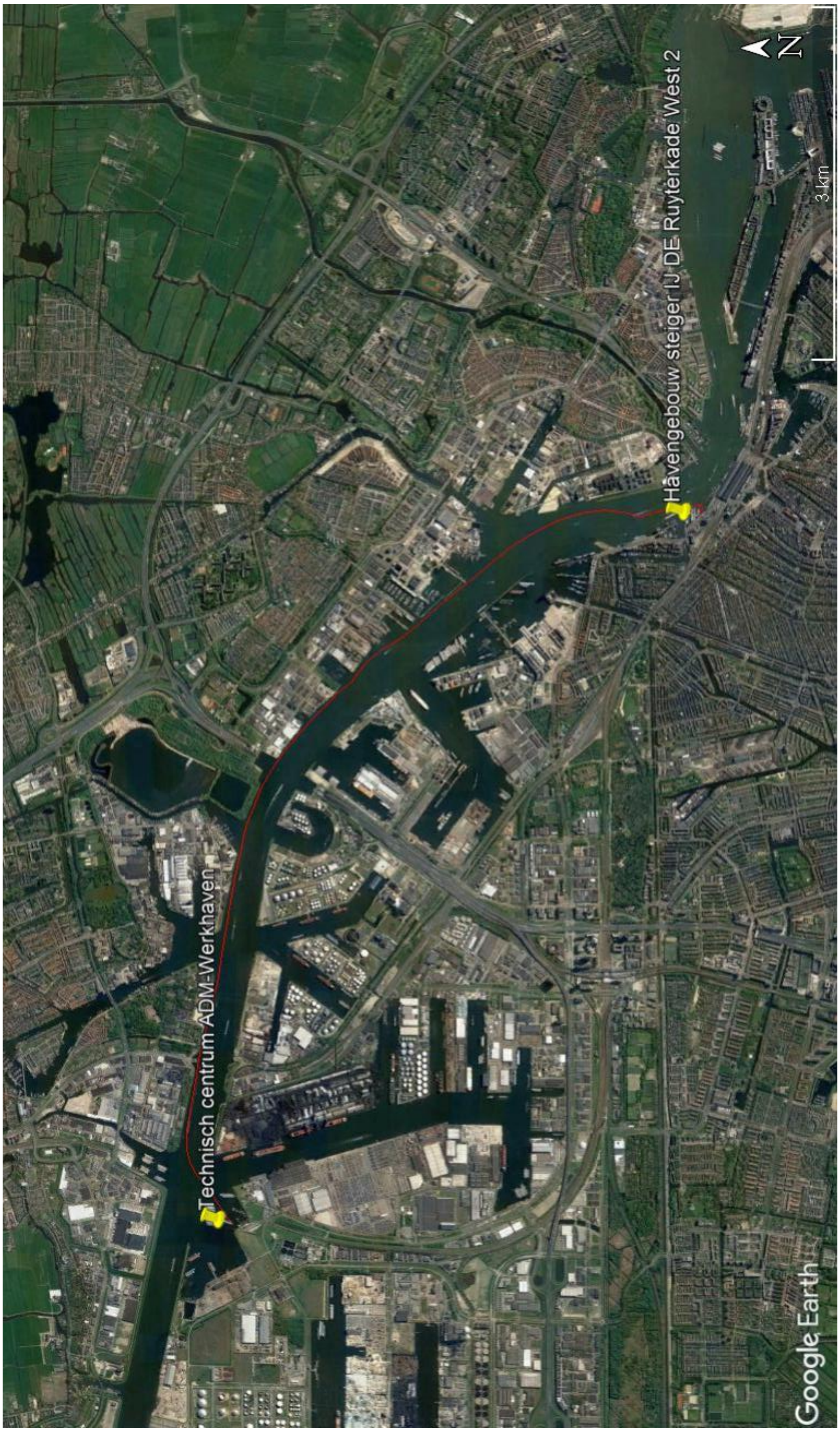

Vaarprofiel E & F: Varen op het Noordzeekanaal

Bijlage C

Grafieken vaarprofiel vermogen & snelheid tegen de tijd

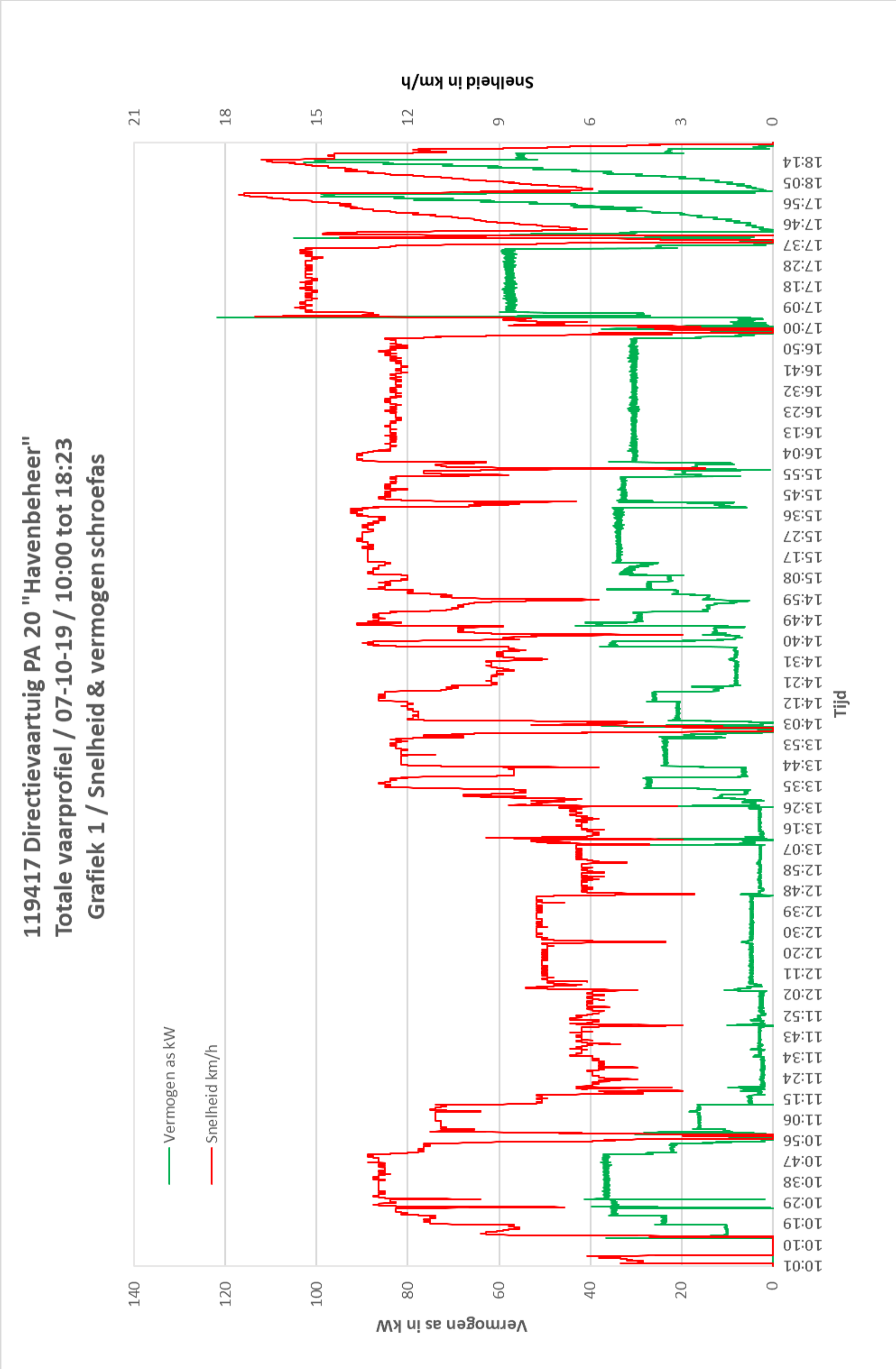
119417 Directievaartuig PA 20 "Havenbeheer"
Totale vaarprofiel / 07-10-19 / 10:00 tot 18:23
Grafiek 1 / Snelheid & vermogen schroefas
Vermogen as kW
Snelheid km/h
Snelheid in km/h
Vermogen as in kW
Tijd

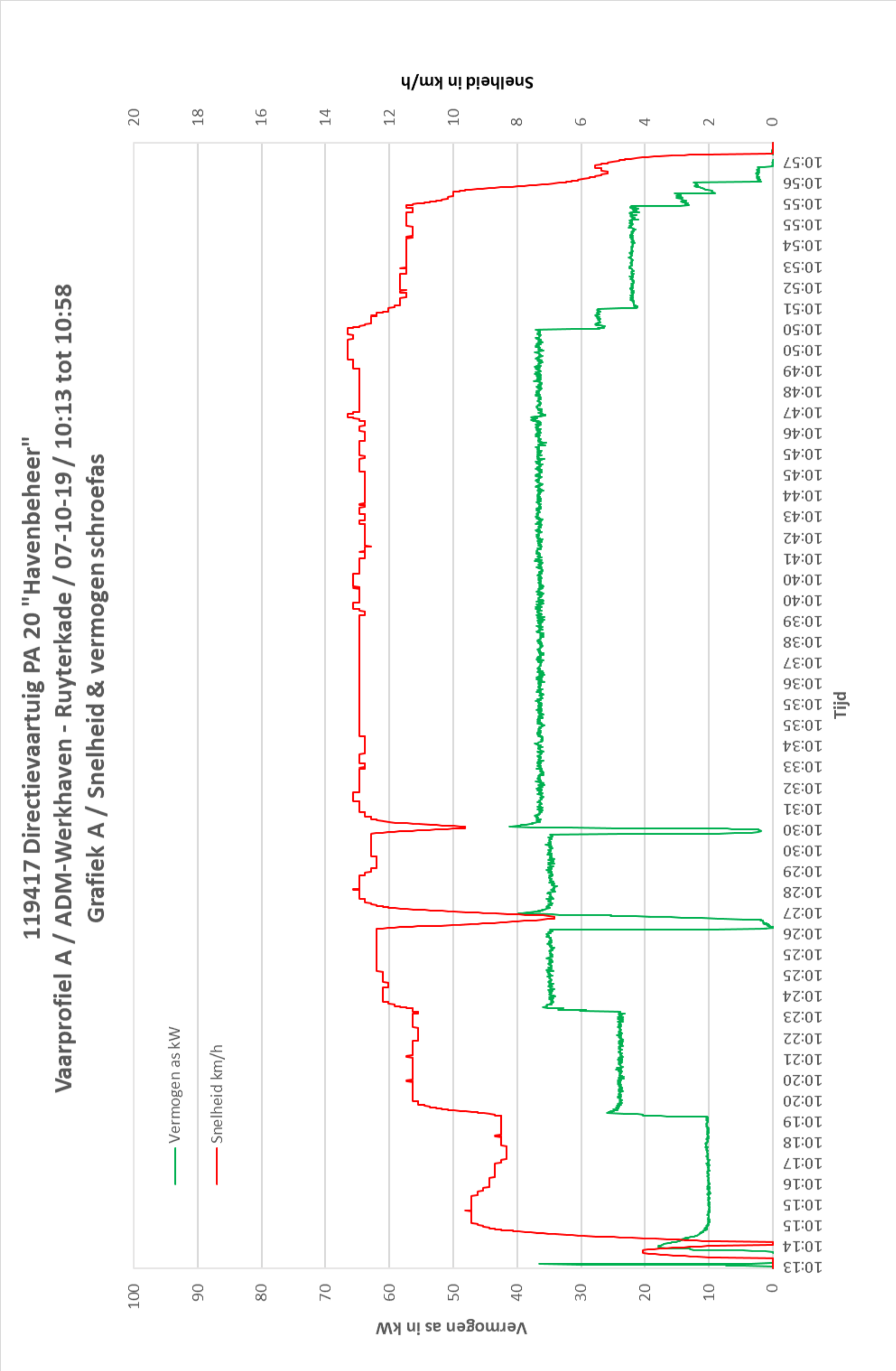
119417 Directievaartuig PA 20 "Havenbeheer"
Vaarprofiel A / ADM-Werkhaven - Ruyterkade / 07-10-19 / 10:13 tot 10:58
Grafiek A / Snelheid & vermogen schroefas
Vermogen as kW
Snelheid km/h
Snelheid in km/h
Vermogen as in kW
Tijd

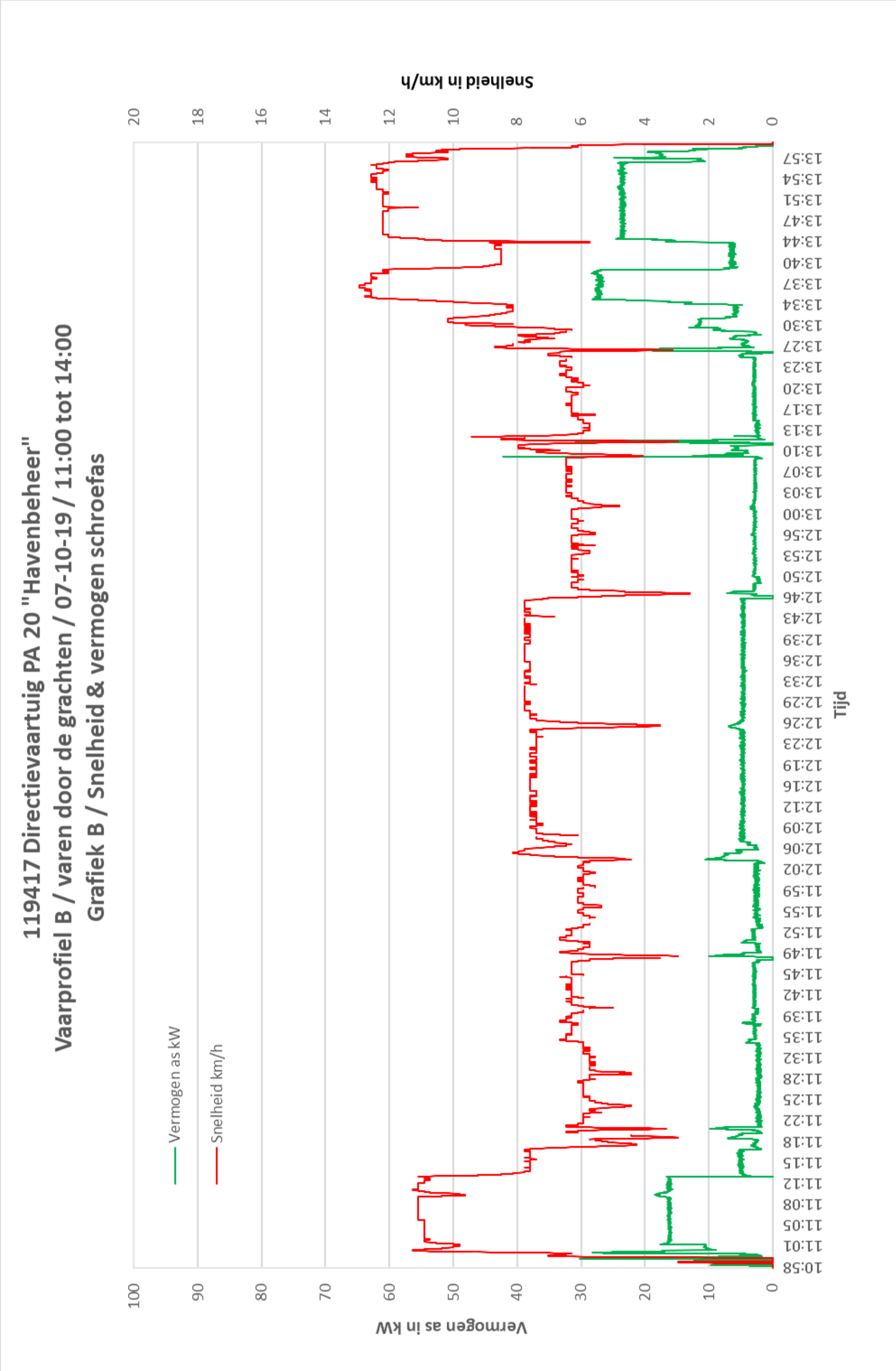
119417 Directievaartuig PA 20 "Havenbeheer"
Vaarprofiel B / varen door de grachten / 07-10-19 / 11:00 tot 14:00
Grafiek B / Snelheid & vermogen schroefas
Vermogen as kW
Snelheid km/h
Snelheid in km/h
Vermogen as in kW
Tijd

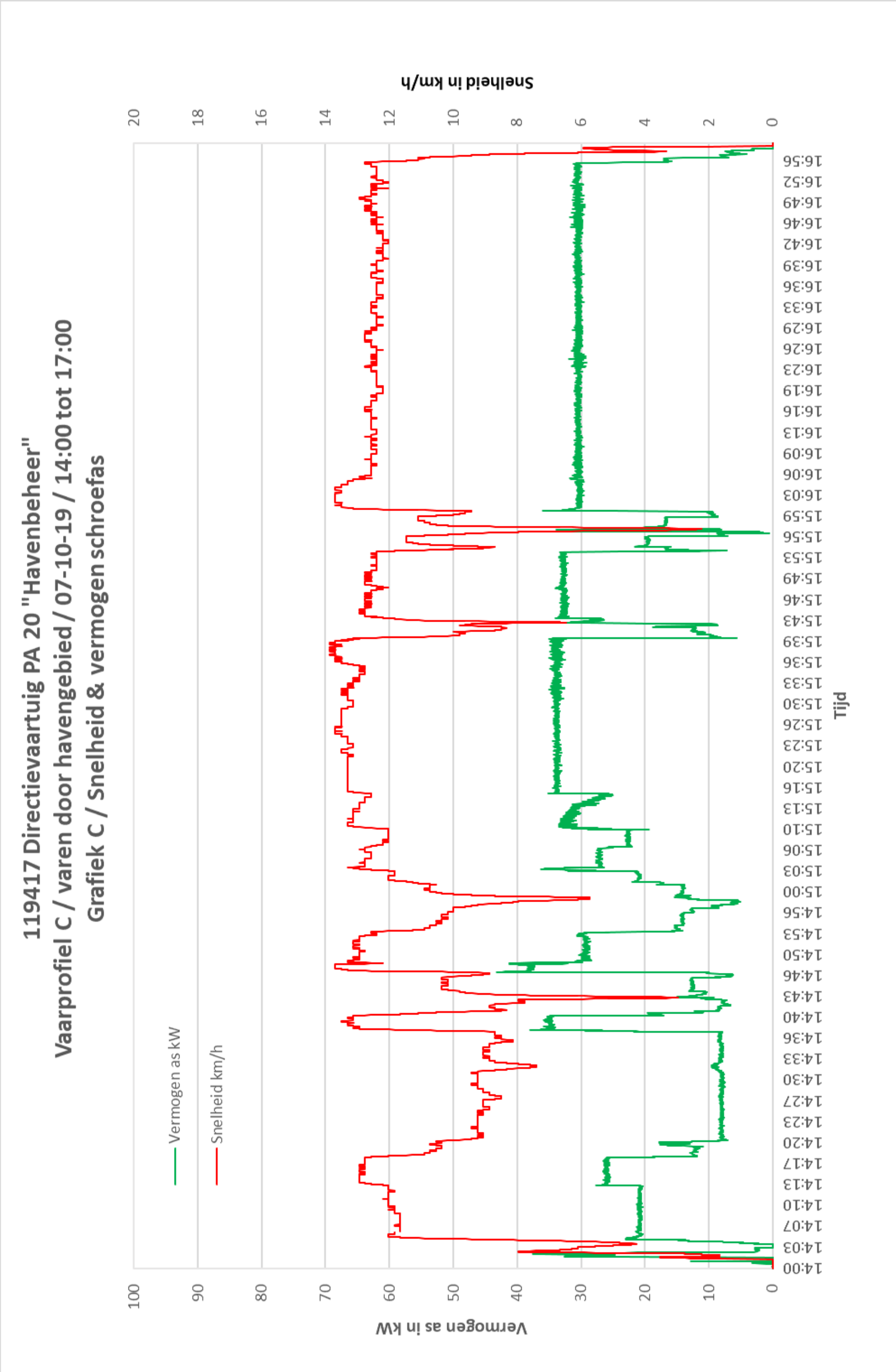
119417 Directievaartuig PA 20 "Havenbeheer"
Vaarprofiel C / varen door havengebied / 07-10-19 / 14:00 tot 17:00
Grafiek C / Snelheid & vermogen schroefas
Vermogen as kW
Snelheid km/h
Snelheid in km/h
Vermogen as in kW
Tijd

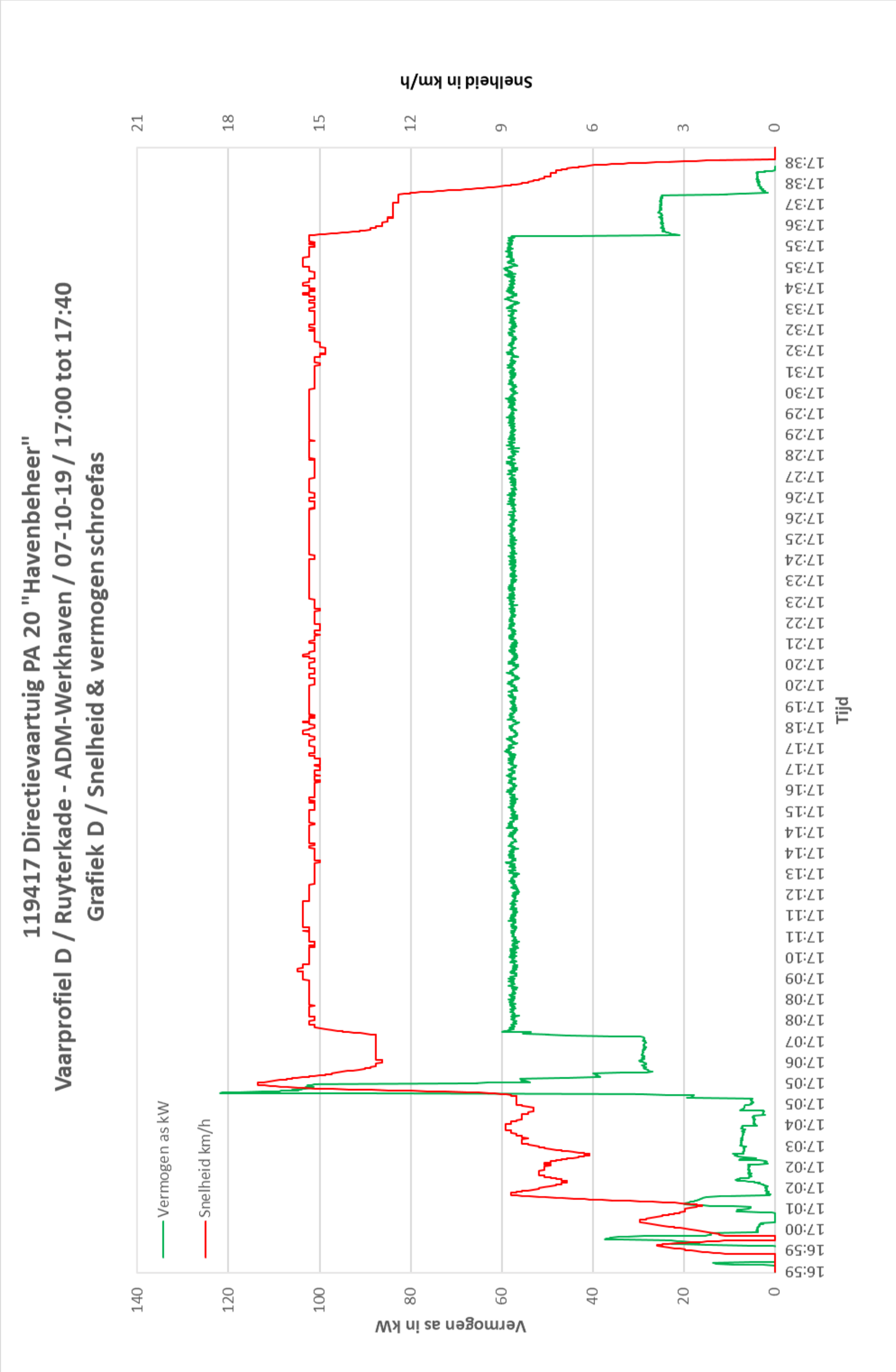
119417 Directievaartuig PA 20 "Havenbeheer"
Vaarprofiel D / Ruyterkade - ADM-Werkhaven / 07-10-19 / 17:00 tot 17:40
Grafiek D / Snelheid & vermogen schroefas
Vermogen as kW
Snelheid km/h
Vermogen as in kW
Snelheid in km/h
Tijd

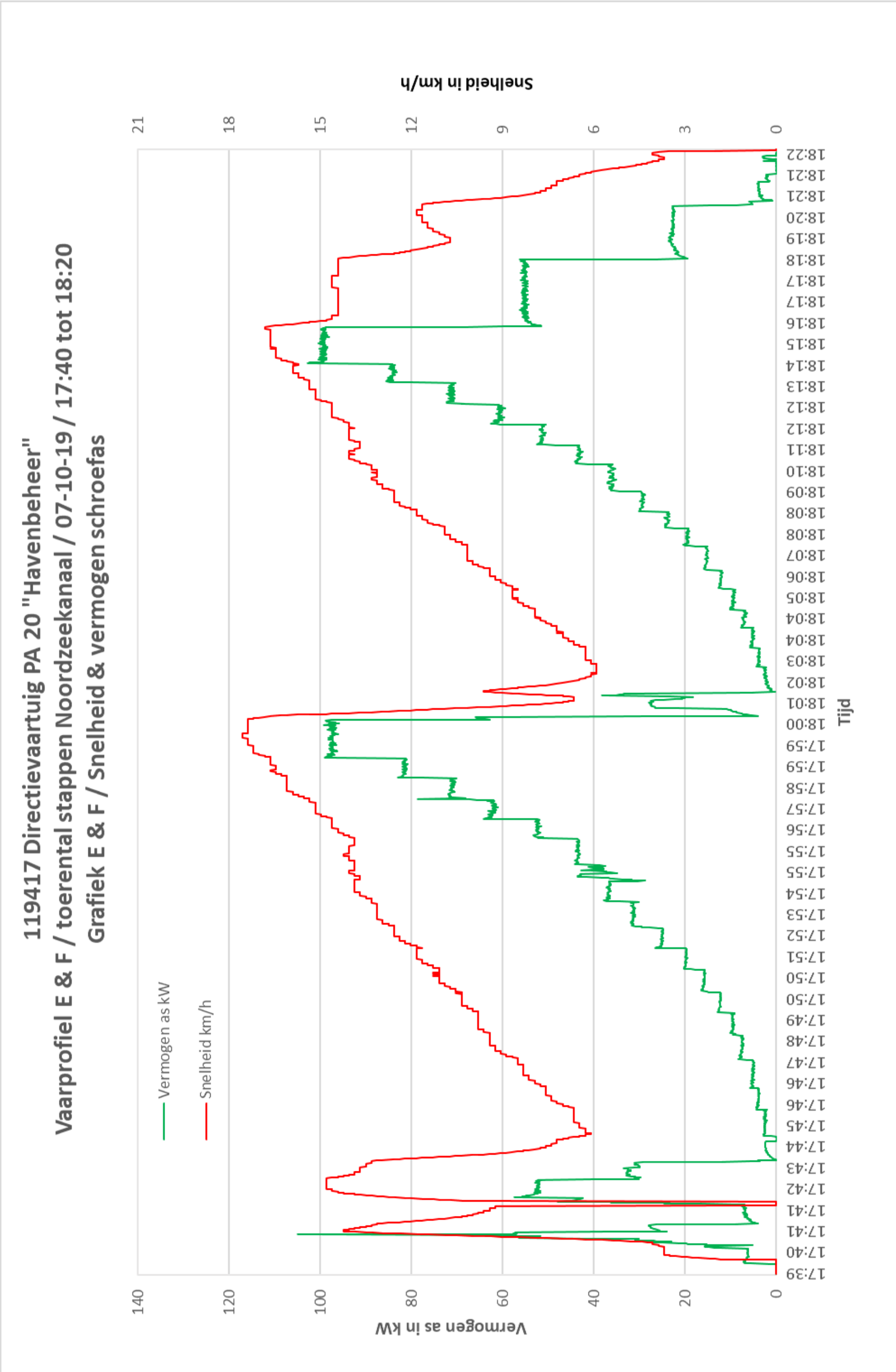
119417 Directievaartuig PA 20 "Havenbeheer"
Vaarprofiel E & F / toerental stappen Noordzeekanaal / 07-10-19 / 17:40 tot 18:20
Grafiek E & F / Snelheid & vermogen schroefas
Vermogen as kW
Snelheid km/h
Vermogen as in kW
Snelheid in km/h
Tijd

C

Productsheet Nedstack MT-FCPP-40 and FCS 10-XXL

PemGen

MT-FCPP-40

The MT-FCPP-40 is a zero-emission shipping enabler as it offers a compact and robust LT-PEM Fuel Cell Power Supply option for a large variety of maritime applications both on inland waterways and in the short-sea domain.

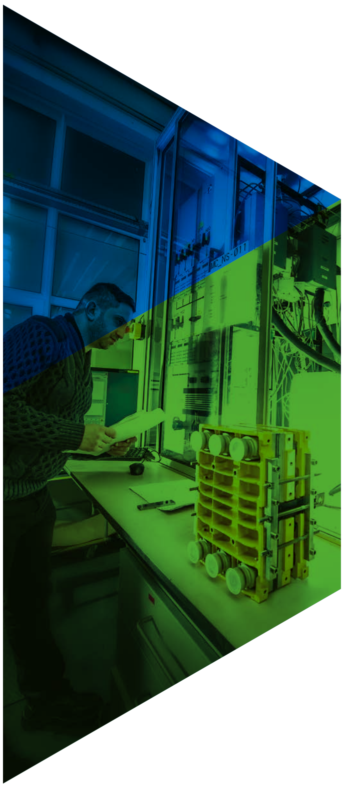

GENERAL	Fuel Cell Type	Low Temperature Proton Exchange Membrane (LT-PEM)
	Fuel Cell Model	4 x Nedstack FCS 10-XXL
ELECTRICAL	Peak Power	40 kWe
	Nominal Power	30 kWe
	Voltage Range	130 – 300 V DC
	Current Range	0 – 230 A
DIMENSIONS	Weight	Approx. 650 kg
	Length	1010 mm
	Width	1010 mm
	Height	1045 mm
HYDROGEN	Quality	Grade ≥ 2.5 (CO < 0.2 ppm)
	Supply Pressure	0.3 – 6 barg
	Max. Consumption	2.5 kg/h
COOLANT	Medium	DI water or BASF FC G20
	Outlet Temperature	65 – 70 °C
	Max. Heat Output	55 kW
AMBIENT CONDITIONS	Operating Temperature	-10 tot 40 °C
	Storage Temperature	5 – 60 °C (optional -20 – 60 °C)
APPLICATION	Intended Use	Main propulsion power or APU for smaller vessels
	Location	Integration in vessel
SAFETY	Compliancy	Class approval on request IEC 60092 IEC 60529 IEC 60533 NEN-EN-50110 ISO 13920 IEC 62282-2 NEN-EN 25817
	Enclosure	IP 55

Nedstack Fuel Cell Technology B.V.
Maritime Power Systems
www.nedstack.com

To be sure.

Westervoortsedijk 73
6827 AV Arnhem
The Netherlands

PRODUCT DATA SHEET

Version: November 2019

NEDSTACK FCS 10-XXL PEM FUEL CELL STACK

Nedstack
PEM FUEL CELLS
To be sure.

SPECIFICATIONS

Electrical - Beginning of Life

Rated power	:	10.6 kWe @ 230 A
Power at lower current	:	see graph

Mechanical

Weight	:	35 kg (approx)
Size	:	499(l)x196(w)x288(h) mm
Cell count	:	75

Hydrogen

Humidification	:	≥ 50% RH at 62 ºC at inlet (75% recommended)
Purity (dry)	:	Grade ≥ 2.5 (max: CO 0.2ppm, CO2 0.5vol%, total sulphur 4ppb, formaldehyde 0.01ppm, formic acid 0.2ppm, ammonia 0.1ppm, total halogenated compounds 0.05ppm, particles 1µg/Nl. Hydrogen specification adapted from ISO 14687-2:2008)
Pressure drop	:	< 0.05 bar at full power
Pressure level	:	0.15 - 0.3 barg
Stoichiometry	:	1.25 - 1.50 for H_2 , minimum flow = 56 Nl/min
Max H2 consumption	:	120 Nl/min at full power

Air

Filtered

Humidification	:	75% RH at 62 ºC
Purity	:	instrument air quality (max: CO 25ppm, Sulphur 0.01ppm, nitrogen dioxide 0.3ppm, ammonia 0.1ppm, particles 1µg/Nl)
Pressure level	:	Ambient (no backpressure allowed)
Pressure drop	:	< 0.12 bar at max power
Stoichiometry	:	≥ 2.0, minimum flow = 105 Nl/min
Max air required	:	572 Nl/min at full power

MEA

Pressure difference		<0.3 bar

Emissions

Noise	:	0
Water production	:	0.5 l/kWh_e(approx.)
H2 respiration	:	60 ml/min (max)

PRODUCT DATA SHEET – NEDSTACK FCS 10-XXL

Cooling

Nominal temperature	:	65 °C
Max temperature	:	70 °C
Capacity	:	< 10 kW_{th} at full power
Medium	:	de-mineralized water or BASF glysantine FC G20
Purity	:	conductivity < 10 $\mu S.cm^{-1}$
Pressure difference	:	< 0.15 bar (DI water) or < 0.45 bar for glysantine
Operating window	:	ΔT < 5K

Note that proper material selection in the tempering device is important to avoid release of ions into the coolant.

Connectors

Coolant	*Standard*	:	Nedstack quick coupling (male)
	Optional	:	quick coupling (female)
Hydrogen	*Standard*	:	Nedstack quick coupling (male)
	Optional	:	quick coupling (female)
Air	*Standard*	:	Nedstack quick coupling (male)
	Optional	:	quick coupling (female)
Current		:	Busbar with 10.5 mm hole (2x)
Cell voltage connector		:	M12 connector (2x)

Appearance Impression

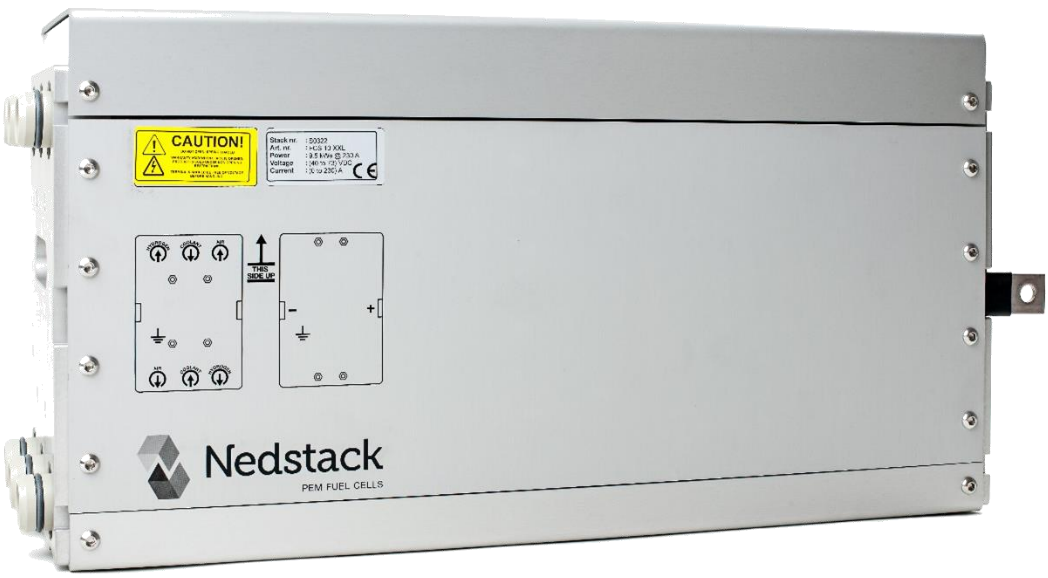

Nedstack
fuel cell technology B.V.

Westervoortsedijk 73
6827 AV ARNHEM

P.O. Box 5167
6802 ED ARNHEM
The Netherlands

Phone +31 (0)26 319 7600
Fax +31 (0)26 319 7601
E-mail info@nedstack.com

Trade Register Arnhem
nr. 09102161

www.nedstack.com

PRODUCT DATA SHEET – NEDSTACK FCS 10-XXL

Nedstack
PEM FUEL CELLS

Electrical specifications
Beginning of Life stack performance data under standard conditions:

Stack temperature = 62 °C, Ambient pressure
Hydrogen: stoichiometry = 1.25; minimum hydrogen flow = 56 Nl/min; RH = 75%.
Air: stoichiometry = 2.0; minimum air flow = 105 Nl/min; RH = 75%

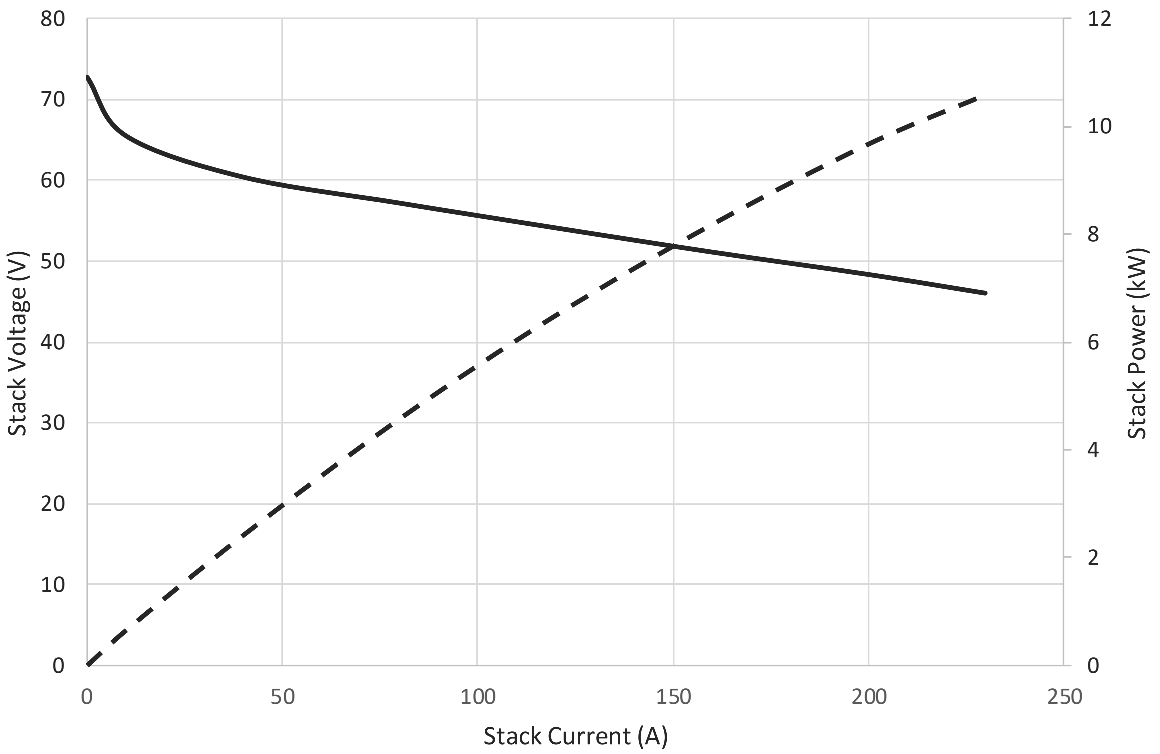

Current (A)	0	40	80	120	160	200	230
Stack Voltage (V)	72.8	60.5	57.2	54.2	51.2	48.4	46.1
Stack Power (kW)	0.0	2.4	4.6	6.5	8.2	9.7	10.6

Nedstack
fuel cell technology B.V.

Westervoortsedijk 73
6827 AV ARNHEM

P.O. Box 5167
6802 ED ARNHEM
The Netherlands

Phone +31 (0)26 319 7600
Fax +31 (0)26 319 7601
E-mail info@nedstack.com

Trade Register Arnhem
nr. 09102161

www.nedstack.com

D

Product sheet Valence XP Modules

LithiumWerks™

Lithium Werks Power Cells

	Product	Voltage	Capacity	Weight	Dimensions L x W x H		Max. Cont. Current	Charge Voltage	Energy
	APR18650M1B	3.3 V	1.2 Ah	39.5 g	Ø18mm x 65mm	-	30 A	3.6 V	3.6 Wh
	ANR26650M1B	3.3 V	2.6 Ah	76 g	Ø26mm x 65mm	-	50 A	3.6 V	8.25 Wh

valence
A LithiumWerks Company

Valence U-Charge® XP Modules with External BMS

	Product	Voltage	Capacity	Weight	Dimensions L x W x H	BCI Group Number	Max. Cont. Current	Charge Voltage	Energy
	U1-12XP	12 V	45 Ah	6.4 kg/ 14.1 lbs	7.76” x 5.12” x 7.17” 197mm x 131mm x 182mm	U1R	90 A	14.6 V	576 Wh
	U24-12XP	12 V	118 Ah	16.3 kg/ 35.8 lbs	10.2” x 6.77” x 8.86” 260mm x 172mm x 225 mm	Group 24	150 A	14.6 V	1510 Wh
	U27-12XP	12 V	144 Ah	19.2 kg/ 42.2 lbs	12.0” x 6.77” x 8.86” 306mm x 172mm x 225 mm	Group 27	150 A	14.6 V	1843 Wh
	UEV-18XP	18 V	75 Ah	14.9 kg/ 32.8 lbs	10.6” x 5.83” x 9.65” 269mm x 148mm x 245mm	-	120 A	21.9 V	1440 Wh
	U24-24XP	24 V	59 Ah	16.3 kg/ 35.8 lbs	10.2” x 6.77” x 8.86” 260mm x 172mm x 225mm	Group 24	118 A	29.2 V	1510 Wh
	U27-24XP	24 V	72 Ah	19.2 kg/ 42.2 lbs	12.0” x 6.77” x 8.86” 306mm x 172mm x 225 mm	Group 27	144 A	29.2 V	1843 Wh
	U27-36XP	36 V	50 Ah	18.7 kg/ 41.1 lbs	12.0” x 6.77” x 8.86” 306mm x 172mm x 225 mm	Group 27	100 A	43.8 V	1920 Wh

Valence Power Module with External BMS

	Product	Voltage	Capacity	Weight	Dimensions L x W x H	BCI Group Number	Max. Cont. Current	Charge Voltage	Energy
	P40-24	24 V	40 Ah	16.5 kg/ 36.3 lbs	10.07” x 6.49” x 10.2” 256mm x 165mm x 260mm	-	up to 600 A*	29.2 V	1024 Wh

* Consult with Lithium Werks about usage conditions

Valence U-Charge® Modules with Internal BMS

	Product	Voltage	Capacity	Weight	Dimensions L x W x H	BCI Group Number	Max. Cont. Current	Charge Voltage	Energy
	U1-12RJ	12 V	45 Ah	6.4 kg/ 14.1 lbs	7.76” x 5.12” x 7.20” 197mm x 131mm x 183mm	U1R	30 A	14.6 V	576 Wh
	U1-12BMS	12 V	45 Ah	6.4 kg/ 14.1 lbs	7.76” x 5.12” x 7.20” 197mm x 131mm x 183mm	U1R	90 A	14.6 V	576 Wh
	U1-24RT	24 V	23 Ah	6.4 kg/ 14.1 lbs	7.76” x 5.12” x 7.20” 197mm x 131mm x 183mm	U1R	30 A	29.2 V	576 Wh

Apr 2019

Bibliography

[1] L. van Biert, M. Godjevac, K. Visser, and P. V. Aravind, *A review of fuel cell systems for maritime applications,* Journal of Power Sources **327**, 345 (2016).

[2] D. J. Durbin and C. Malardier-Jugroot, *Review of hydrogen storage techniques for on board vehicle applications,* International Journal of Hydrogen Energy **38**, 14595 (2013).

[3] T. Hua, R. Ahluwalia, J.-K. Peng, M. Kromer, S. Lasher, K. McKenney, K. Law, and J. Sinha, *Technical assessment of compressed hydrogen storage tank systems for automotive applications,* International Journal of Hydrogen Energy **36**, 3037 (2011).

[4] *Fuel Cell Technologies Office | Department of Energy,* .

[5] T. Umegaki, J.-M. Yan, X.-B. Zhang, H. Shioyama, N. Kuriyama, and Q. Xu, *Boron- and nitrogen-based chemical hydrogen storage materials,* International Journal of Hydrogen Energy **34**, 2303 (2009).

[6] L. O. Valøen and M. I. Shoesmith, *THE EFFECT OF PHEV AND HEV DUTY CYCLES ON BATTERY AND BATTERY PACK PERFORMANCE*, Tech. Rep.

[7] L. Ouyang, W. Chen, J. Liu, M. Felderhoff, H. Wang, and M. Zhu, *Enhancing the Regeneration Process of Consumed NaBH ₄ for Hydrogen Storage,* Advanced Energy Materials **7**, 1700299 (2017).

[8] U. B. Demirci, A. Ouardia, J. Andrieux, J. Hannauer, R. Chamoun, and P. Miele, *Sodium borohydride hydrolysis as hydrogen generator: issues, state of the art and applicability upstream from a fuel cell,* Fuel Cells **10** (2010), 10.1002/fuce.200800171ï.

[9] Y. Wu, *Hydrogen storage via sodium borohydride,* Current Status, Barriers, and R&D Roadmap, Millenium … (2003).

[10] N. Renewable, *Go / No-Go Recommendation for Sodium Borohydride for On-Board Vehicular Hydrogen Storage I n d e p e n d e n t R e v i e w,* (2007).

[11] J. Baldic, P. Osenar, N. Lauder, and P. Launie, *<title>Fuel cell systems for long duration electric UAVs and UGVs</title>,* Defense Transformation and Net-Centric Systems 2010 **7707**, 770703 (2010).

[12] K. Kim, T. Kim, K. Lee, and S. Kwon, *Fuel cell system with sodium borohydride as hydrogen source for unmanned aerial vehicles,* Journal of Power Sources **196**, 9069 (2011).

[13] T. Kim, *NaBH4 (sodium borohydride) hydrogen generator with a volume-exchange fuel tank for small unmanned aerial vehicles powered by a PEM (proton exchange membrane) fuel cell,* Energy **69**, 721 (2014).

[14] S.-m. Kwon, S. Kang, and T. Kim, *Development of NaBH4-Based Hydrogen Generator for Fuel Cell Unmanned Aerial Vehicles with Movable Fuel Cartridge,* Energy Procedia **158**, 1930 (2019).

[15] Y. Kojima and T. Haga, *Recycling process of sodium metaborate to sodium borohydride,* International Journal of Hydrogen Energy **28**, 989 (2003).

[16] C.-L. Hsueh, C.-H. Liu, B.-H. Chen, C.-Y. Chen, Y.-C. Kuo, K.-J. Hwang, and J.-R. Ku, *Regeneration of spent-NaBH4 back to NaBH4 by using high-energy ball milling,* International Journal of Hydrogen Energy **34**, 1717 (2009).

[17] S. Basting, P. Vermeir, V. V. B., and G. Haesaert, *Waterstofproductie uit natriumboorhydride via een heterogene kobaltgebaseerde polymeerharskatalysator Sjoerd Basting,* (2015).

[18] C.-t. F. Lo, K. Karan, and B. R. Davis, *KINETICS , CATALYSIS , AND REACTION ENGINEERING Kinetic Studies of Reaction between Sodium Borohydride and Methanol , Water , and Their Mixtures,* , 5478 (2007).

[19] S. Murugesan and V. R. Subramanian, *Effects of acid accelerators on hydrogen generation from solid sodium borohydride using small scale devices,* **187**, 216 (2009).

[20] C. Grimmer, R. Zacharias, M. Grandi, B. Cermenek, A. Schenk, S. Weinberger, F. A. Mautner, B. Bitschnau, and V. Hacker, *Carbon Supported Ruthenium as Anode Catalyst for Alkaline Direct Borohydride Fuel Cells,* Journal of Physical Chemistry C **119**, 23839 (2015).

[21] F. M. V. Nievelt, *Maritime applications of sodium borohydride as an energy carrier Intermediate presentation,* , 1.

[22] S. S. Muir and X. Yao, *Progress in sodium borohydride as a hydrogen storage material: Development of hydrolysis catalysts and reaction systems,* International Journal of Hydrogen Energy **36**, 5983 (2011).

[23] B. H. Liu and Q. Li, *A highly active Co-B catalyst for hydrogen generation from sodium borohydride hydrolysis,* International Journal of Hydrogen Energy **33**, 7385 (2008).

[24] H. B. Dai, Y. Liang, P. Wang, X. D. Yao, T. Rufford, M. Lu, and H. M. Cheng, *High-performance cobalt – tungsten – boron catalyst supported on Ni foam for hydrogen generation from alkaline sodium borohydride solution,* **33**, 4405 (2008).

[25] Y. Liang, P. Wang, and H.-b. Dai, *Hydrogen bubbles dynamic template preparation of a porous Fe – Co – B / Ni foam catalyst for hydrogen generation from hydrolysis of alkaline sodium borohydride solution,* **491**, 359 (2010).

[26] V. G. Minkina, S. I. Shabunya, V. I. Kalinin, and A. Smirnova, *Hydrogen generation from sodium borohydride solutions for stationary applications,* International Journal of Hydrogen Energy **41**, 9227 (2016).

[27] W. S. Abdul-Majeed, M. T. Arslan, and W. B. Zimmerman, *Application of acidic accelerator for production of pure hydrogen from NaBH4,* International Journal of Industrial Chemistry **5**, 15 (2014).

[28] J. Andrieux, L. Laversenne, O. Krol, R. Chiriac, R. Tenu, J. J. Counioux, C. Goutaudier, J. Andrieux, L. Laversenne, O. Krol, R. Chiriac, and Z. Bouajila, *Revision of the NaBO2 – H2O phase diagram for optimized yield in the H2 generation through NaBH4 hydrolysis HAL Id : hal-01612021 Revision of the NaBO 2 -H 2 O phase diagram for optimized yield in the H 2 generation through NaBH 4 hydrolysis,* (2017).

[29] J. C. S. Pak, B. O. Na, N. O. Solutions, C. Academy, O. Nabo, O. Nabo, and O. Nabo, *Density , Electrical Conductivity , Acidity , Viscosity and Raman Spectra of Aqueous which indicated many hydrates of sodium metaborate sodium tetraborate potential raw material was electro-reduced to NaBH 4 few data appear in the International Critical T,* **35**, 1066 (2013).

[30] V. G. Gude, *Energy consumption and recovery in reverse osmosis,* Desalination and Water Treatment **36**, 239 (2011).

[31] T. Tronstad, H. H. Åstrand, G. P. Haugom, and L. Langfeldt, *Study on the use of Fuel Cells in Shipping,* , 1 (2017).

[32] W. Commons, *Proton exchange fuel cell diagram,* (2015).

[33] W. Commons, *Solid oxide fuel cell,* (2007).

[34] D. Zhou, A. Al-Durra, F. Gao, A. Ravey, I. Matraji, and M. Godoy Simões, *Online energy management strategy of fuel cell hybrid electric vehicles based on data fusion approach,* Journal of Power Sources **366**, 278 (2017).

[35] E. contributors, *dod,* .

[36] L. Werks, *Anr226650m1b dischrage voltage profiles,* (2019).

[37] I. Buchman, *Battery university, how do lithium batteries work?* (2019).

[38] M. N. Hashemnia and B. Asaei, *Comparative study of using different electric motors in the electric vehicles,* (2017), 10.1109/ICELMACH.2008.4800157.

[39] J. L. Kirtley, A. Banerjee, and S. Englebretson, *Motors for Ship Propulsion,* Proceedings of the IEEE **103**, 2320 (2015).

[40] J. D. Widmer, R. Martin, and M. Kimiabeigi, *Sustainable Materials and Technologies Electric vehicle traction motors without rare earth magnets,* SUSMAT **3**, 7 (2015).

[41] M. Fedkin, *6.5 efficiency of converters,* (2019).

[42] R. D. Geertsma, R. R. Negenborn, K. Visser, and J. J. Hopman, *Design and control of hybrid power and propulsion systems for smart ships: A review of developments,* Applied Energy **194**, 30 (2017).

[43] A. M. Bassam, A. B. Phillips, S. R. Turnock, and P. A. Wilson, *Development of a multi-scheme energy management strategy for a hybrid fuel cell driven passenger ship,* International Journal of Hydrogen Energy **42**, 623 (2017).

[44] S. Njoya Motapon, L. A. Dessaint, and K. Al-Haddad, *A comparative study of energy management schemes for a fuel-cell hybrid emergency power system of more-electric aircraft,* IEEE Transactions on Industrial Electronics **61**, 1320 (2014).

[45] T. Zhang, P. Wang, H. Chen, and P. Pei, *A review of automotive proton exchange membrane fuel cell degradation under start-stop operating condition,* Applied Energy **223**, 249 (2018).

[46] Unknown, *Boot koningsvaart is gereed,* (2013).

[47] M. G. Parson, *Parametric design,* in *Ship design and construction vol 1-2*, edited by T. Lamb (Society of Naval architects and Marine Engineering, 2004) Chap. 11, pp. 11.3–11.46.

[48] J. Holtrop and G. Mennen, *An approximate power prediction method,* (1982).

[49] F. C. B. BV, *Nemo h2: rondvaart op waterstof,* (2011).

[50] M. Oosterveld and P. van Oossanen, *Further computer analyzed data of the wgaeningen b-screw series,* (1978).

[51] unknown, *Pias manual: resistance prediction with emperical methods,* (2019).

[52] P. van Mensch and R. P. Verbeek, *Electric Shipping in the City of Amsterdam,* , 1 (2015).

[53] G. L. Se and G. L. Se, *FUEL CELLS IN MARITIME APPLICATIONS CHALLENGES , CHANCES AND EXPERIENCES,* , 1 (2010).

[54] H. Grimmelius, *Control of Hybrid Ship Drive Systems Control of Hybrid Ship Drive Systems,* (2016).

[55] B. Geng, S. Member, J. K. Mills, D. Sun, and S. Member, *Two-Stage Energy Management Control of Fuel Cell Plug-In Hybrid Electric Vehicles Considering Fuel Cell Longevity,* **61**, 498 (2012).